5-2008

ASSESSING THE IMPACT OF WATER HARVESTING ON WATER RESOURCES

Jennifer Oblinger
Clemson University, felidae369@gmail.com

ASSESSING THE IMPACT OF WATER HARVESTING ON WATER RESOURCES IN RURAL INDIA

A Thesis
Presented to
the Graduate School of
Clemson University

In Partial Fulfillment
of the Requirements for the Degree
Master of Science
Hydrogeology

---

by
Jennifer Ann Oblinger
May 2008

Accepted by:
Dr. Stephen Moysey, Committee Chair
Mr. Scott Brame
Dr. Fred Molz
Dr. Abdul Khan

ABSTRACT

Clean water supplies, like all natural resources, are becoming scarce all over the world, but especially in developing countries where special interest groups (such as city governments, commercial farmers, other villages downstream, etc.) fight over water rights. The Foundation for Ecological Security (FES) is a non-government organization in India whose mission is to restore degraded lands through cooperation with rural villages. In order to increase the water supply to the ecosystem, FES constructs water harvesting structures (WHS) which impound rainfall, water that would have otherwise runoff and contributed to erosion, in surface storage. This study was conducted to assess the impact of the WHS on the environment and the effectiveness of extending the water supply through the dry season. To accomplish this task, a surface water balance was formulated to estimate the natural hydrologic characteristics of the system and an analytical balance over the WHS was designed to approximate the infiltration from the standing pool.

A conceptual model of the hydrogeology of the Deccan Traps was created to determine the approach to the solution of the water balance. Digital data provided by FES was compiled and organized using ESRI's ArcGIS. The geology of the study area was surveyed in the spring of 2007 through surface mapping and vertical electrical sounding. A geologic map was drawn and a basic conceptualization of the flow of groundwater through the subsurface was formulated.

It is hoped that this study will be the beginning of a project which will aid FES, other NGO's and the Indian government in promoting self-management and cooperative usage of available water resources in rural villages.

DEDICATION

To my family whose support has been unwavering throughout my graduate career. To Adam whose love and encouragement has carried me through the final and most difficult parts of this project.

ACKNOWLEDGMENTS

I would like to thank Ravi Ravindranath, Chiranjit Guha, and the Foundation for Ecological Security, they are the driving force behind this project. I would also like to thank the Moysey Research and Creative Inquiry Groups, Dr. Himanshu Kulkarni, and the India Water Portal team for their valuable contribution to this project.

TABLE OF CONTENTS

Table of Contents (Continued)

Page

LIST OF TABLES

List of Tables (Continued)

Table Page

LIST OF FIGURES

List of Figures (Continued)

Figure Page

List of Figures (Continued)

Figure Page

List of Figures (Continued)

Figure Page

CHAPTER 1: INTRODUCTION

1.1 MOTIVATION

People are dependent on water for survival. In developing countries this dependence can be exacerbated by insufficient knowledge on the controls of water occurrence be it surficial or subsurface. This problem of water scarcity is particularly prevalent in India where 70% of the population lives in rural areas (Macdonald, 1995) and where groundwater provides more that 80% of drinking water supplies (Saha, 2006). In addition, 65% of the total area of India is covered by hard rock (Saraf, 1998) where water storage and transmission is controlled by fractures and other secondary porosity (Saha, 2006). This geologic complexity coupled together with variable rainfall (Macdonald, 1995) makes water resource management difficult.

The rising demand for water often confounded by a lack of comprehension of the dynamics of groundwater flow and storage has led to overexploitation of groundwater resources. The overdraft of groundwater can have numerous unforeseen consequences which not only directly affect the groundwater supply through the lowering of water tables, but can also change or reduce surface water resources. Wells are drying up because the aquifers cannot recover from the stress of excessive extraction and some villages are under such strain that potable water has to be brought in on tanker trucks during dry months (Kulkarni, 2004). In addition, extraction of groundwater and lowering of water tables results in increased infiltration and decreased runoff generated from rainfall (Kumar, 2005; Macdonald, 1995). The reduction in runoff ultimately reduces surface streams to flow primarily during the high intensity monsoon.

To aid in counteracting the effects of overextraction and to sustain local water supply throughout the year, surface impoundments have been constructed on pre-existing stream channels in an attempt to capture monsoonal rain water which would have otherwise runoff downstream. The goal of this study is to determine the contribution these structures make to groundwater.

1.2 Background on Water Management

Historically, groundwater was efficiently and effectively used as a source for drinking water and irrigation without much conflict between the two. Most crops were drought-tolerant plants and water supplies were supplemented through the use of irrigation storage tanks, check dams on small streams, and groundwater obtained through large-diameter wells (Narasimhan, 2006). Surface water storage tanks and intricate irrigation systems were built and maintained since 300 BC. These systems were constructed by commoners, for the benefit of their communities, as well as royalty, as a part of their religious and social obligations (Iyengar, 2007). Water abstraction was obtained through manual or animal powered means which limited the volume of water that could be extracted from the groundwater reserve (Macdonald, 1995).

With Indian independence in 1947 came a push to reduce famine and increase agricultural production (Moench, 2003). During this time the number of wells sunk increased dramatically and electrical water pumps were introduced to increase the volume of water extracted (Macdonald, 1995). Faith in the new technology led to the neglect of the traditional water storage systems (Iyengar, 2007). Agricultural production

increased more than five fold during this period at the expense of groundwater quantity and quality (Narasimhan, 2006; Narula, 2001).

Today the level of groundwater development is assessed by the Indian national government based upon the reasoning that water supplies can be quantified using pre- and post-monsoon water level fluctuation, rainfall measurements, and estimates of groundwater extraction (Moench, 2003). The assessment of development, which is basically a balance between the recharge and withdraw of groundwater, determines the level of financial support for further development offered to local regions and is calculated as (Moench, 2003)

$$\text{level of development} = \frac{\text{net yearly draft}}{\text{utilizable resource for irrigation}} \tag{1.1}$$

The net yearly draft is based on well surveys and estimated pumping time usage while the utilizable resource for irrigation is calculated using the water table fluctuation method which is estimated by multiplying recharge from rainfall by the specific yield of the aquifer and the area of interest (Moench, 2003). Both of these estimates are fraught with uncertainties and possibilities of inadequate and inaccurate data. The water table fluctuation method is particularly conspicuous because it requires not only a detailed network of wells for collecting water table measurements, but an estimate of specific yield of the aquifer which can be difficult to determine in fractured rock systems (Healy, 2002; Moench, 2003).

Despite these problems, estimates for the above values are obtained and the level of financial support provided to local regions is determined using Table 1.1.

Table 1.1: The Government of India's schema for allocating financial support for groundwater development (Moench, 2003)

Categories of Groundwater Development		
Level	Description	Financing
Safe	<70% development with no significant decline in long term water levels	Open
Critical	90-100% development with declines in water levels -or- >100% development with no declines in water levels	Somewhat restricted Local surveys and intensive monitoring required
Overexploited	>100% development with pre- and post-monsoon water levels displaying significant, long-term declines	Highly restricted Local surveys and intensive monitoring required

This funding scheme attempts to remediate overabstraction of groundwater; however, the system falls short of its goal as a result of unreliable estimates upon which it is based. The reliance on this system for funding allocation can ultimately result in more problems because of inadequate data analysis.

1.3 Background on Water Harvesting

Numerous techniques have been proposed to attempt to alleviate the groundwater crisis, from redirection of major rivers (Shankar, 2004) to groundwater recharging schemes (Patel, 2007) and communal management of resources (Kulkarni, 2004). Recently, the most popular option has been the construction of water harvesting structures (WHS). These structures are small earthen dams built on stream systems. The objective of water harvesting is to store water on the surface while simultaneously recharging the groundwater supply and reducing erosion caused by flooding streams. Some regional water harvesting constructions have been funded by the government,

either state or national, but most of the smaller, local structures have been funded by non-governmental organizations (NGOs) or by local villages.

An example of an NGO which has been successful in promoting WHS construction is the Foundation for Ecological Security (FES). This organization has made it their mission to restore degraded lands and water supply through recharge and storage via cooperation with rural villages (FES, 2003). FES has used a variety of techniques including protection of common lands, soil and water conservation, and construction of water harvesting structures.

Water harvesting structures are a traditional, simple technology which has had great success in the past. The groundwater recharge produced by the structures has resulted in the farmer's realization that water needs to be recharged and managed, that it is not an infinite resource (Kumar, 2006; Ray, 2006). Unfortunately, the WHSs are sometimes constructed based upon the common beliefs rather than governing principles of watershed hydrology. Some examples of the beliefs motivating WHS construction include: the monsoon rains contribute an immense amount of water which will eventually end up in the ocean if it remains uncaptured, local water needs are small and thus local water supplies should handle the demands of that scale, incremental structures built on the same stream will lead to incremental benefits, etc. (Kumar, 2006; Patel, 2007).

Upon these premises, the number of WHSs have increased dramatically over the past decade following severe droughts in 1999 and 2000 (Patel, 2007). Unanticipated effects of water harvesting, such as interruption of streamflow from upstream to

downstream (Kumar, 2006; Narasimhan, 2006; Ray, 2006), are beginning to be recognized. Additional concerns such as the water collection potential of the structures are also coming to light. The structures capacity can be reduced by logistical controls such as WHS overflowing within the first monsoonal rains and high degree variability of rainfall patterns (Kumar, 2006; Patel, 2007). The importance of the underlying geology beneath WHSs is being realized; however, there is no general comprehension of the impact of water harvesting on the hydrogeology due to the scarcity of studies on the topic (Kumar, 2006).

Overall, there is a wealth of anecdotal evidence of the hydrologic effects of the WHS, both positive and negative, but there is general lack of quantitative understanding of the effects on both small and large scales (Patel, 2007). Not only is there a deficiency of geological and hydrological information, but the only prevalent data available that is required as a part of a water balance is rainfall because of the ease of monitoring such data. Other parameters, such as evapotranspiration (ET), streamflow, and water table levels, are either not measured or they are not readily available due to the confidentiality of internal reports (Shankar, 2004). Since most of the smaller structures are built by local agencies, these parameters cannot be generated due to a lack of funding for comprehensive hydrogeological investigations (Kumar, 2006). To compensate for the missing data, many studies have used inappropriate data, such as figures from discrete locations which were over generalized to represent much larger areas (Kumar, 2006; Shankar, 2004). An example of such an extrapolation is the use of water level data obtained from a handful of wells and application of the results to large areas and the use

of specific yield estimates from studies which may or may not be applicable to the area of interest (Moench, 2003). Thus, there remains a lack of understanding of the effects of WHSs on the local and regional hydrology due largely to the use of inappropriate data in studies examining WHSs.

1.4 Study Objective

This study was conducted to investigate the impact of one WHS on the hydrology of a local basin. This task was accomplished by (i) characterizing the hydrogeologic system through field mapping, (ii) investigating the natural water cycle, and (iii) comparing natural recharge in the watershed to the artificial recharge generated by the WHS to understand groundwater impacts.

Geology is a key factor to understanding the groundwater component of the hydrologic cycle since the hydrogeologic properties of the rock determines the flow path and patterns of subsurface water. Additionally, the geology will control the rate of progression of the recharge plume from WHSs (Kumar, 2006). A water balance, a quantitative formula assessing the inputs, outputs, and changes in storage over a particular area, was formulated to characterize the hydrologic cycle of the watershed. An analytical formulation based on atmospheric data was compiled for the surface water balance to constrain the variables of a groundwater balance designed to describe the controls on the infiltration from and the impacts of the WHS. Ultimately, the goal of this study is to assist NGOs and the associated communities in understanding the controls of artificial recharge from the WHS through a hydrogeological survey and thus allow

them to make informed decisions on the construction and maintenance of current and future structures.

1.5 Study Area Description

The study was conducted near the village of Salri, Shajapur district, state of Madhya Pradesh, India; the approximate coordinates are 23.7° N and 76.1° E. The area is generally flat with few undulating hills (FES, 2003) rising about 100m over the 2.6km^2 area. The biome is barren, dominated by dry, deciduous scrub and thorny forests. Land use is predominantly for grazing livestock with some productive agricultural fields. Water is used for domestic and irrigation purposes.

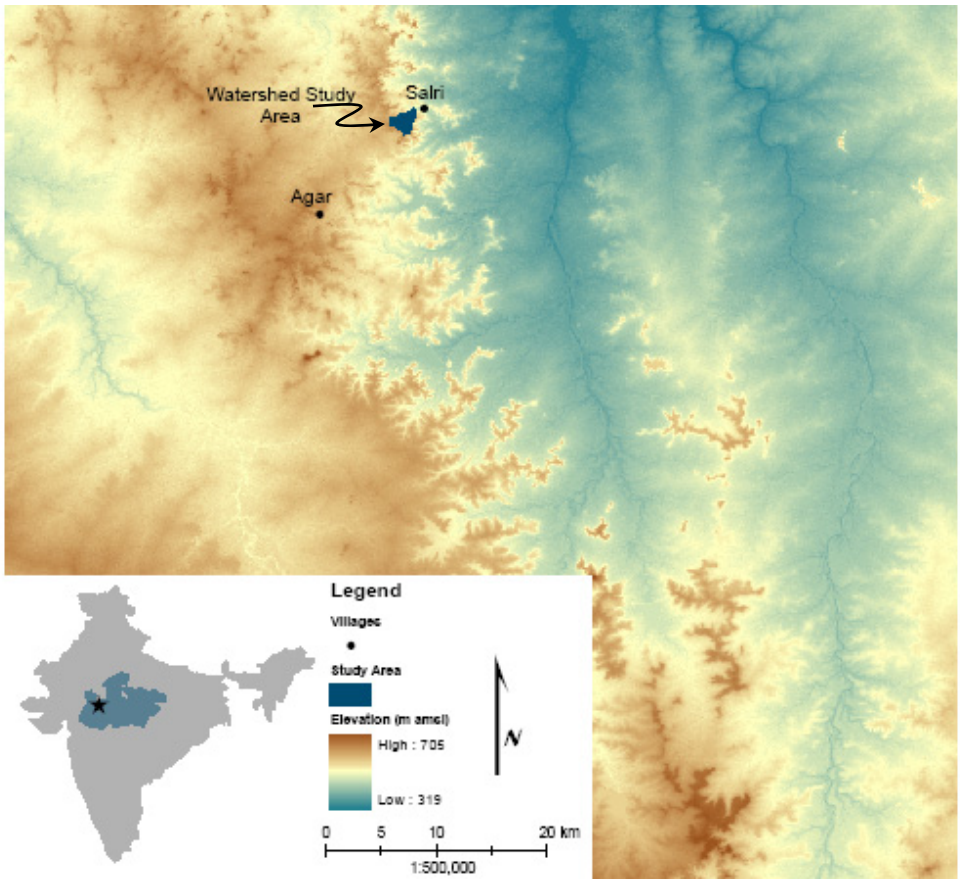

Figure 1.1: Regional map of the study area

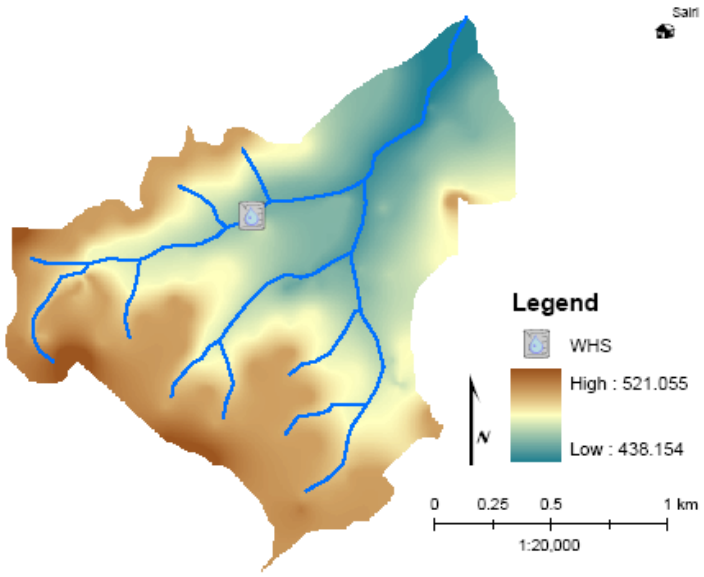

Figure 1.2: Local map of the study area

The region is characterized as a semiarid climate which experiences two distinct periods: a wet (monsoon) season and a dry season. The water supply is recharged by the southwest monsoon, from mid-June to October, but 80% of the rain typically falls from July through September (Saha, 2006; Scanlon, 2006). These three months are dominated by heavy rainfall over short periods of time that leads to frequent flooding (FES, 2003; Patel, 2007; Saha, 2006; Saraf, 1998).

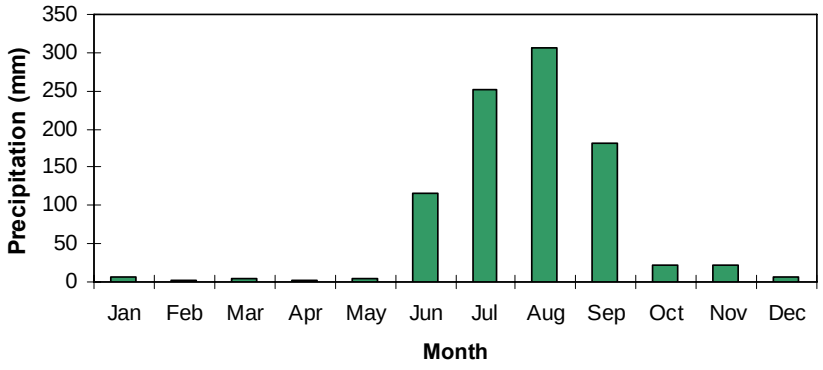

Figure 1.3: Average total monthly rainfall over 1952 and 2002

Immediately after monsoon, water supplies are easily attainable, but water is scarce for the remainder of the year as seen in Figure 1.4 and Figure 1.5. As a result, the streams in the area are seasonal and the vegetation is composed primarily of xerophytes (FES, 2003; Scanlon, 2006). WHS are filled during monsoon and most maintain a surface water supply until March at which point the shallow wells downstream of the WHS become the primary source of water (FES, 2003).

Figure 1.4: River between Ujjain and Agar, July 17 2006

Figure 1.5: River between Ujjain and Agar, May 2 2007

The geology of the area is dominated by a sequence of heterogeneous basalt flows known as the Deccan Traps. This dense volcanic rock can be highly fractured (either vertically through columnar joints or horizontally through sheet joints), extensively vesicular and glassy, or massive sections of compact rock (Saha, 2006). The arrangement and characteristics of each type of basalt determine its ability to transmit or store water.

1.6 Thesis Synopsis

Chapter 1 illustrates the problems associated with water resources in India, describes how the issues evolved through time and illustrates the need for a more comprehensive understanding of the geologic controls on groundwater storage, flow, and occurrence. Chapter 2 describes the geologic setting of the Salri watershed and details the field work and interpretation of the hydrogeologic situation. Chapter 3 explains the soil water balance model used to estimate the natural surface water balance of the area and discusses the components of the groundwater balance. Chapter 4 presents the visual and numerical modeling performed to estimate the recharge from the WHS. Chapter 5 concludes the comparison of natural recharge and artificial recharge of the WHS and offers recommendations for future work and general management of scarce water resources.

CHAPTER 2: GEOLOGY OF THE SALRI WATERSHED

As mentioned in the previous chapter, the geologic structure is the main factor which controls groundwater distribution, flow, and storage. Particularly in the heterogeneous environment of the Deccan Traps, where groundwater movement is dominated by flow through fracture systems, high groundwater productivity areas can occur in randomly arranged, discrete locations (Kulkarni, 2004, 1994). In actuality, with a thorough understanding of the fracture controls and patterns, groundwater potential in a particular area should be relatively predictable.

2.1 REGIONAL CONTEXT: DECCAN BASALTS

The Deccan basalts of India are the fourth largest continental flood basalt in the world covering half a million square kilometers (Kulkarni, 1997; Saha, 2006). The basalts were formed as a result of the northward migration of the India plate over a hotspot (Nair, 2001). The hotspot, basically an upwelling of hot mantle material, melted the overlying crust and forced basalt to pour out of fissures. This eruption had a very slow rate, but it occurred over four million years to produce the observed large volume of basalt which inundated valleys and depressions and covered the low hills of the bedrock which was previously exposed for a long duration (Jerram, 2005).

The Deccan basalts are considered as a stack of individual lava flows ranging in thickness from a few meters to hundreds of meters (Kulkarni, 2000). Each individual flow exhibits the same basic pattern of characteristics: a glassy section indicating the top of the flow underlain by a bubbly vesicular or amygdular layer with a base of compact

basalt which is fractured by vertical columnar joints in the top and horizontal joints at the bottom (Kulkarni, 2004, 2000, 1994).

The glassy top of the flow, commonly referred to as red bole, is usually weathered to clay as a result of the long exposure time between eruptions (Saraf, 1998). The vesicular basalt formed when dissolved gasses in lava escape to produce bubbles. Vesicular basalt is termed amygdular if the vesicles are filled with calcite, zeolite, or quartz as a result of chemical weathering due to prevalent sheet joints (Kulkarni, 1994; Saraf, 1998). The compact basalt, which represents the majority of the flow, is more fine-grained than the vesicular portion with two different fracture patterns creating characteristic subsets (Kulkarni, 2000; Saraf, 1998). The majority of the compact basalt is dominated by vertical or subvertical joints, known as columnar joints, with few horizontal fracture zones. The lower portion of the layer is characterized by either a low density of fractures or an approximately equal ratio of horizontal to vertical fractures (Kulkarni, 2000). The upper compact layer will from this point forward be termed columnar basalt due to the large amount of columnar jointing while the lower compact basalt will be termed massive basalt due to the tendency of this section to fracture into large blocks. Overall, individual lava flows exhibit a similar pattern of decreasing weathering with depth with the majority of weathering occurring to the glassy and vesicular/amygdular layers (Athavale, 1983). A conceptual representation of the parts of each flow is presented in Figure 2.1.

Figure 2.1: Conceptual stratigraphic column representing the common portions of Deccan trap lava flows (note that photos are at different scales)

As a result of the long eruption period and the movement of the location of volcanic activity, there exists a high degree of heterogeneity of the basalts with respect to weathering and fracturing properties (Saha, 2006). Individual flows can be traced variably for kilometers to hundreds of kilometers, but they commonly pinch out or change in character (Jerram, 2005). In addition, basic lithologic characteristics, such as

weathering and fracturing patterns, tend to change dramatically over short distances (Kulkarni, 1994) making correlation between flows difficult.

2.2 Geology of the Malwa Plateau

The Malwa Plateau, where the present study is located, represents some of the oldest eruptions of the Deccan basalts (Jerram, 2005; Nair, 2001). As such, these basalts appear slightly different from the highly studied basalts of the Western Ghats region. The Malwa basalts tend to exhibit little or no evidence of the glassy top and vesicular/amygdular layers of individual flows leaving only the columnar and massive basalts (Kulkarni, 2007). The reasons for the absence of the top two layers of typical flows could be that the conditions for forming these two layers were not optimal and the layers were never present, or the top two layers were so easily weathered that they were eroded away before the next lava flow was laid down. The exact reasoning for the layer's nonexistence is not of great importance to this particular study, but it is significant to note that this Malwa region is different from most of the studied areas of the Deccan traps.

2.3 Geology of the Salri Watershed

In order to fully understand the hydrogeology of the area, a basic understanding of the geology must be developed. From the previous section, it can be inferred that columnar basalt, being highly fractured vertically, would most likely generate vertical preferential flow of water while massive basalt, being generally equally fractured vertically and horizontally, would have relatively similar amounts of flow in either

direction. Knowledge of the extents of the individual basalts would therefore allow for a more accurate representation of the hydrology of the area. To this end, the geology of the watershed was investigated by mapping and electrical resistivity studies.

2.3.1 Geologic Mapping

Lithologic descriptions were collected at outcrops throughout the watershed. The particular locations were collected using the MobileMapper function of the Thales Promark 3 GPS system. The purpose of logging data points in this fashion is to allow for simple integration of the collected data into a GIS database. Collecting GPS points using the

Figure 2.2: Thales GPS MobileMapper setup

MobileMapper feature involves collecting waypoints and adding attribute data with the handheld receivers without the use of external antennas. Using only the handheld receiver with a smaller occupation time results in less data accuracy as opposed to the use of two GPS receivers with their respective external antennas in survey mode (i.e.,

differential GPS). However, the less accurate but more rapid data collection model was well suited for the present study. To ensure data retention, the positions and elevations were noted in a field notebook in addition to digitally logging the point using the MobileMapper feature. GPS data collection took place over the course of two days. On May 4, 2007, the entire FES field team from Agar participated in mapping basin 1 (Figure 2.3). The purpose of having everyone walk down together was to ensure that the lithologies were being identified accurately and consistently. The next day, May 5, the adjacent basins were logged by splitting into two teams: one team walked the stream valley marked two and the other walked the valley marked three in Figure 2.3. The lower basin could not be visually mapped because the region was much flatter and there was a general lack of exposures due to an excess of weathered bedrock covering the bedrock.

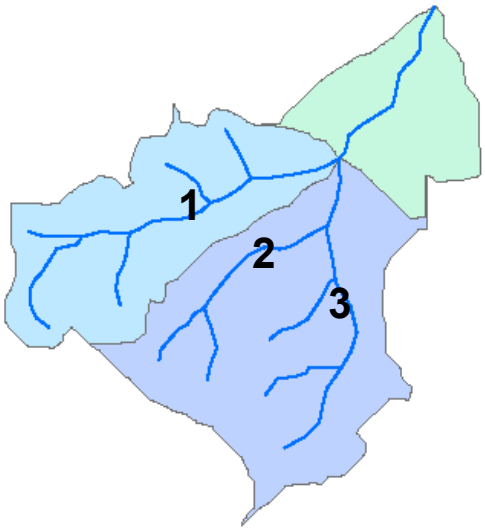

Figure 2.3: Visually mapped transects of the basins of the Salri watershed

CLASSIFICATION OF BASALTS

There are three basic basalt characters observed in the field: weathered, columnar, and massive. The weathered basalt is a result of the chemical and mechanical breakdown

of exposed rock. This decomposed layer of basalt exists at the top of each lava flow and increases in thickness with increased exposure to the elements. Columnar basalt, as discussed previously, is rock that is primarily fractured vertically. Massive basalt is fractured equally horizontally and vertically. These basic characteristics defined the classification scheme of the field mapping; examples are shown in Figure 2.4 to Figure 2.6.

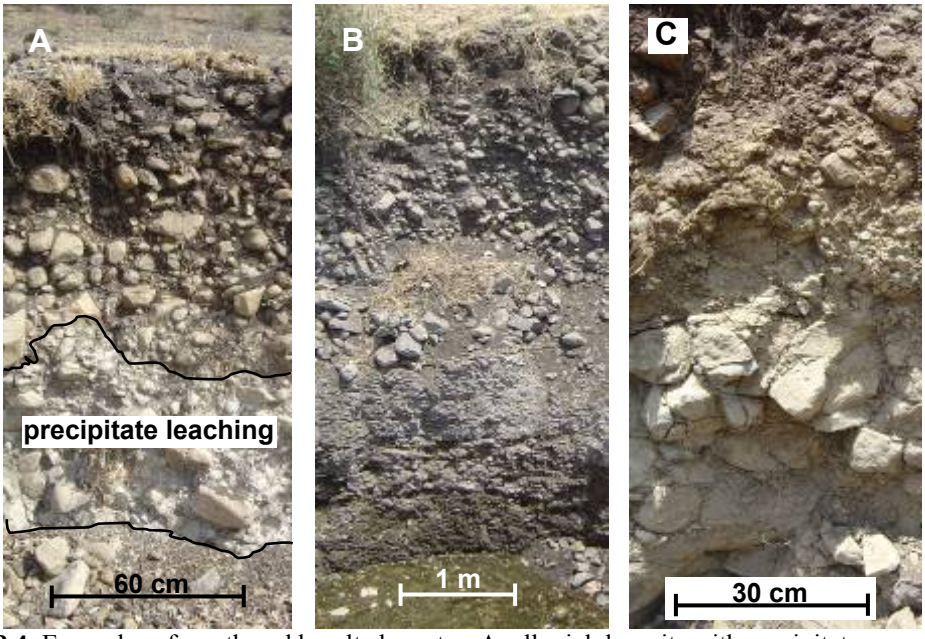

Figure 2.4: Examples of weathered basalt character: A. alluvial deposits with precipitates as a result of chemical weathering in a dry streambed, B. alluvial deposits overlying highly chemically weathered material in a dug well, C. recently disturbed soil transitioning down to weathered basalt cobbles in a WHS construction excavation site

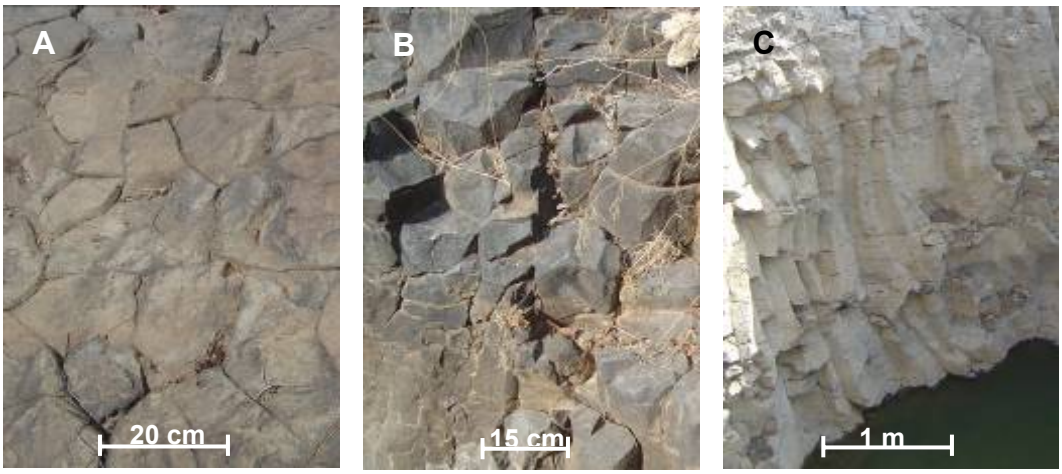

Figure 2.5: Examples of columnar basalt character: A. surface view of columns directly downstream of the WHS in basin 1, B. partially weathered columnar basalt at the southwestern divide, C. columnar basalt in a dug well on the southwestern divide

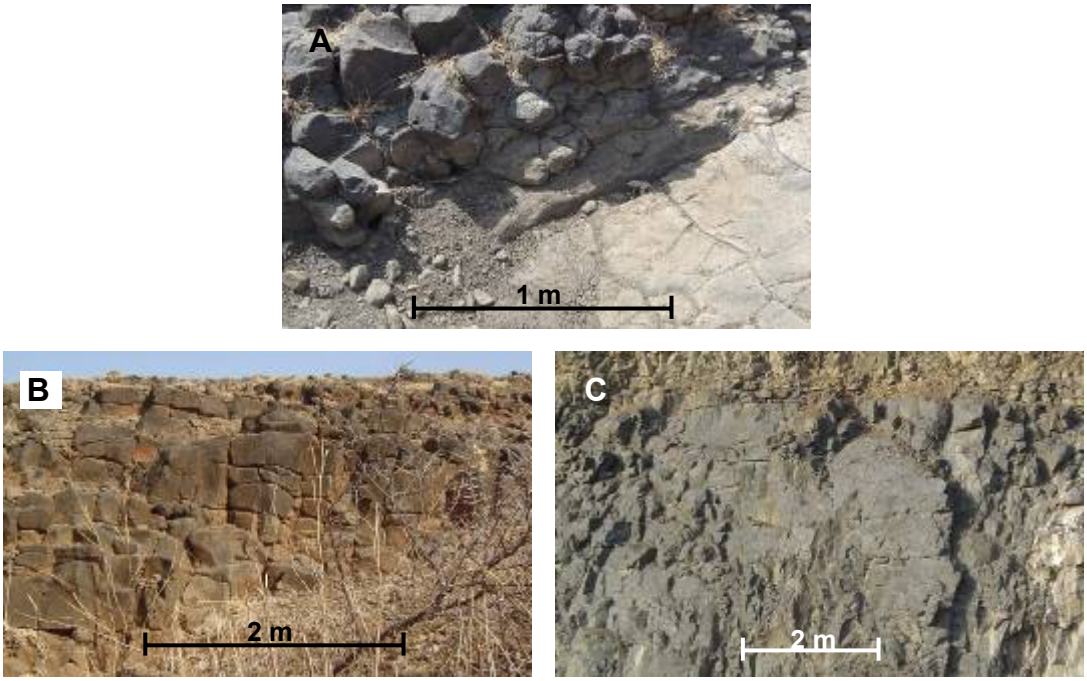

Figure 2.6: Examples of massive basalt character: A. surface view of massive basalt in basin 2, B. partially weathered massive basalt in basin 1 (scale is approximate), C. massive basalt at a quarry south of the study area

OUTCROP OBSERVATIONS

The results of the field mapping are shown in Figure 2.7. There were a few cases where vesicular basalt was observed, and in the cases where it could not be clearly

determined if the basalt was columnar or massive, the transitional classification was used. As mentioned before, the lower basins could not be visually mapped because of the flatness of the topography and thus the excess of weathered basalt (Figure 2.4) obscuring any exposures. The weathered classification was not used in the final results because this classification yields no information regarding the successive lava flows, only the inevitable result of surface exposure.

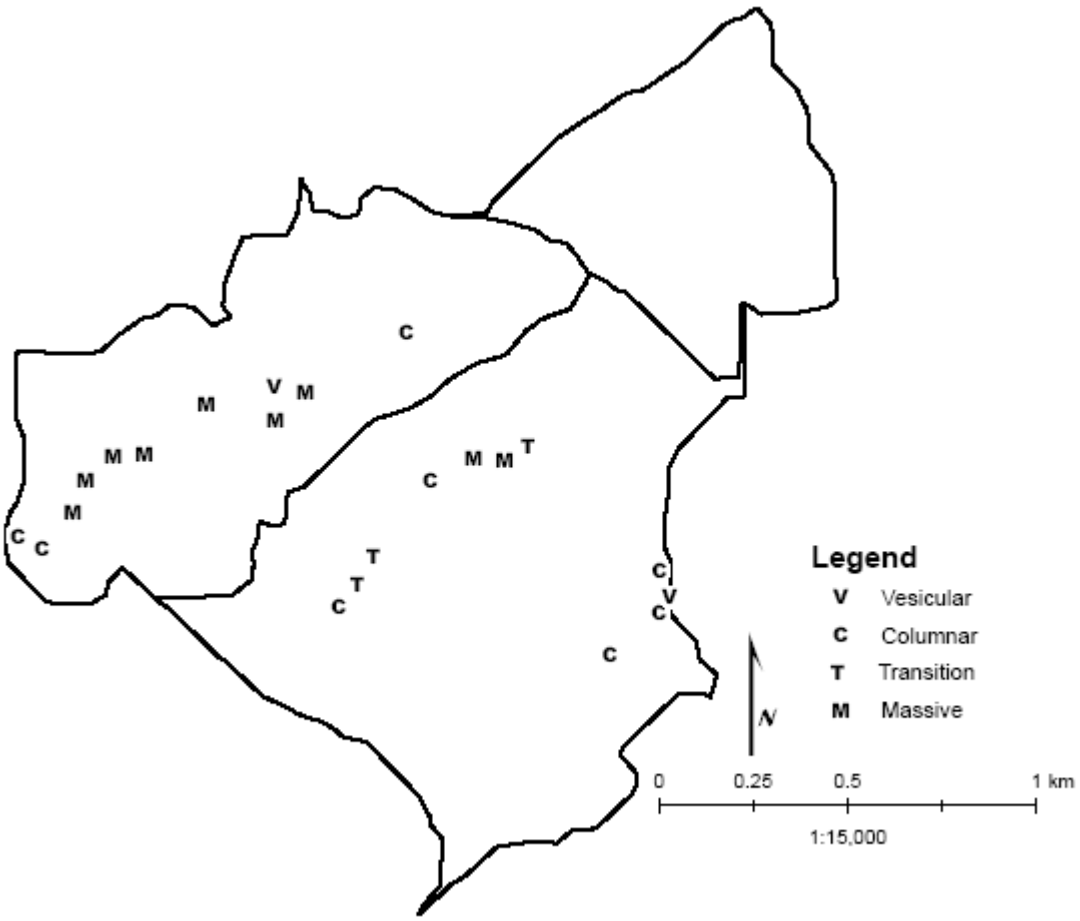

Figure 2.7: Locations of logged geologic waypoints

POSSIBLE ERRORS/FUTURE WORK SUGGESTIONS

Difficulties were encountered that could result in errors during the mapping of geologic features. The handheld GPS systems were not as accurate as they were when

used in conjunction with the external antennas. It was noticed that the elevation measurements were particularly troublesome, for example, two points were taken near the WHS in basin 2, one on the top of the retention structure and the other at a lower elevation downstream of the WHS. The GPS receivers read a higher elevation at the downstream point than at the WHS. It is estimated that the error with the elevation could be as high as 10 meters. In addition, the receivers required the user to remain stationary for some time (at least one minute) to get accurate readings, but this observation was not noted until the second day of mapping. Finally, the rocks were commonly obscured by thick soils or weathered zones and were difficult to consistently classify in terms of their cooling character (as seen in Figure 2.4 to Figure 2.6) because of similarities between or differences within categories. It is suggested that a more detailed study be performed where surface observations are combined with lithologic well logs to obtain a more accurate representation of the study area. In addition, more accurate GPS elevation measurements should be obtained.

2.3.2 Electrical Surveys

In this study, electrical resistivity surveys were conducted to qualitatively identify hydrogeologic trends and boundaries. Resistivity surveys are useful for identifying water saturated and dry zones in the subsurface without disturbing the material by excavation or drilling. The basic principle of resistivity surveying is that the ability of a material to impede the flow of electrical current, i.e., the electrical resistivity of the material, is dependent upon the volume and connectivity of pore space (porosity), amount of water

(water content), and electrical characteristics of the geologic material (Singhal, 1999). Salinity is an additional factor that strongly affects electrical resistivity.

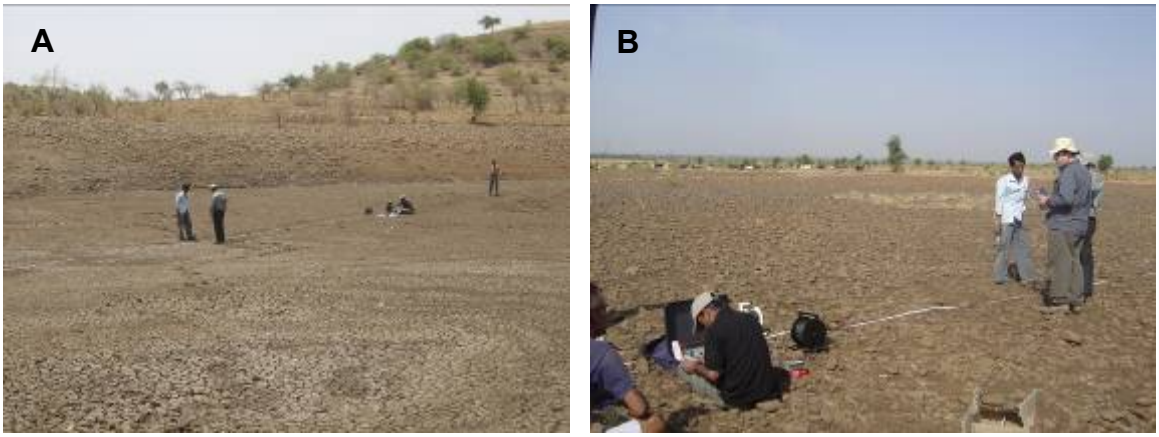

Figure 2.8: Resistivity setup: A. wide view of resistivity survey within the reservoir of the WHS (survey point #3), B. resistivity on the ridge

The geophysical surveys were conducted as vertical electrical soundings which assumes that the subsurface is composed of laterally homogeneous horizontal layers and involves increasing the spacing between electrodes to profile deeper levels of the subsurface (Singhal, 1999). The two most common electrode configurations are the Wenner and the Schlumberger arrays. The Schlumberger array was used in this study because it requires less space and time to complete than the Wenner array (Reynolds, 1997). The Schlumberger array is also easier to complete manually as only the current electrodes need to be moved for deeper profiles, whereas the spacing between all electrodes must be maintained at a constant in a Wenner array.

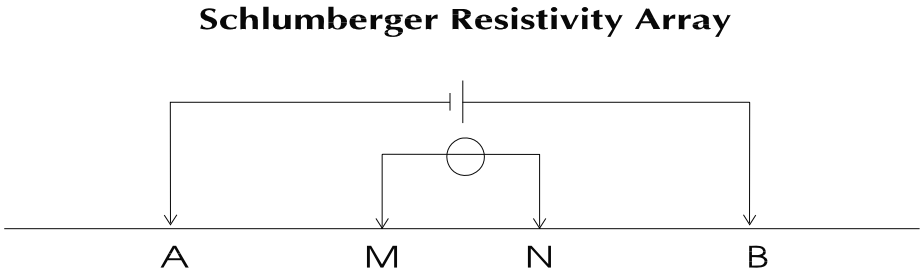

Figure 2.9: Schematic diagram of a Schlumberger array (Cooper, 2000)

A resistivity measurement involves the use of four electrodes as seen in Figure 2.9: electrodes A and B (current electrodes) inject current into the ground, while the potential electrodes, M and N, register the average voltage drop due to the resistance of the subsurface (Singhal, 1999). One half of the distance between the current electrodes is approximately equal to the effective depth of current penetration and this distance is changed to obtain data at different depths.

A resistivity measurement at a given depth is not a true resistivity of the material but an apparent resistivity which is an average of the effects of all the layers from the investigation depth to the surface (Singhal, 1999). Interpretations from the resistivity can be made qualitatively through the analysis of the curve shape or comparison with master curves or quantitatively through computer modeling (Reynolds, 1997).

Resistivity surveys were performed at six locations, as shown in Figure 2.10. Due to a shortage of GPS receivers, only 5 survey locations and elevations were recorded. Although only the surveys at those 5 locations were analyzed in detail here, the fifth point generally agrees with the geologic trend of the area identified by the other resistivity survey locations.

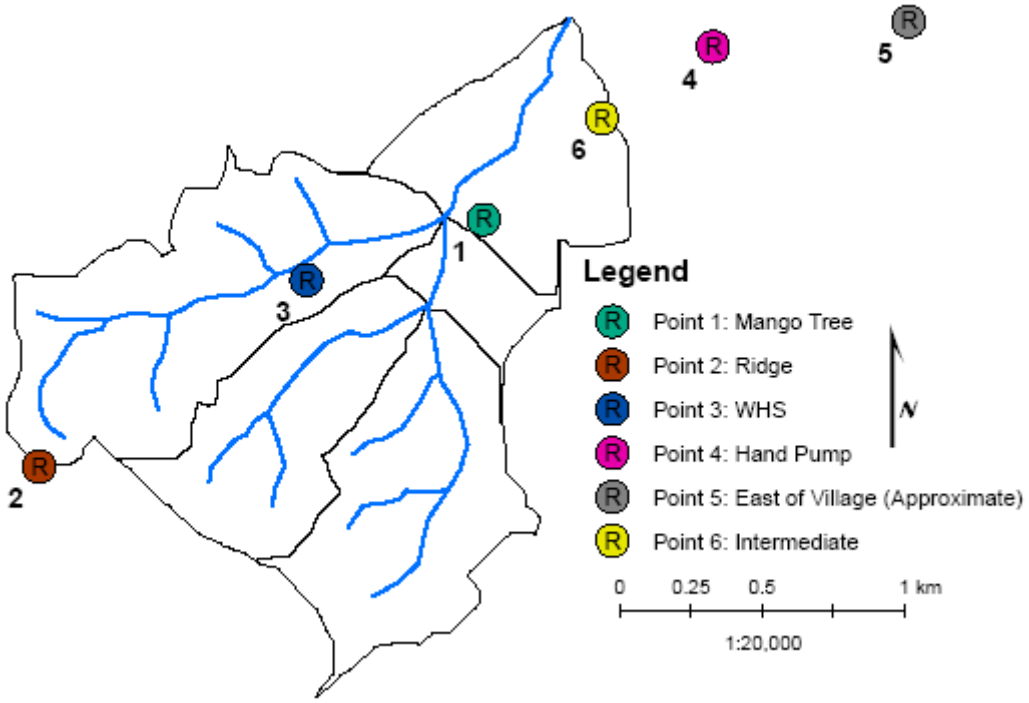

Figure 2.10: Locations of resistivity logs (point 5 is an approximate location because a GPS was not available)

Initial interpretations of the resistivity data were formulated using the conceptual model of alternating columnar and massive basalt characters. These interpretations were tested using forward and inverse modeling to determine the level of detail that could be extracted from the raw data. For a full explanation of the resistivity modeling process, see Appendix B. Given the sensitivity of the resistivity data limited information about resistivity variations with depth could be obtained. The interpretation that was drawn from the data is that resistivity increases with depth, the weathered zone thickness increases in correlation with distance from the ridge, and a sense of the basalt character which directly underlies the weathered zone was determined. The lithology of the basalt under the weathered zone is consistent with the conceptual model of the geology as

defined by field observations. These interpretations are given in Figure 2.11; note that the actual thickness of the underlying lithology is unknown.

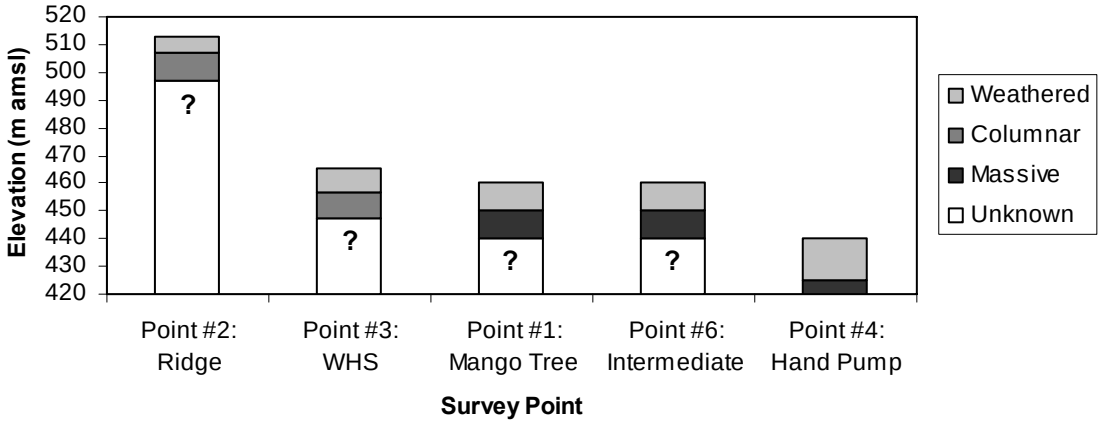

Figure 2.11: Overall interpretation of resistivity surveys

2.3.3 GEOLOGICAL INTERPRETATION

The synthesis of all the data relied heavily on direct observations from field mapping supported by the resistivity data and historical information from the Irrigation Department (Susner Irrigation Department, 1987). Areas of similar basalt character, excluding weathered, were grouped together and outlined along lines of equal elevation assuming the basalt flow contacts are generally horizontal, as suggested by Kulkarni (2000). This process, supported by field observations and by evidence of general trends from the resistivity models, yielded 3 packages of columnar overlapping massive basalts, representing 3 distinct flow events (flow 4-2) as seen in Figure 2.12 and Figure 2.13.

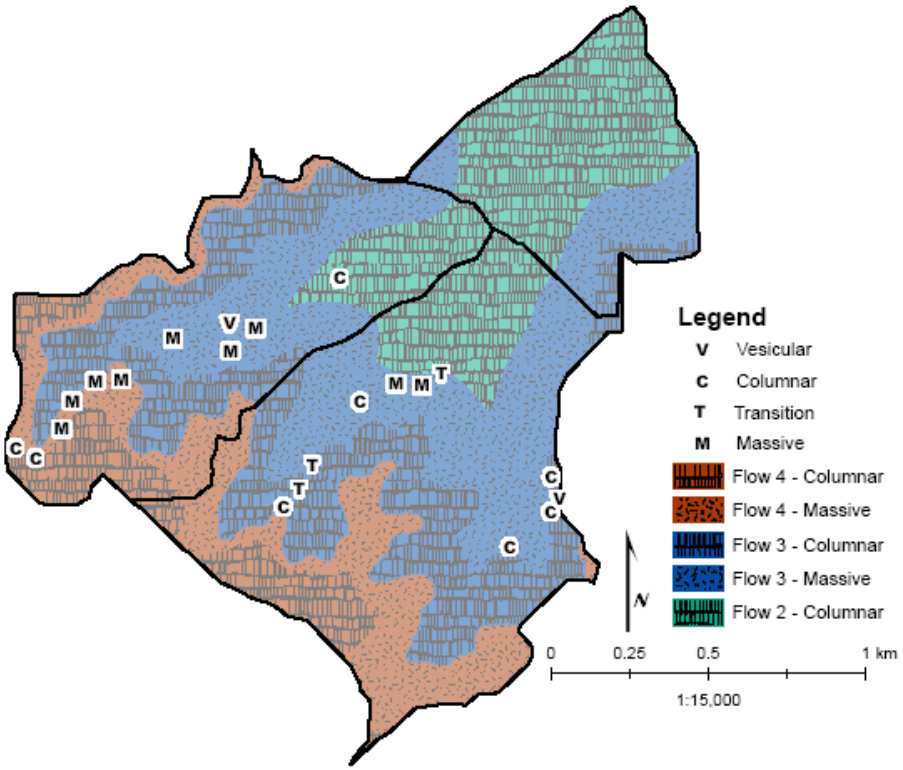

Figure 2.12: Geologic interpretation based on field mapping

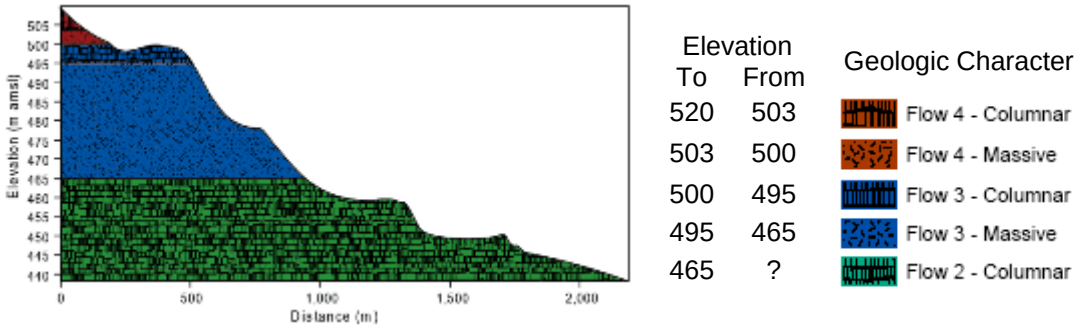

Figure 2.13: Cross section of lithologic interpretation based on field mapping (15x vertical exaggeration)

The resistivity surveys suggest that below the lowest columnar basalt there exists a layer of massive basalt. Downstream of the WHS in basin 1 (Figure 2.3) classification of basalt character was not possible because solid rock was obscured by a thick blanket of weathered basalt, thus the lower massive layer was not seen in the field. The lower limit

of the columnar basalt of flow 2 was chosen to coincide with the 460 contour because this boundary would result in similar thicknesses of all columnar layers.

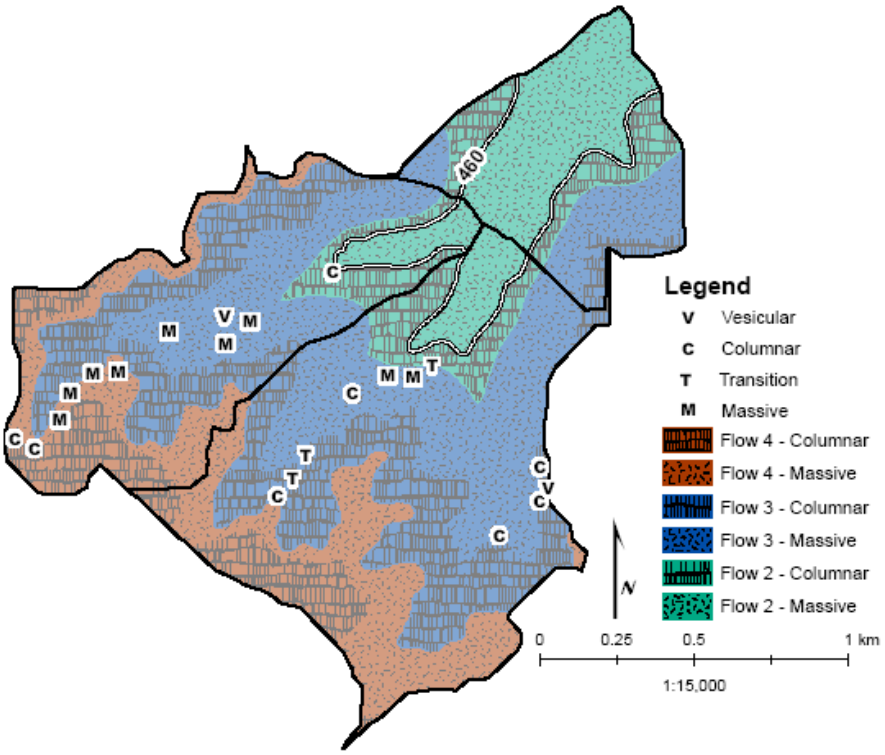

Figure 2.14: Geologic interpretation based on field mapping and resistivity modeling

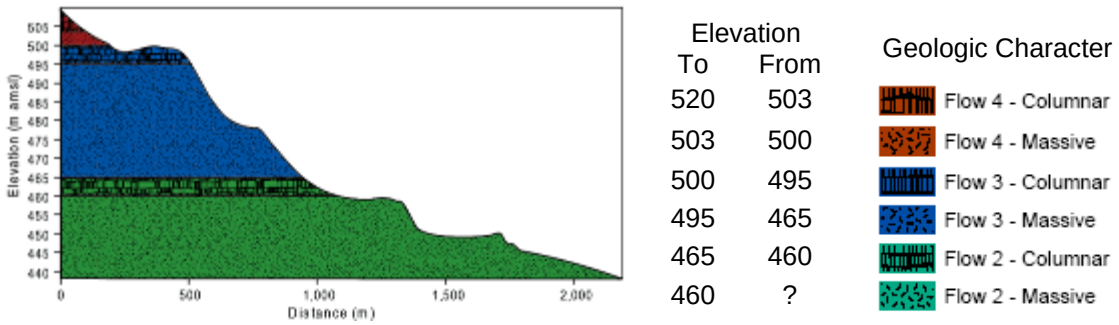

Figure 2.15: Cross section of lithologic interpretation based on field mapping and resistivity modeling (15x vertical exaggeration)

A report by the Irrigation Department of the Government of Madhya Pradesh suggests there is a flow below these layers (called flow 1 in this paper) with an upper boundary

along the 440 m contour which consists only of massive basalt (1987). A complete geologic map of the Salri watershed is presented in Figure 2.18.

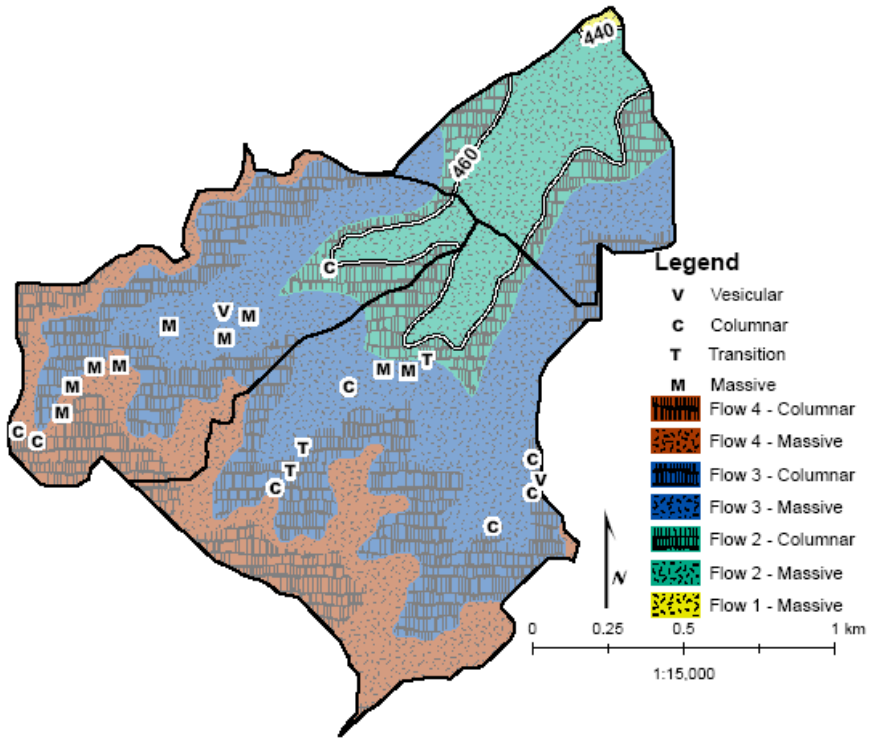

Figure 2.16: Geologic interpretation based on field mapping, resistivity modeling, and government paper

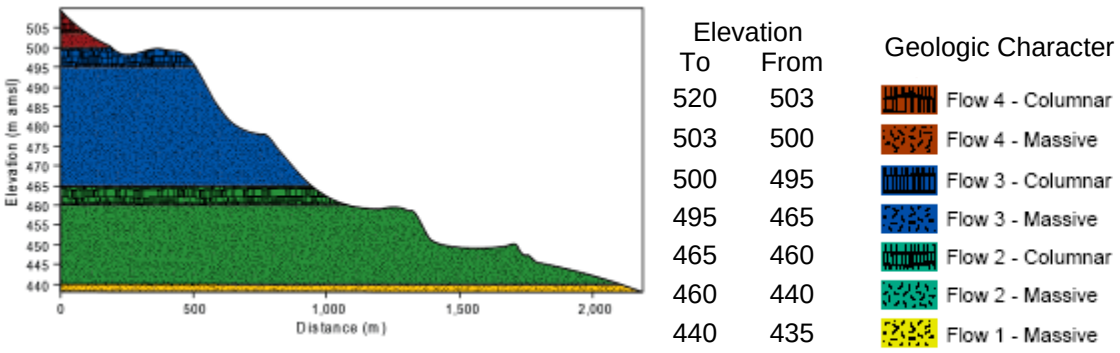

Figure 2.17: Cross section of lithologic interpretation based on field mapping, resistivity modeling, and government paper (15x vertical exaggeration)

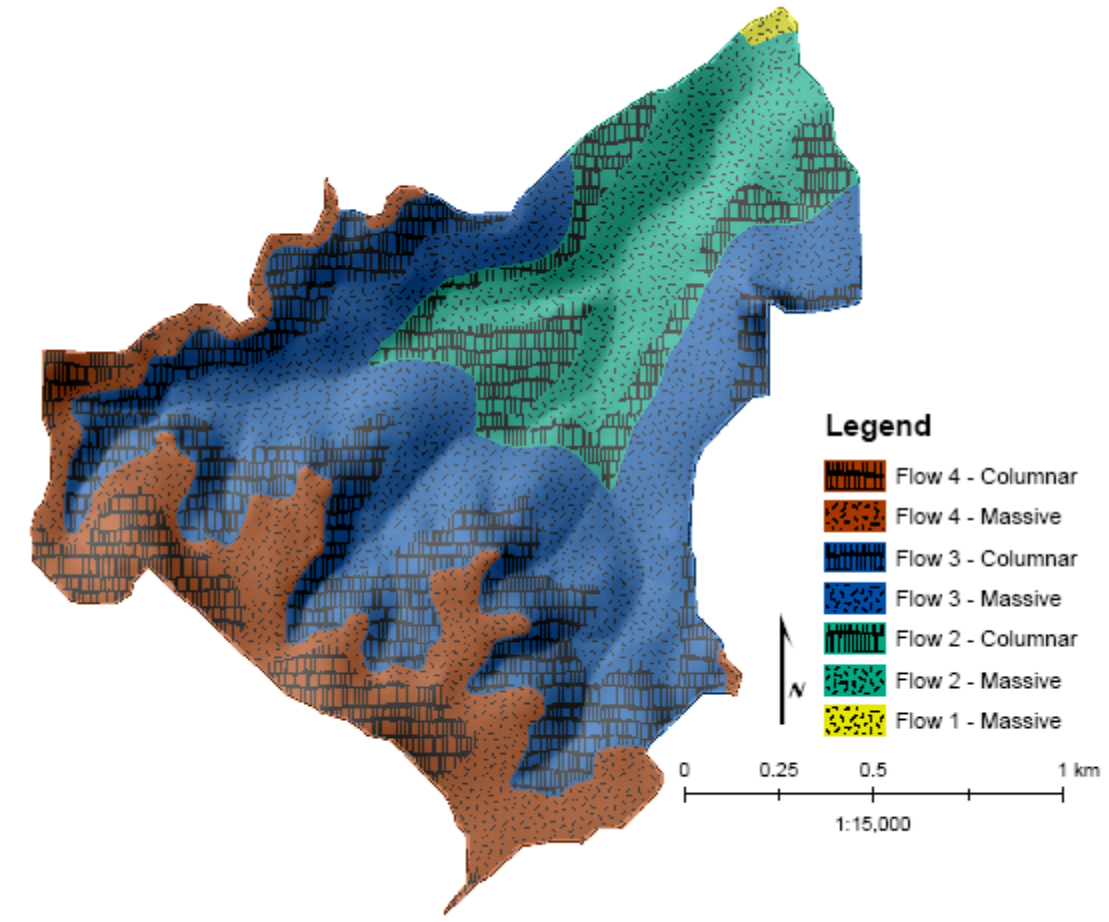

.

Figure 2.18: Geologic map of the Salri watershed

2.4 Aquifer Formation of the Deccan Traps

Productive aquifers in the Malwa Plateau occur in one of two situations: (1) in the near surface weathered zone ("shallow aquifer") (Gore, 1998; Kulkarni, 1994; Macdonald, 1995; Narasimhan, 2006) or (2) at the boundary of vesicular transitioning into compact basalt within a single flow due to a decrease in overall permeability (Kulkarni, 1997, 2000) . A third aquifer type may include fracture zones in the basalt, which could lead to enhanced transmission of water but probably lacks significant storage capacity.

2.4.1 Aquifer Formation of the Salri Watershed

Aquifers within the Salri watershed exist as shallow aquifers in the weathered zone and in some form at depth. As stated previously, the basalts of the Malwa plateau exhibit little or no vesicular portion of lava flows, hence the deeper aquifers beneath the weathered, shallow aquifer do not exist in the same sense as in other areas. A hypothesis on the formation of semiconfined aquifers is discussed below.

The unconfined shallow aquifer (type 1) is tapped by numerous hand dug wells and according to anecdotal evidence is recharged directly by the WHS. According to the villagers, soon after the WHS was constructed the water supply in the dug wells increased and many of the nearby downstream wells maintain water throughout the year.

It is hypothesized that the aquifers below the weathered aquifer are formed as a result of differing fracture orientation and density. The columnar basalt acts as a vertical conduit for water to percolate into the subsurface at which point the vertical movement is hindered by the massive basalt which acts as an aquiclude as a result of its fracturing tendencies. These semiconfined "boundary aquifers" (type 2) exist as a result of the differing fracture orientation and density between the columnar and massive basalts (Figure 2.19). Water in the columnar basalt will flow vertically and pool on top of the massive basalt as a result of the reduction in hydraulic conductivity of the lower unit. The water eventually chemically weathers the columnar basalt forming a mostly continuous unit with enhanced storage. The basis for the hypothesis of this type of formation was observed at a quarry outcrop south of the study area (Figure 2.19; Appendix A). A competing hypothesis for the origin of the formation, however, is that

the weathered zone at the top of a lava flow, formed at the surface through chemical weathering, is preserved even though it was subsequently covered by a more recent flow. In either case, it is expected that the hydraulic behavior of the formation would be similar. These formations may also be recharged by the WHS, if directly or indirectly connected by fractures in the basalts, and may also act as a source of water to penetrating wells.

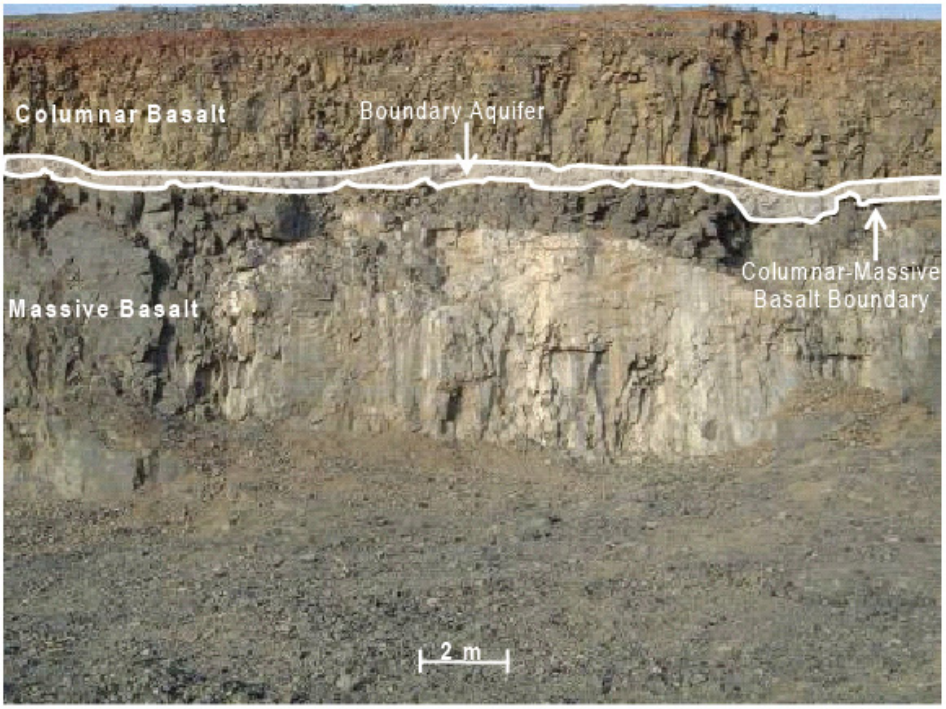

Figure 2.19: Outcrop illustrating the character of the geologic unit of the boundary aquifer

Through these observations in the field and using the completed geology from the previous section, two types of aquifers, shallow and boundary, were hypothesized. Shallow unconfined aquifers occur fairly continuously over the entire study area at the bottom of the weathered zone and thus could not be appropriately delineated in the hydrostratigraphic section. Approximate locations of boundary aquifer occurrences, which form as a result of a difference in porosity and permeability at the contact between

columnar and massive basalt, are indicated on Figure 2.20 and Figure 2.21 as blue lines. It is hypothesized that these aquifers are recharged through vertical fractures which cut across impermeable layers, i.e. massive basalt. Springs, areas of high fracture density and water producing potential, were not incorporated into the hydrostratigraphic interpretation because they are laterally discontinuous and thus affect only small areas, though they are important indicators of the hydrogeologic regime.

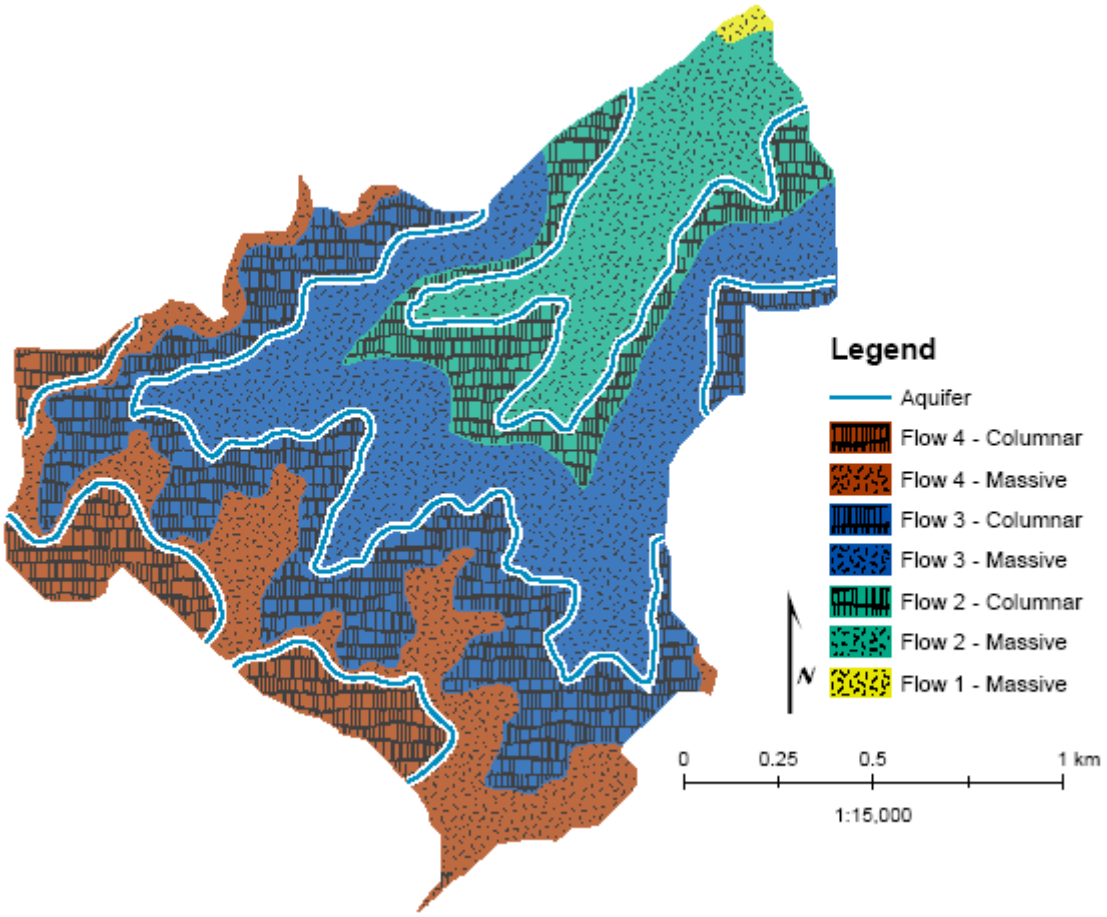

Figure 2.20: Positions of boundary aquifers

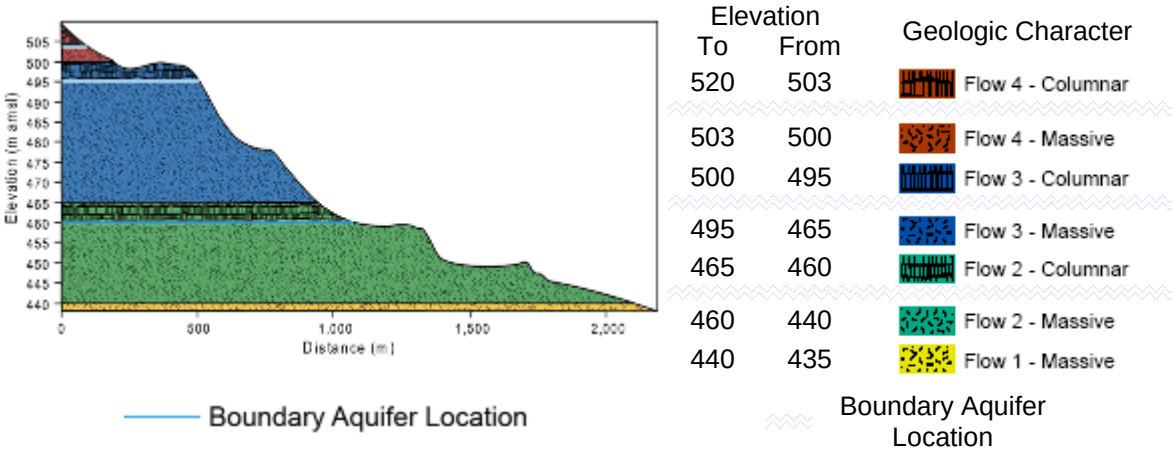

Figure 2.21: Hydrostratigraphic cross section of the Salri watershed (15x vertical exaggeration)

2.4.2 Future Work

The aquifer locations suggested in Figure 2.20 and Figure 2.21 are based entirely on the knowledge that differing fracture orientations control the flow of water and on possibly circumstantial observations made in the field (Figure 2.19). A more detailed study including observations of well logs, pumping tests, villager surveys, groundwater modeling, etc. is needed to confirm or refute the hydrostratigraphy suggested in this thesis. It is hoped that this document will provide a basis for future work on this matter.

CHAPTER 3: CONCEPTUAL MODEL OF THE SALRI WATERSHED

After establishing the foundation of the study through the geology and hydrogeology, the analytical formulation of a water balance can be discussed. The main method of examination of natural water supply is through the use of a water balance which accounts for the inputs, outputs, and storage of water in a specified volume (in this case a watershed) throughout a specified time period. The development of a realistic conceptual model helps describe and forecast basin behavior (Sutcliffe, 1986). The natural water balance calculation will be used as a comparison for the modeled infiltration from the WHS.

3.1 COMPREHENSIVE WATER BALANCE

The individual pieces of the water balance each has a role in the comprehensive water balance illustrated in Figure 3.1.

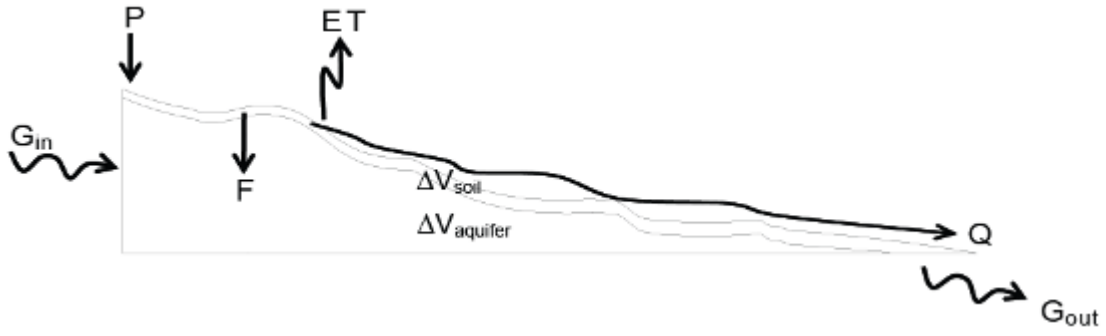

Figure 3.1: Conceptual model of the natural water balance

Where P is precipitation, ET is evapotranspiration, F is infiltration from soil storage, Q is surface runoff resulting from precipitation in excess of the maximum soil holding capacity, ΔV_{soil} is the change in volume per month of soil moisture storage, $\Delta V_{aquifer}$ is the change in volume of water per month stored in the aquifer, G_{in} is the

volume per month of groundwater entering the watershed, and G_{out} is the volume per month of groundwater leaving the watershed.

3.2 Surface Water Balance

The surface water balance is defined by atmospheric parameters, precipitation and evapotranspiration, and basin characteristic parameters, runoff and infiltration. The surface water balance was calculated using the Thornthwaite and Mather approach (Thornthwaite, 1957). This method is useful because it is designed to estimate evapotranspiration, runoff, and infiltration in areas lacking primary data as it only requires mean values of monthly or daily air temperature and precipitation in addition to an estimate of the water holding capacity of the soil. This technique is a soil water balance where the difference between the precipitation and potential evapotranspiration drives the calculations of actual evapotranspiration, soil moisture, runoff, and infiltration (Thornthwaite, 1957). For a full explanation on the application of the Thornthwaite-Mather technique to this study, see Appendix C.

Table 3.1: Thornthwaite-Mather soil moisture balance for 2007

Month	Precipitation (mm)	Evapotranspiration (mm)	Runoff (mm)	Infiltration (mm)
January	0.0	15.0	9.3	1.6
February	2.6	23.6	4.6	0.8
March	0.0	22.0	2.3	0.4
April	8.6	34.6	1.2	0.2
May	18.0	33.0	0.6	0.1
June	68.5	74.5	0.3	0.1
July	438.8	135.7	84.1	14.8
August	314.8	121.0	175.8	31.0
September	141.9	137.7	148.2	26.2
October	0.0	78.0	74.1	13.1
November	0.0	41.0	37.1	6.5
December	0.0	17.0	18.5	3.3

Precipitation

Rainfall is mostly restricted to the monsoonal months, June-October, and occurs as large storm events over short durations of time. The data used in the surface water balance was obtained from the Foundation for Ecological Security. Site-specific data collected over long periods of time, at least tens of years, is not available for the immediate study area. However, the India Water Portal (Arghyam, 2008), an online platform for water management, supplies meteorological data given over a 0.5° x 0.5° latitude-longitude grid for years the 1901-2002.

Evapotranspiration

Evapotranspiration represents the opposite of precipitation where liquid water is returned to the atmosphere (Thornthwaite, 1955). Direct estimates of evapotranspiration are difficult to obtain because it is challenging to measure. There are, however, a variety of methods of calculating evapotranspiration depending on the amount of atmospheric data available, such as solar radiation, wind speed, atmospheric pressure, and humidity. The Thorthwaite-Mather approach approximates evapotranspiration through monthly temperatures and an annual heat index. This value is then adjusted to account for the latitude of the study location through the use of a correction factor based on the monthly duration of sunlight.

Soil Moisture Storage, Runoff, and Infiltration

Water that is input through precipitation and not lost through evapotranspiration goes into soil storage. When the soil storage volume is saturated as a result of the precipitation rate exceeding the infiltration capacity, the excess water will either

contribute to surface runoff or infiltrate to groundwater. According to the Thornthwaite-Mather approach, for large basins half of the surplus is available to runoff and infiltration each month. The method states that values would be different for smaller basins, but gives no suggestion as to what the breakdown should be. As a result, the 50% release of water from surplus was used in this study. Of this available surplus it has been assumed that 85% will go to surface runoff and 15% will be infiltrated to the water table. The basis for this assumption is that runoff will occur at a much higher rate than infiltration. The actual proportion of runoff to infiltration probably changes throughout the year. Furthermore, the proportion of infiltration to direct surface runoff could vary significantly depending on the specific properties of a basin leading to a large potential range in yearly infiltration volume. For example, if infiltration were to range from 5-50% of the available monthly surplus, the overall basin infiltration could range from 85,000-850,000m^3. However, lacking streamflow or groundwater level data for calibration, a yearly assumption of 85% runoff to 15% infiltration was used. With this assumption, the Thorthwaite-Mather method estimates the annual infiltration to be 256,000m^3 over the 2.61km^2 study area.

3.3 Groundwater Processes

The groundwater balance is defined by surface water and groundwater interactions, such as recharge by infiltration and discharge at springs and streams, and groundwater flow in and out of the watershed. Each process is described in detail below.

GROUNDWATER DISCHARGE

Discharge represents the opposite in the water balance of infiltration. Discharge allows transfer of groundwater to surface water, usually in the form of baseflow to streams or flowing springs. Springs occur because of a variety of factors that are influenced by geology, hydrology, hydraulic, and even biology (Naik, 2002), but the main controls on spring formation are hydrogeologic in nature. Changes in the geologic character of the rock, for example decreases in porosity and permeability due to decreasing weathering or changes in fracture character, are the main cause for spring formation in the Deccan traps (Naik, 2002). These changes from high to low porosity and permeability lead to pooling of water on top of the less hydraulically conductive material; thus the water travels horizontally along the boundary until it discharges at the surface as a spring.

In the study area, springs form as a result of horizontal fractures or fracture zones, so springs tend to occur in the massive basalts which are characterized as having a relatively equal ratio of horizontal to vertical fractures, as opposed to columnar basalts which are dominated by vertical fractures. Springs in massive basalt are common in the Deccan traps and are usually seen as seepage zones rather than distinct springs (Naik, 2001, 2002). Local villagers identified springs in the study area and indicated that discharge occurs for approximately 3-4 months per year, from the end of monsoon, typically in September, through November or December. Two examples of such springs are shown in Figure 3.2. The locations of these springs are shown in Figure 3.3 which displays the geology of the area overlain by spring locations.

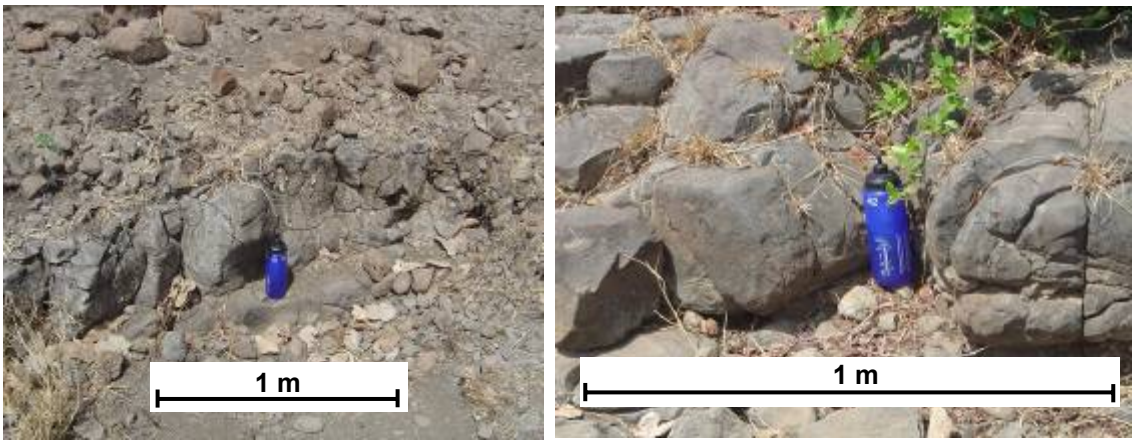

Figure 3.2: Examples of two different seeps in massive basalt, the bottle marks the location of water discharge

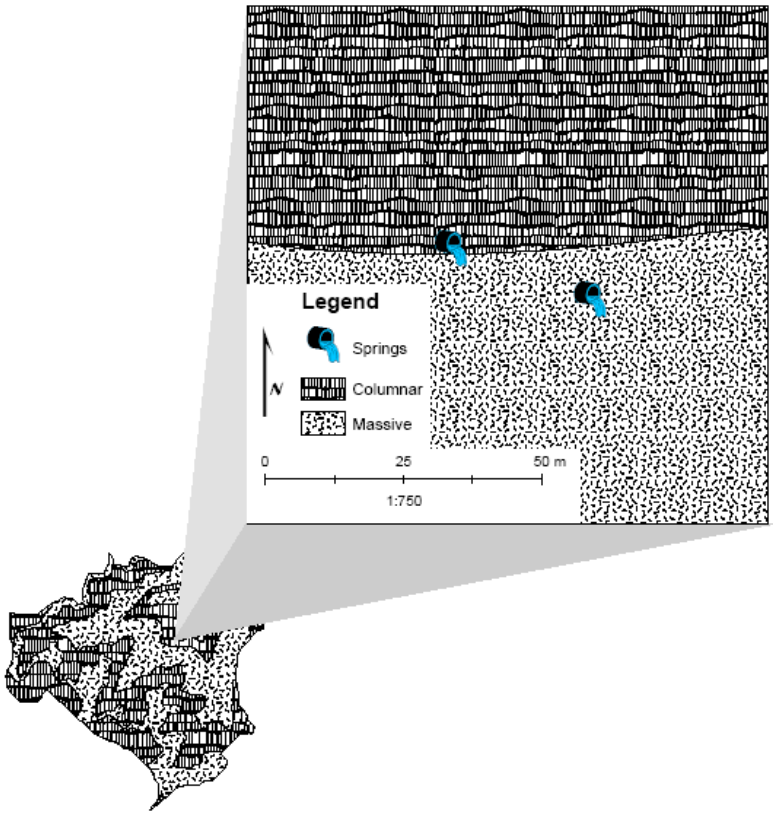

Figure 3.3: Locations of 2 villager-described springs and the relation to massive basalt

GROUNDWATER FLOW IN AND OUT

Groundwater occurs in weathered and fractured zones in both shallow unconfined aquifers and in deeper confined or semi-confined conditions (Kumar, 2005; Macdonald,

1995; Saraf, 1998). Over the watershed defined by the study area, the groundwater flow into the basin is expected to be zero because the inflow areas are bounded by a topographic divide and in hard-rock geology, groundwater divides typically coincide with topographic divides (Narasimhan, 2006). Groundwater maps created by the Irrigation Department in 1981 suggest that regional flow out of the area occurs generally in the north to northeast part of the basin (Madhya Pradesh Irrigation Department, 1981). Groundwater flow also probably follows general flow patterns over region scale, but these flow paths are out of the scope of this particular study.

GROUNDWATER STORAGE

The effective amount of subsurface water storage in aquifers is dependent on the hydrogeologic characteristics, storativity and transmissivity, of the aquifer material. Several studies have been conducted in the Deccan traps to estimate the water holding and transmission properties of the rock (Kulkarni, 1997, 2000, 1994; Kumar, 2005; Lalwani, 1995; Macdonald, 1995; Naik, 2001; Narula, 2001; Saha, 2006; Sutcliffe, 1981). The formation and degree of weathering and fracturing are the two most important factors which control groundwater movement and storage (Gore, 1998). Different basalt formations may have different primary porosities, crystallization, and fracture patterns depending on conditions such as cooling temperature. Degree of weathering refers to the amount of in situ chemical weathering that has degraded the basalt. The tops of individual lava flows were exposed to the elements for long periods of time (Jerram, 2005) allowing for percolating water to breakdown the basalt into clays. The degree of fracturing refers to the amount of discontinuities in the rock that formed

primarily as a result of cooling stresses. These fractures can either be vertical, as for the columnar basalts, or horizontal, as for the massive basalts.

Columnar and massive basalts, taken together as compact basalt, of which the majority of the study area is composed, has a porosity varying between 0.1% and 1% with decreasing porosity with increasing age (Saha, 2006) while the porosity of weathered or fractured basalt is approximately 10-17% (Singhal, 1999). The hydraulic conductivity of dense basalt ranges from 10^{-11}-10^{-8} m/s while fractured or weathered basalt ranges from 10^{-9}-10^{-2} m/s (Singhal, 1999). The specific yield of compact basalt varies from 0.01 to 0.03 (Kumar, 2006; Patel, 2007) while the specific yield of weathered crystalline rock varies from 0.1 to 0.2 (Singhal, 1999). From these values, it can be interpreted that the weathered basalt exhibits at least one order of magnitude greater porosity and specific yield than the compact basalt. The hydraulic conductivity of weathered basalt can be anywhere from 2 to 6 orders of magnitude greater than dense, unfractured basalt.

3.4 Summary

The surface water balance was calculated using the Thornthwaite-Mather method which estimates evapotranspiration, runoff, and infiltration through a soil moisture balance driven by atmospheric measurements. Through this balance an estimate of the total natural infiltration for 2007 was estimated to be 256000m^3 from multiplying the total yearly infiltration (98.1mm) by the total area of the watershed (2.61km^2). This natural

infiltration value will be used as a comparison with the artificial recharge estimation in the following chapter.

General descriptions of the components of the groundwater balance were also detailed. Overall, weathered basalt has a greater capacity for storage of groundwater than dense basalt. Fractures in unweathered basalt contribute primarily to the transmission of groundwater.

CHAPTER 4: WATER HARVESTING STRUCTURE MODELING

The goal of this chapter is to characterize the amount of infiltration contributed by water harvesting structures. In order to accomplish this task, the WHS was surveyed to obtain a representation of the storage characteristics. An analytical model of a water balance over the WHS was then formulated and numerically solved to estimate the parameters involved in the loss of water retained in the structure through time.

4.1 WATER HARVESTING STRUCTURE INVESTIGATION

The surface storage in the basin is represented by the volume of water held in the reservoir of the WHS. The volume of the water harvesting structure was estimated based on topographic surveys using the Thales Promark 3 GPS system. Two receivers with their corresponding antennas were used: one unit acted as the base station and was stationary during the survey while the other unit acted as the rover which collected the survey points. The base station was set on static survey mode with a recording interval of 2 seconds, thus the base station collected a continuous stream of satellite position data every 2 seconds. In order to record specific data points to define the WHS, the rover was set to stop and go survey mode with a recording interval of 2 seconds and an occupation time of 1 minute on each station. The external antennas and the use of a base station result in less spatial error of the logged points, as compared to the usage of a single handheld GPS receiver. The accuracy associated with the use of the external antennas is less than one centimeter while the accuracy of the GPS without external antennas is less than one meter according to the manufacturer ("ProMark3 Reference Manual," 2005). The satellite positions collected by the base station are compared with those of the rover

and position differences (vectors) are calculated to determine the relative position of each point to the stationary reference point ("ProMark3 Reference Manual," 2005).

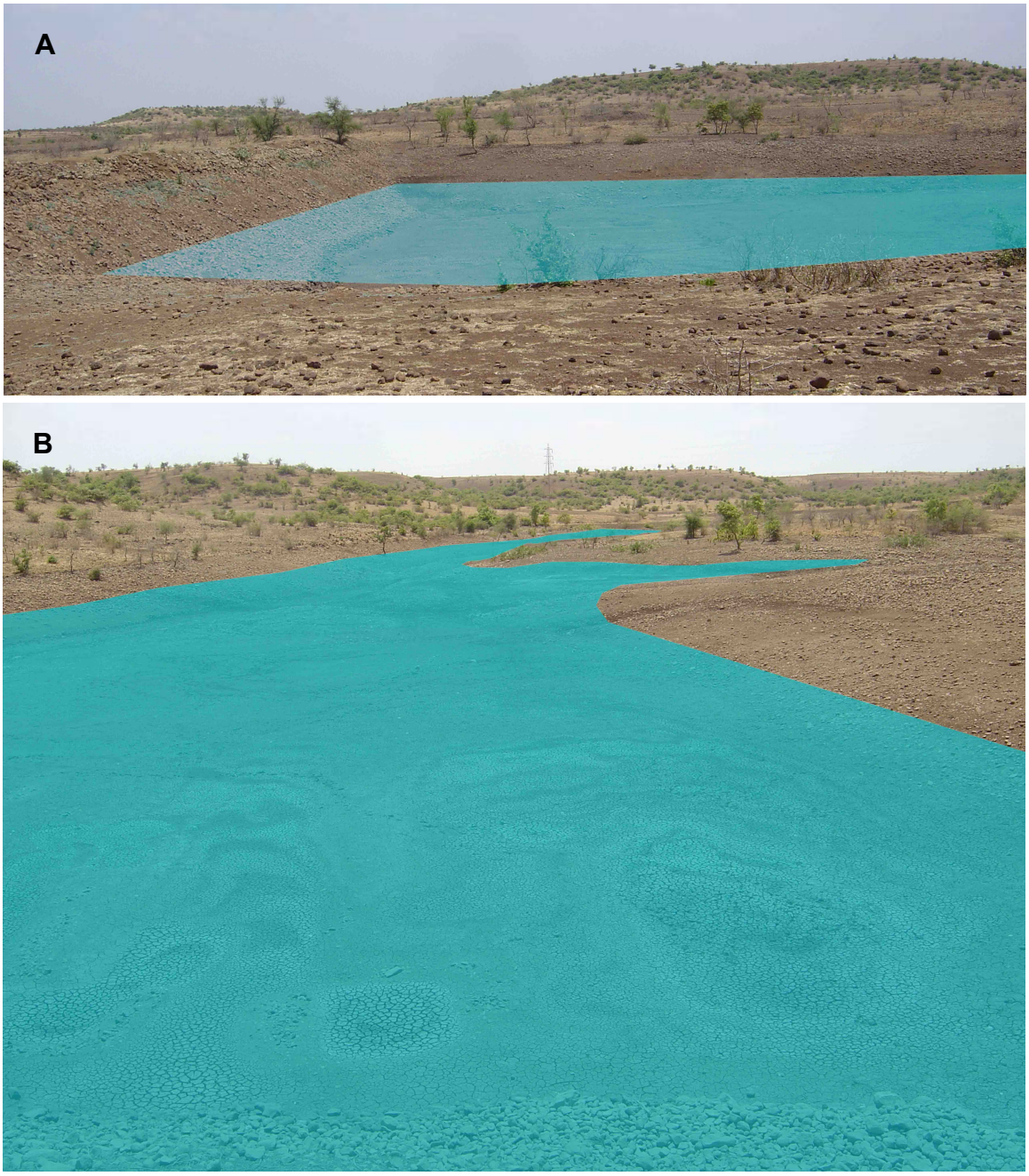

Figure 4.1: WHS reservoir (hypothetical water level shaded) A. side view, B. upstream view from retaining structure

Figure 4.2: Thales GPS survey setup

Surveying was completed over three days; however, technical problems with the base station resulted in unrecoverable data points on the second day. Therefore only the data from two days of surveying were used. The first day, May 6, 2007, two transect lines covering the top and bottom of the dam structure were recorded and on the third day, May 10, 2007, the area upstream of the structure was surveyed.

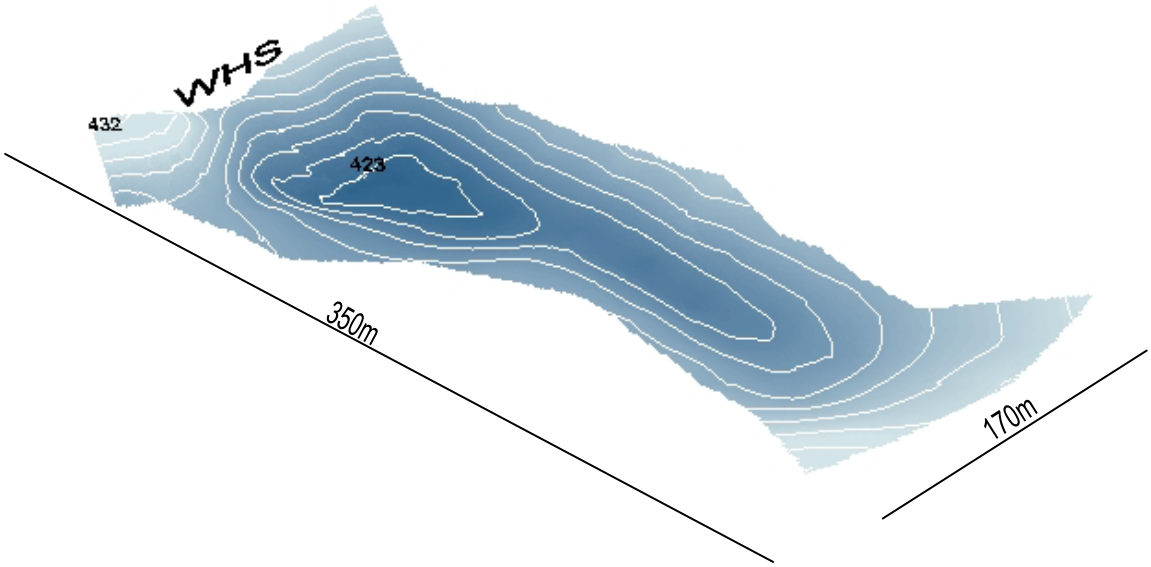

Figure 4.3: ArcScene visualization of the WHS (1meter contour interval)

The volume of water stored at any given elevation can be calculated using the surface volume tool in ArcScene. The only input needed is the elevation to which the volume should be calculated, the reference plane, which represents the stage of the water in the WHS measured in meters above mean sea level (m amsl). Since the lowest elevation of the WHS is 422.4m, any reference plane would need to be above this elevation. An example use of the tool is presented in Figure 4.4 where the reference plane is 430m, notice the result of the tool is in the calculation dialog.

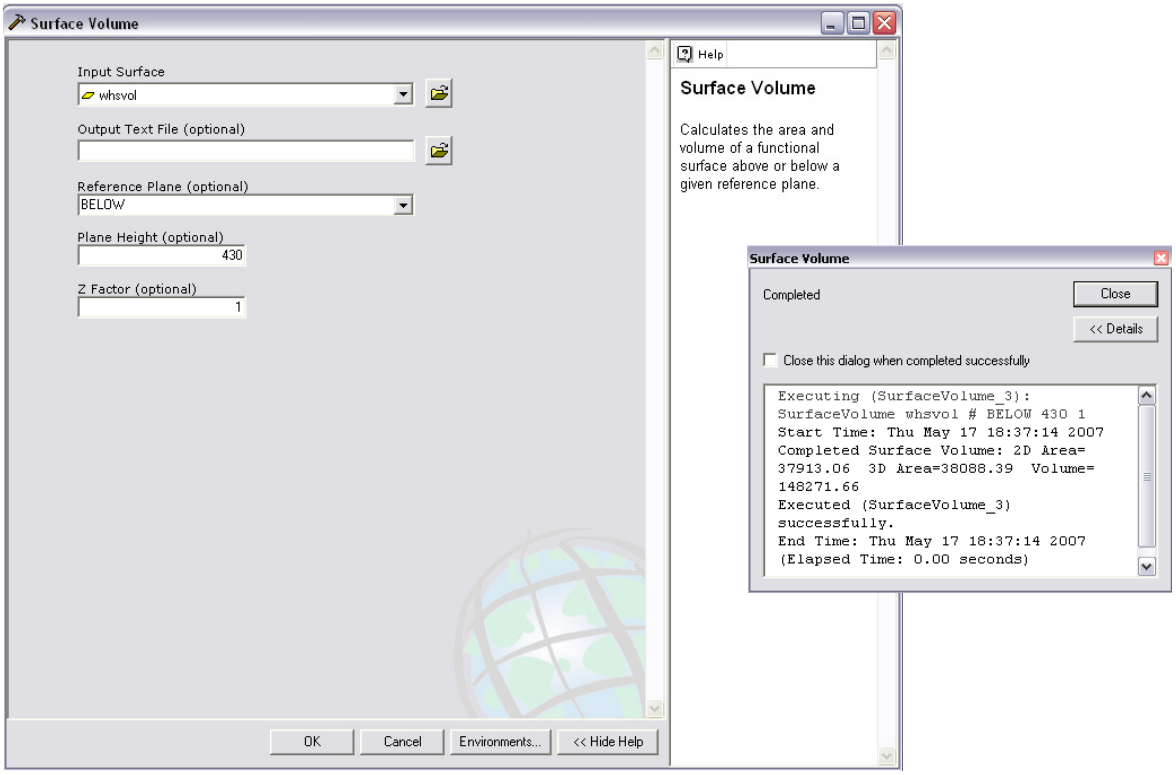

Figure 4.4: ArcScene tool for calculating the volume of water stored in the WHS

A key point to note is that the input surface needs to be in Universal Transverse Mercator (UTM) coordinates and the reference plane height in meters, thus the resulting volume will be in cubic meters (in our example the volume is 148271.66m^3). If access to ArcScene is not possible, a rough estimate of the volume of water stored can be obtained using Equation 4.1 given the stage of the WHS and setting the lowest elevation in the structure, 422.4m amsl, as the datum.

$$V_{WHS} = \begin{cases} 1695.5h^2 - 251.99h + 4.5707; & h \le 2 \\ -222.82h^3 + 6090.2h^2 - 16222h + 17106; & h > 2 \end{cases} \quad R^2 = 1 \qquad (4.1)$$

where V_{WHS} is the volume of water stored in the WHS (m^3) and h is the stage of the water in the WHS (m).

4.2 Pressure Transducer Data

A pressure transducer was installed in the WHS to record the change in level of surface water stored after the WHS was filled during the monsoon season. The transducer recorded pressure readings every 30 minutes from September 2, 2007 to December 14, 2007. Data were missing from September 23 to October 12 due to a transducer malfunction. The transducer recorded the total pressure exerted on the device, meaning the pressure of the water and the barometric pressure of the atmosphere.

In order to obtain the stage of water in the WHS, the effect of the barometric pressure needed to be removed from the data. Since barometric pressure data were not available for the immediate area, the data were corrected in two ways. Daily fluctuations were smoothed out using a moving average and regional pressure variations were removed by subtracting off barometric pressures obtained from surrounding areas.

The data were refined by using a central moving average of 24 hours. The window of 24 hours was chosen because barometric pressure fluctuates diurnally as a result of atmospheric tides, similar to oceanic tides; therefore, averaging over 24 hours should reduce if not eliminate the daily barometric effect.

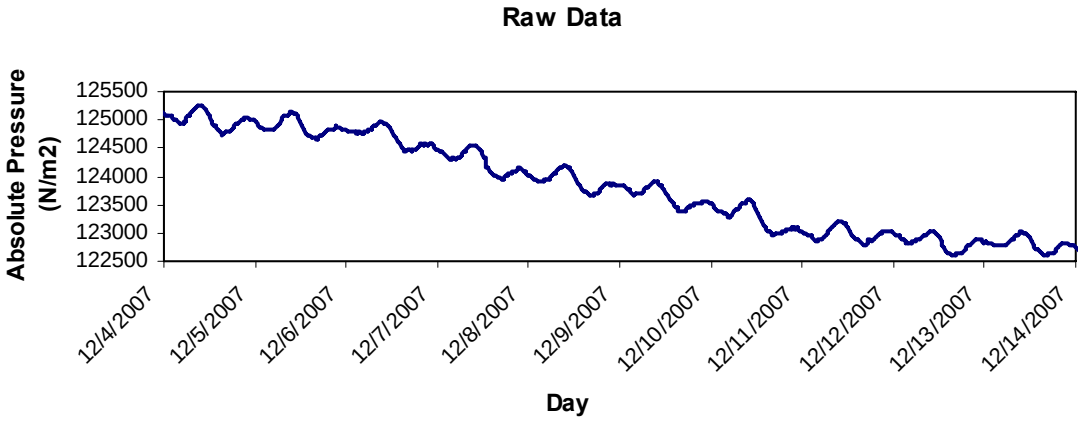

Figure 4.5: A portion of uncorrected pressure data collected from the WHS to illustrate diurnal variations

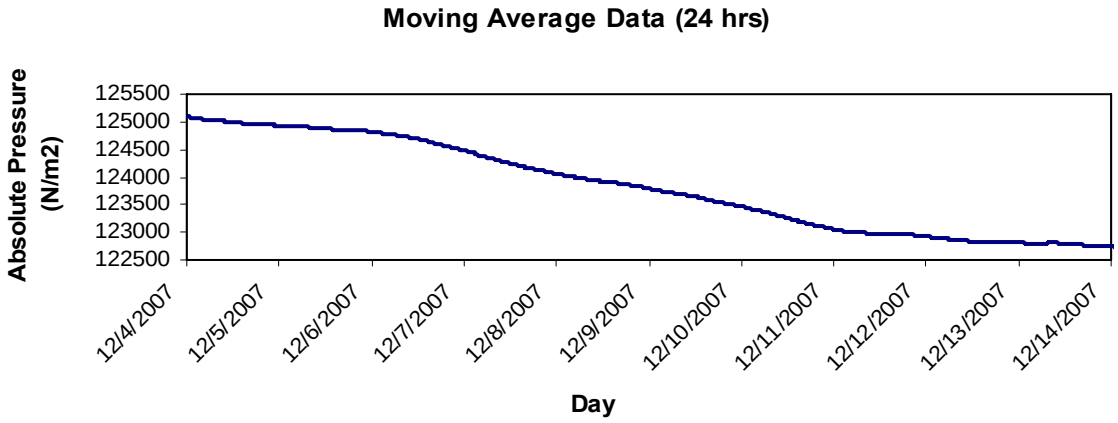

Figure 4.6: A portion of corrected pressure data collected from the WHS to illustrate removal of diurnal variations

To account for the change in barometric pressure associated with weather systems moving through the area, daily barometric pressure readings were obtained from three surrounding cities (Indore, Bhopal, and Kota) because a station was not located at the field site (The Weather Underground, 2008).

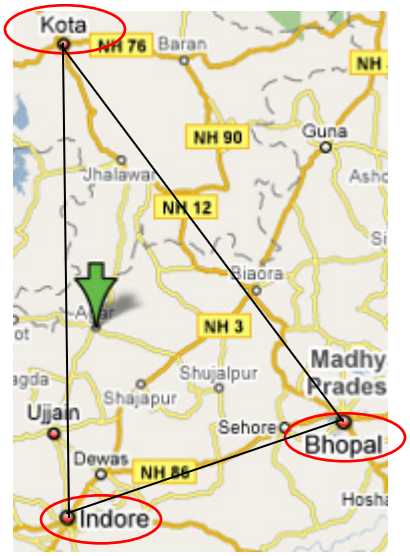

Figure 4.7: Locations of weather stations used for regional barometric pressure data (green arrow marks Agar, location of interest) (Google, 2008)

Barometric pressures were collected from October 12, 2007 through December 14, 2007 at 1 pm. The time of day was selected because it was determined by subtracting the moving average data from the original pressure data that the difference was zero, thus the effect of the daily fluctuation would be minimal at that time.

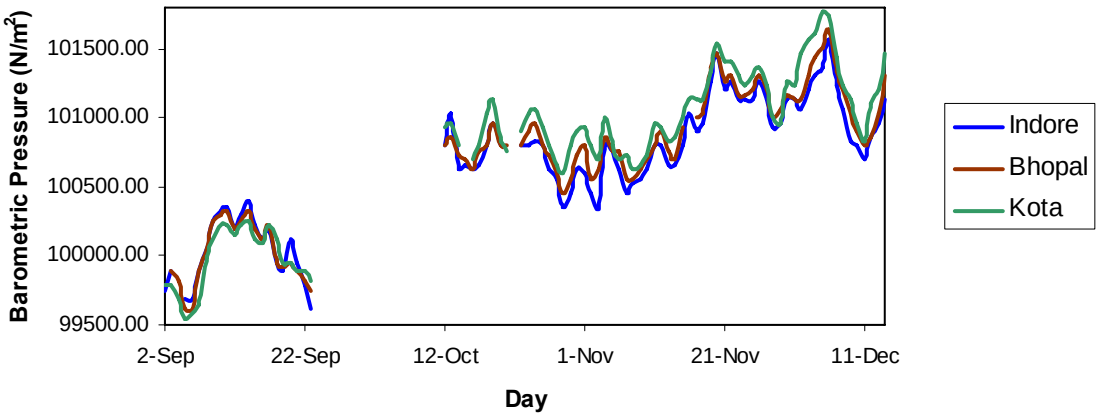

Figure 4.8: Barometric pressures at sampled weather stations (The Weather Underground, 2008)

The overall trends in the three locations were similar, but the variations were not identical at each station, for example one location did not always exhibit higher pressure than the

other two. Therefore, the data from the three stations were averaged using inverse distance weighting to estimate the barometric pressure at the study location. These daily values were then interpolated using Matlab to obtain half-hourly readings to match the time step of the pressure transducer data. Finally, the barometric pressure data were subtracted from the moving averaged pressure transducer data to obtain pressure readings representing only the pressure exerted by the water in the WHS. The pressure data were then converted to heights using the formula

$$h = \frac{P}{\rho g} \tag{4.2}$$

where h is the stage of water in the WHS in meters, P is the pressure reading from the pressure transducer in N/m^2, ρ is the density of water (1000 kg/m^3), and g is the acceleration due to gravity (9.8 m/s^2).

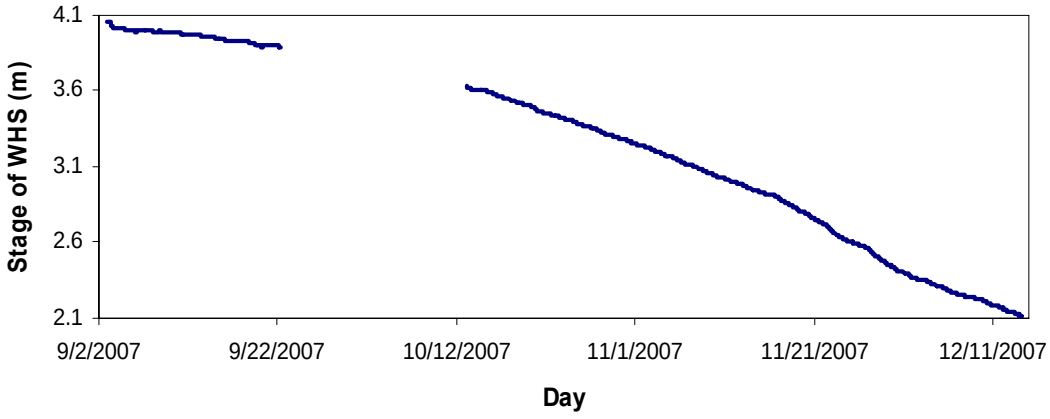

Figure 4.9: Stage of water in the WHS as recorded by pressure transducer

4.3 Water Harvesting Structure Infiltration Modeling

Water balances on man made water retention structures are usually estimated through the use of gauging stations on rivers upstream and downstream of the structure. Given that the study area lacks gauging stations, two strategies for estimating the volume contribution of infiltration from the WHS were formulated. The first assumes the lowering of the water level in the WHS is due to either evaporation from the surface or recharge to groundwater. The second involves the use of a generalized water balance for which unknown terms could be solved for numerically.

4.3.1 Minimum Infiltration Volume Estimate

The height of the water harvesting structure over the time period recorded by the pressure transducer (from September to December 2007) has a decreasing trend. As such a simple water balance can be equated by assuming negligible inflows during the study period:

$$\Delta \text{ Volume of WHS} = \text{Evaporation} + \text{Recharge} + \text{Use} \qquad (4.3)$$

Under this assumption, the water lost from storage in the WHS must have either evaporated, infiltrated, or been extracted for use by people or animals. Since the storage losses from the WHS were measured, if volume of water evaporated and extracted for use can be estimated, then the amount of infiltrated can be estimated. Note that if inflows to the WHS are considered, e.g., via surface runoff, direct precipitation, or groundwater flow, the infiltration estimate would increase accordingly thus making the infiltration determined here a minimum estimate.

The change in volume was estimated by subtracting the last height measurement from the first and using Equation 4.1 to convert the change in height to volume. Monthly total evaporation volumes were obtained from the weather station in Agar and used to estimate the total volume of water removed from the WHS through evaporation. A daily water need estimate for drinking and bathing purposes was obtained from a village survey conducted by the International Water Management Institute and the Sir Ratan Tata Trust (Tiwary, 2005). This estimate did not include irrigation; however, if the WHS surface storage volume is used for irrigation purposes, an estimate of the water drawn for this purpose should be incorporated. This daily value of $5.15\ {}^{m^3}\!/_{\text{person}}$ was multiplied by the number of people in the village (132) and scaled to the study period. To find the infiltration from the WHS, the evaporation over this period and the usage was subtracted from the change in volume. The infiltration estimated using this method over the study period is approximately $21{,}000 m^3$.

Table 4.1: Calculation of minimum recharge from WHS

Δ Volume of WHS (m^3)	Evaporation (m^3)	Use (m^3)	Recharge (m^3)
28872.42	7291.37	628.86	20952.19

This estimate considers only the outflows from the WHS and as such represents the minimum volume that could be estimated from September through December, 2007.

4.3.2 Water Balance Modeling

A simple water balance over the WHS was designed to better approximate the artificial recharge. The water balance inflows include baseflow from groundwater and surface runoff from the upstream basin which contributes directly to the WHS. The

outflows are evaporation from the surface of the WHS, use by villagers or animals, and recharge to the groundwater.

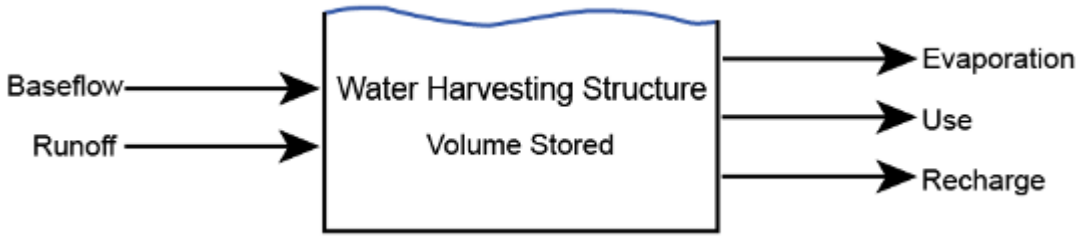

Figure 4.10: Conceptual model of the water harvesting structure water balance

WATER BALANCE DERIVATION

The purpose of this exercise is to estimate the volume of water lost via infiltration to the groundwater supply by matching a predicted stage of the water stored to the observed data collected from the pressure transducer. The water harvesting structure model is conceptualized as a group of interconnected tanks.

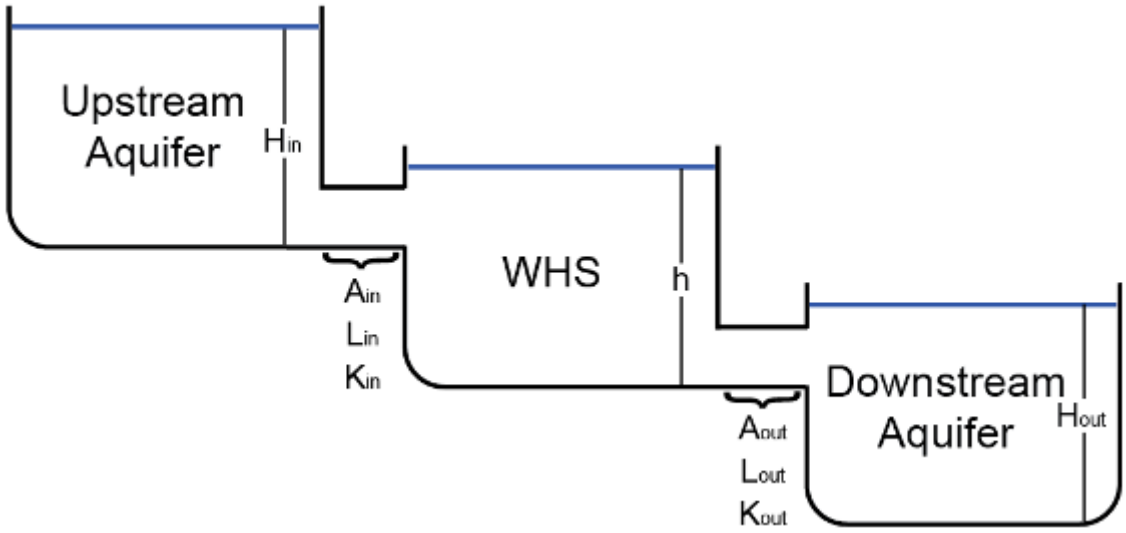

Figure 4.11: Conceptual model of the WHS as a group of interconnected tanks

Where H_{in} is the head in the upstream aquifer, h is the head in the WHS, H_{out} is the head in the downstream aquifer, A_{in} and A_{out} are the area of hypothetical flow tubes in and out of the WHS respectively, L_{in} and L_{out} are the length of hypothetical flow tubes in and out of the WHS respectively, and K_{in} and K_{out} are the hydraulic conductivities of the hypothetical flow tubes in and out of the WHS respectively. The datum of the water balance was defined as the bottom of the WHS. However, this datum was physically set as the elevation of the pressure transducer installed in the WHS to record the stage of the water. It was assumed that the pressure transducer was located at the bottom of the WHS at an elevation of 422.4m above mean sea level.

The analytical model describing the head in the WHS is defined using the water balance

$$dV/dt = Q_b + Q_r - Q_i - Q_e - Q_u \tag{4.4}$$

where dV/dt is the change in volume of the WHS through time, Q_b is the inflow into the WHS through baseflow, Q_r is the inflow from surface runoff, Q_i is the water lost through recharge, Q_e is the water removed by direct evaporation, and Q_u is the water taken out of the WHS for use by villagers or animals. Of these six parameters, only Q_r and Q_e could be calculated separately and entered directly into the water balance. All other parameters need to be estimated. Precipitation directly onto the WHS itself was neglected because the surface area of the WHS is much smaller than that of the total watershed. Therefore, any contribution from the direct precipitation would be insignificant compared with the other parameters.

Each term in the water balance is derived below

$$
\begin{aligned}
Q_b &= \frac{A_{in}K_{in}}{L_{in}}\left(H_{in}-h\right) \\
Q_r &= RA_{shed} \\
Q_i &= \frac{A_{out}K_{out}}{L_{out}}\left(h-H_{out}\right) \\
Q_e &= A_{WHS}\,{dh_{evap}}/{dt} \\
Q_u &= 0
\end{aligned}
\tag{4.5}
$$

where R is storm runoff, A_{shed} is the area of the watershed that directly contributes to the WHS, ${dh_{evap}}/{dt}$ is the change in height of water lost by evaporation per unit change in time, A_{WHS} is the surface area of the WHS, and Q_u is removed from this formulation. As a result of a lack of data, it was not possible to separate the effect of the Q_u term from the other estimated terms, Q_b or Q_i, thus the Q_u term was removed to reduce the number of parameters. H_{in} was approximated using an exponential decay curve to simulate the declining head in the aquifer with a constant of five to keep the head in the aquifer above the stage of the WHS.

$$H_{in} = \alpha e^{-\beta \Delta t} + 5 \tag{4.6}$$

The volume of the water stored was approximated as the average surface area of the water multiplied by the height of the water $\left(V = \bar{A}h\right)$ at each time step. The average surface area was defined as

$$\bar{A} = \frac{\int_0^h A\,dz}{\int_0^h dz} = {V}/{h} \tag{4.7}$$

Thus the change in volume per unit change in time $\left(dV/dt\right)$ can be expressed as

$$\frac{d\overline{A}h}{dt} \tag{4.8}$$

Differentiating the change in volume using the product rule yields

$$h\frac{d\overline{A}}{dt}+\overline{A}\frac{dh}{dt} \tag{4.9}$$

Conceptually, WHS volume is estimated by transforming the actual reservoir volume to a reservoir with vertical sides of equivalent volume. Thus the change in volume at a particular time (ΔV) is calculated through the use of addition of the volumes represented by $hd\overline{A}$ and $\overline{A}dh$ as seen in Figure 4.12.

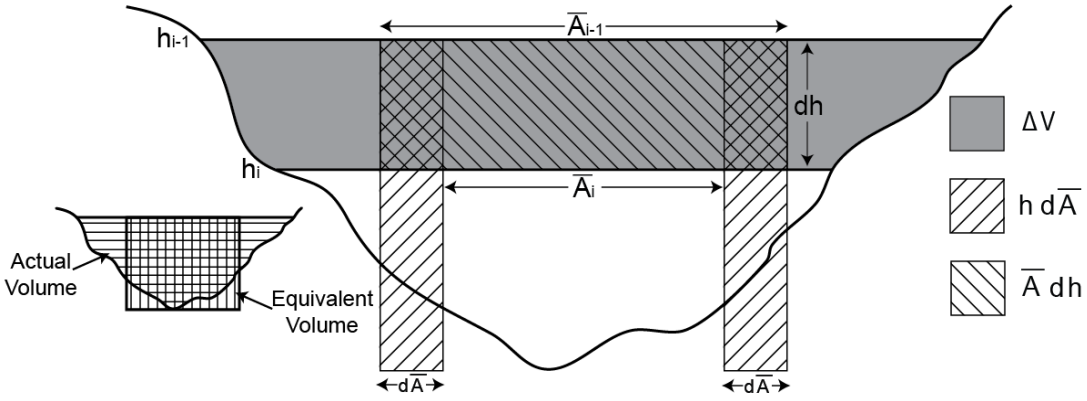

Figure 4.12: Conceptualization of the volume calculation using $\overline{A}$

Entering in the derived terms into the water balance gives

$$h\frac{d\overline{A}}{dt}+\overline{A}\frac{dh}{dt}=\frac{A_{in}K_{in}}{L_{in}}\left(H_{in}-h\right)+RA_{shed}-\frac{A_{out}K_{out}}{L_{out}}\left(h-H_{out}\right)-A_{WHS}\,dh_{evap}/dt \tag{4.10}$$

Since the attributes of the hypothetical flow tubes in and out of the WHS are unknown variables, constants are substituted to give

$$h\frac{d\overline{A}}{dt}+\overline{A}\frac{dh}{dt}=C_{in}\left(H_{in}-h\right)+RA_{shed}-C_{out}\left(h-H_{out}\right)-A_{WHS}\,{dh_{evap}}/{dt} \quad (4.11)$$

The factoring $\frac{dh}{dt}$ out of the volume term gives

$$h\frac{d\overline{A}}{dh}\frac{dh}{dt}+\overline{A}\frac{dh}{dt}=C_{in}\left(H_{in}-h\right)+RA_{shed}-C_{out}\left(h-H_{out}\right)-A_{WHS}\,{dh_{evap}}/{dt} \quad (4.12)$$

Solving for $\frac{dh}{dt}$

$$\left(h\frac{d\overline{A}}{dh}+\overline{A}\right)\frac{dh}{dt}=C_{in}\left(H_{in}-h\right)+RA_{shed}-C_{out}\left(h-H_{out}\right)-A_{WHS}\,{dh_{evap}}/{dt}$$

$$\frac{dh}{dt}=\frac{C_{in}\left(H_{in}-h\right)}{\left(h\frac{d\overline{A}}{dh}+\overline{A}\right)}+\frac{RA_{shed}}{\left(h\frac{d\overline{A}}{dh}+\overline{A}\right)}-\frac{C_{out}\left(h-H_{out}\right)}{\left(h\frac{d\overline{A}}{dh}+\overline{A}\right)}-\frac{A_{WHS}\,{dh_{evap}}/{dt}}{\left(h\frac{d\overline{A}}{dh}+\overline{A}\right)} \quad (4.13)$$

The final step is to discretize $\frac{dh}{dt}$ and solve for h_i

$$\frac{h_i-h_{i-1}}{\Delta t}=\frac{C_{in}\left(H_{in}-h_i\right)}{\left(h_i\frac{d\overline{A}}{dh}+\overline{A}\right)}+\frac{RA_{shed}}{\left(h_i\frac{d\overline{A}}{dh}+\overline{A}\right)}-\frac{C_{out}\left(h_i-H_{out}\right)}{\left(h_i\frac{d\overline{A}}{dh}+\overline{A}\right)}-\frac{A_{WHS}\,{dh_{evap}}/{dt}}{\left(h_i\frac{d\overline{A}}{dh}+\overline{A}\right)}$$

$$h_i-h_{i-1}=\left(\frac{C_{in}\left(H_{in}-h_i\right)}{\left(h_i\frac{d\overline{A}}{dh}+\overline{A}\right)}+\frac{RA_{shed}}{\left(h_i\frac{d\overline{A}}{dh}+\overline{A}\right)}-\frac{C_{out}\left(h_i-H_{out}\right)}{\left(h_i\frac{d\overline{A}}{dh}+\overline{A}\right)}-\frac{A_{WHS}\,{dh_{evap}}/{dt}}{\left(h_i\frac{d\overline{A}}{dh}+\overline{A}\right)}\right)\Delta t \quad (4.14)$$

$$h_i=\left(\frac{C_{in}\left(H_{in}-h_i\right)}{\left(h_i\frac{d\overline{A}}{dh}+\overline{A}\right)}+\frac{RA_{shed}}{\left(h_i\frac{d\overline{A}}{dh}+\overline{A}\right)}-\frac{C_{out}\left(h_i-H_{out}\right)}{\left(h_i\frac{d\overline{A}}{dh}+\overline{A}\right)}-\frac{A_{WHS}\,{dh_{evap}}/{dt}}{\left(h_i\frac{d\overline{A}}{dh}+\overline{A}\right)}\right)\Delta t+h_{i-1}$$

This formula gives the predicted height of the free surface in the WHS which is compared to the observed free surface collected by the pressure transducer (see Appendix E).

The surface area of the WHS was described using a fitted equation derived from the ArcScene WHS volume visualization (see Appendix D). The average surface area of the WHS was obtained by dividing the volume of the WHS by the height and fitting a curve to those points. The storm runoff was assumed to be 50% of precipitation for a given time period. Direct evaporation was input using total monthly pan evaporation data obtained from a weather station in Agar.

The final equation in Equation Set 4.14 was programmed as a set of functions in Microsoft Excel using Visual Basic. The predicted stage of water in the WHS was fitted to the observed stage using the Solver tool in Excel (Appendix F) to estimate values for the five unknown parameters in the final equation (C_{in}, C_{out}, α, β, and H_{out}).

RESULTS

The predicted and observed stages are given in Figure 4.13.

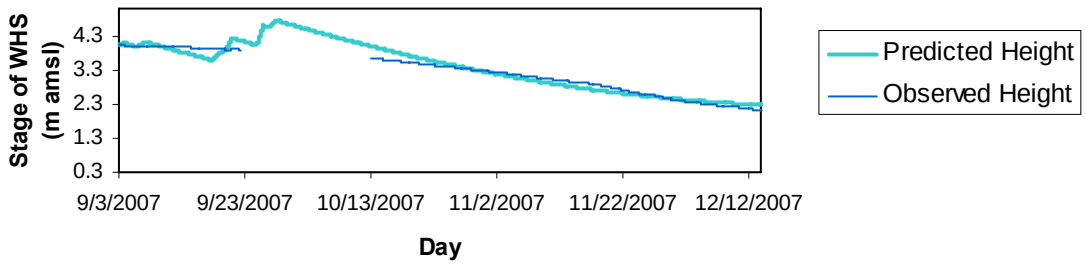

Figure 4.13: Predicted (modeled) and observed stage of the WHS

The fit of the curves was determined by minimizing the sum of square errors and fitting

the R^2 value close to one. R^2 was calculated as

$$1 - \frac{\text{Sum of Squared Errors}}{\text{Sum of Squared Means}} \tag{4.15}$$

The R^2 value was 0.94 and the sum of square errors was 77.8m^2, visually, the fit does not appear to be as good as the error terms suggest. This discrepancy might be a result of the lack of data points in late September and early October because this section of time is not being fit into the error approximation. The predicted data matches closer to the observed data where there are more data points.

Other calibration points that were checked in addition to minimizing error are the total recharge volume and the total baseflow volume. The minimum recharge volume was calculated by subtracting evaporation from the total change in volume stored in the WHS over the time period. The infiltration for the water balance method must be greater than this previously calculated minimum. In addition, the total baseflow into the WHS must not exceed the total annual precipitation. Both of these objectives were met in this solution.

The predicted curve appears to jump during September as a result of the runoff inflow term. September was the only month during the study time period where precipitation fell. Since the runoff term was calculated as 50% of the rainfall on a daily time step, the jumps are a result of rain falling on particular days.

The infiltration determined from this model from September 2, 2007 to December 31, 2007 is 97,000m^3. This value represents 38% of the total annual natural infiltration as calculated by the Thornthwaite- Mather approach for the entire watershed and thus does

not seem like a reasonable value. A better approximation may be possible through the implementation of a term that represents the overflow of the WHS.

SPILLWAY APPROXIMATION

A spillway was constructed on the WHS to allow for water in excess of the storage capacity to continue downstream without over flowing and eroding the retention structure itself. The actual height of the spillway is unknown as a result of data lost from GPS surveying, but it is assumed to be at the level of 4 meters above the lowest point in the structure because the transducer data appears to level off in early September around 4 meters.

In order to incorporate the spillway into the Visual Basic code, an if-then statement was added. This statement basically set the highest predicted elevation to be 4 meters. If the estimated predicted elevation as calculated using the final equation of Equation Set 4.14 was higher than 4 meters, the output height was set to 4 meters; otherwise, the predicted value was retained as the output.

The predicted and observed stages with the spillway at 4 meters are given in Figure 4.14.

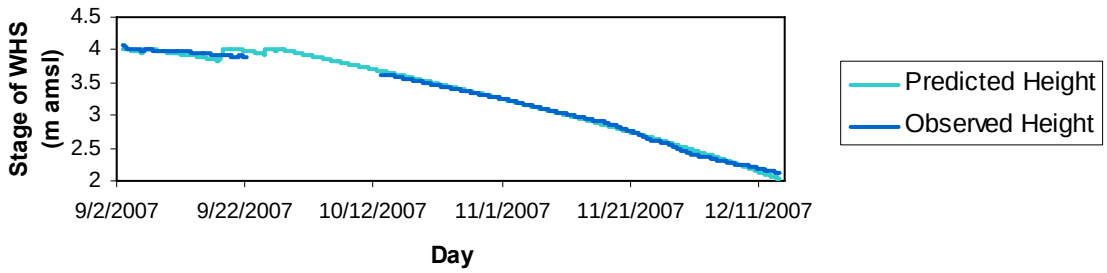

Figure 4.14: Predicted (modeled) and observed stage of the WHS with a spillway at 4 meters

The R^2 value of this approximation was 0.996 and the sum of squared errors was 5.92m^2. This model visually looks like a better fit than without the spillway. The same supplementary constraints of the recharge being greater than the minimum estimation and the baseflow being less than the annual precipitation used in the previous model are valid.

The infiltration determined from this model from September 2, 2007 to December 31, 2007 is 39,000m^3. This value represents 15% of the total annual natural infiltration as calculated by the Thornthwaite-Mather approach, which is a more reasonable value though still a significant contribution relative to infiltration over the entire basin.

Sensitivity Analysis

Each parameter value was varied up to 50% of the solved value in order to understand the sensitivity of the parameters. Figure 4.15 through Figure 4.19 presents the results of this analysis. Each figure presents a graph of the variation of the stage in the WHS given a 10% change in the parameter and a graph of the percent change in R^2 varying the parameter 5, 10, 25, and 50% of the original value. Note the vertical scale on the B portions of each figure is different depending on the parameter they are representing. For C_{in}, α, and β the maximum value on the scale is 0.5 while for parameters C_{out} and H_{out} the maximum value is 1.

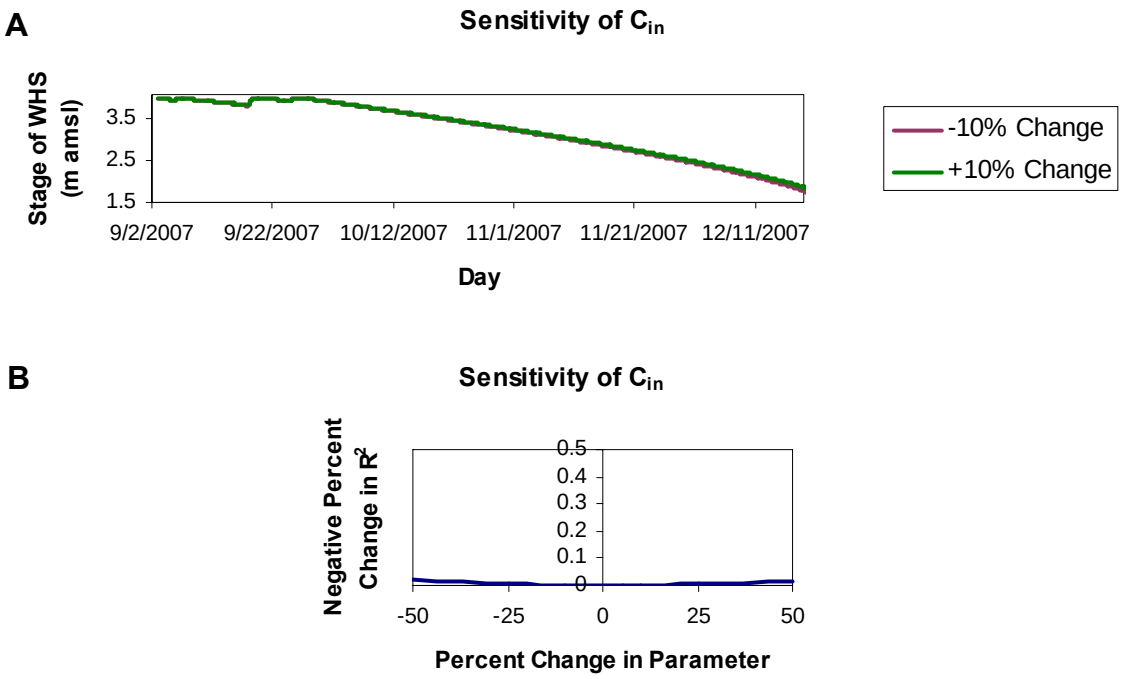

Figure 4.15: Sensitivity of C_{in}: A. difference in stage with 10% change in C_{in}, B. percent change in R^2

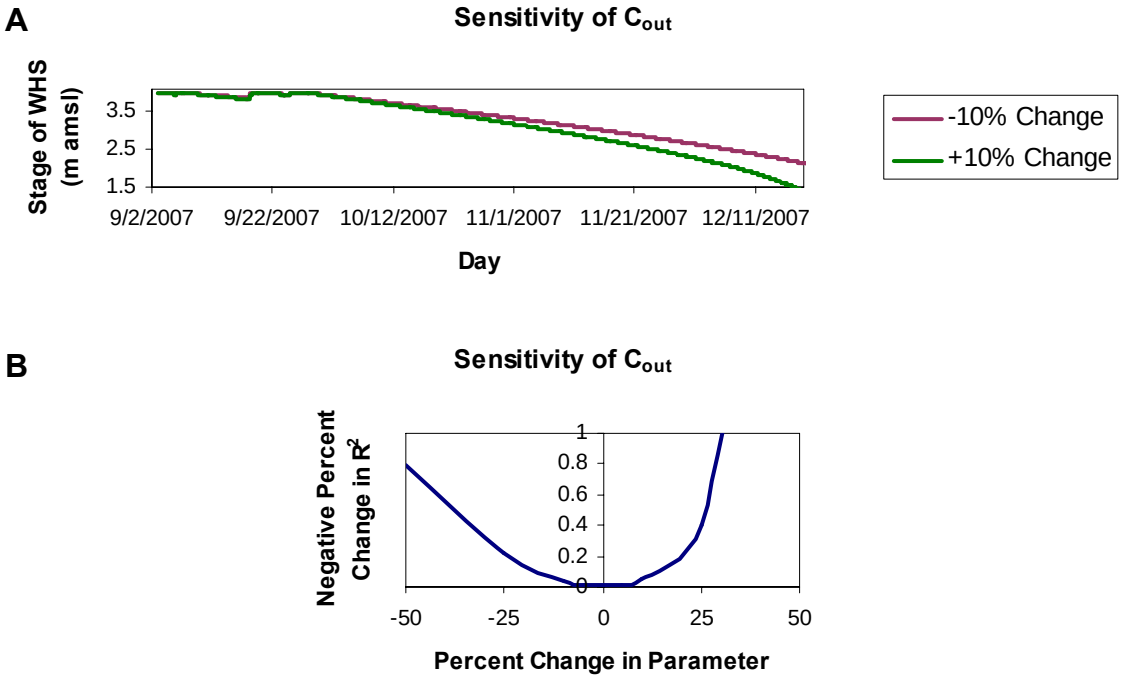

Figure 4.16: Sensitivity of C_{out}: A. difference in stage with 10% change in C_{out}, B. percent change in R^2

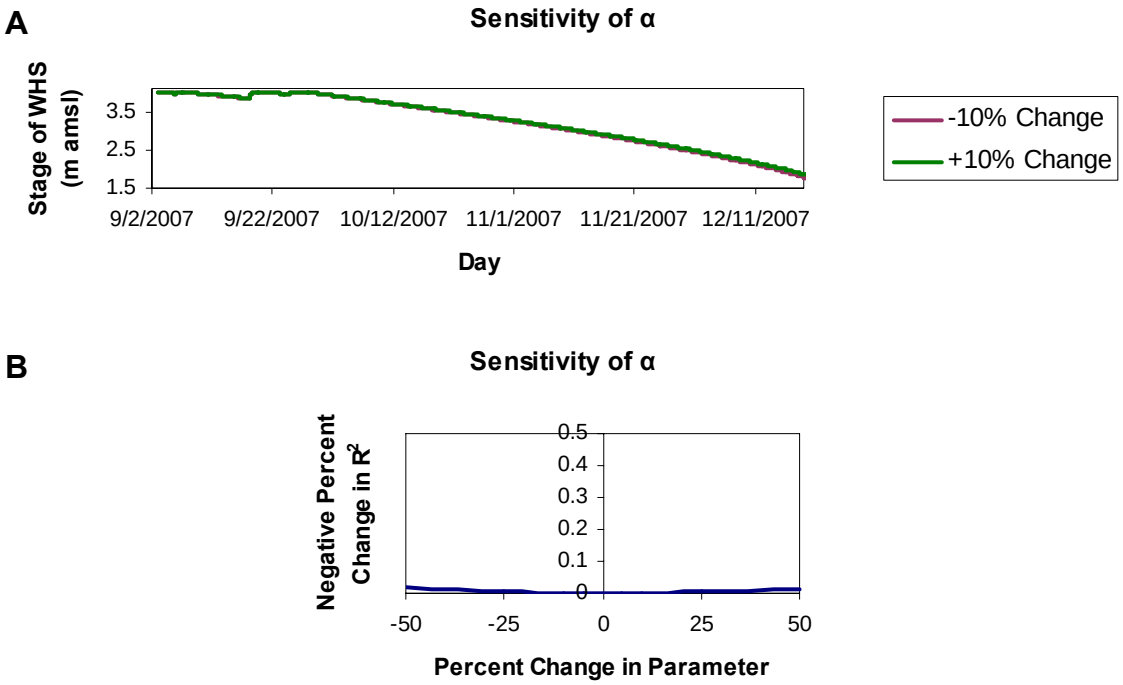

Figure 4.17: Sensitivity of α: A. difference in stage with 10% change in α, B. percent change in R^2

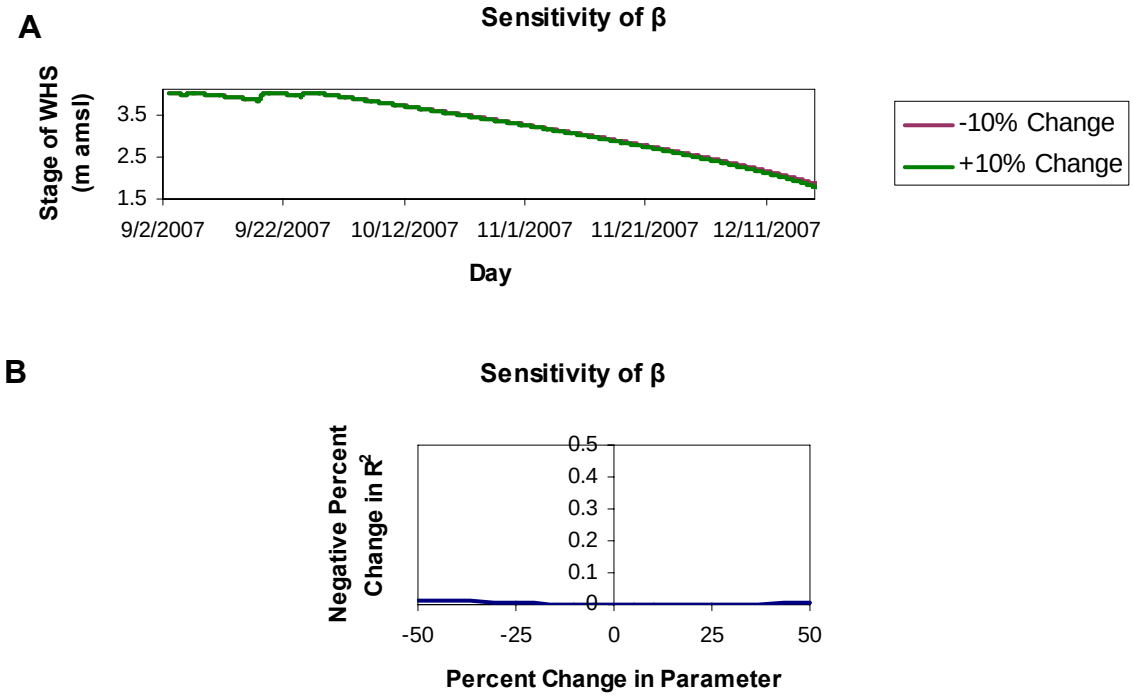

Figure 4.18: Sensitivity of β: A. difference in stage with 10% change in β, B. percent change in R^2

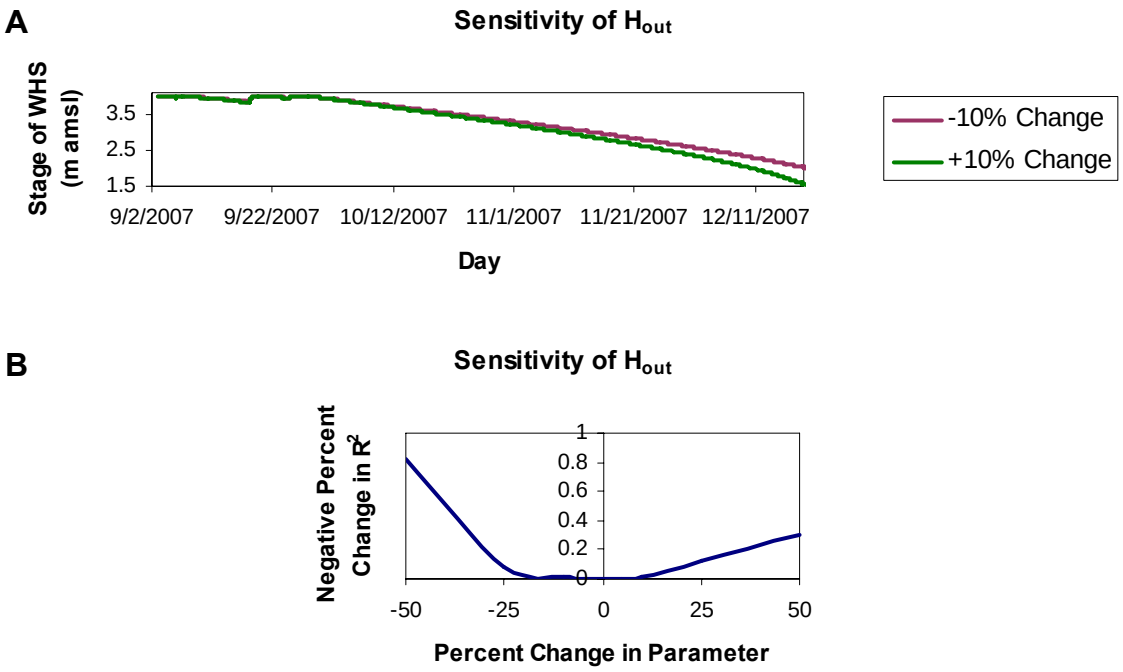

Figure 4.19: Sensitivity of H_{out}: A. difference in stage with 10% change in H_{out}, B. percent change in R^2

The parameters controlling the outflow from the WHS (C_{out} and H_{out}) are more sensitive than the parameters controlling the inflow to the WHS (C_{in}, α, and β). A general understanding of the mathematical controls on the model is necessary to analyze the sensitivity of the parameters. There are two mathematical considerations which need to be addressed: the relationship of the constants, C, to their respective H terms and the calculation of H_{in}.

The H terms are dependent on the respective C terms through multiplication, but the C term is somewhat independent because it appears again in a separate term.

$$\begin{aligned} Q_b &= C_{in}\left(H_{in} - h\right) = C_{in}H_{in} - C_{in}h \\ Q_i &= C_{out}\left(h - H_{out}\right) = C_{out}h - C_{out}H_{out} \end{aligned} \tag{4.15}$$

In addition, the use of the exponential decay to approximate H_{in} decreased the sensitivity of the aquifer, or inflow into the WHS, terms while the outflow terms are held constant throughout the simulation. The estimated parameters are generally equally sensitive with the exception of C_{out} and H_{out}.

The C_{out} and H_{out} terms are very well constrained as any change in the parameters caused a large change in error. The C_{in}, α, *and* β terms are not well constrained as variations up to 50% in the fitted parameter value did not alter the error significantly as compared with the outflow terms. Therefore, the model is sensitive primarily to the outflow terms.

The C_{out} term can vary up to 10% and the H_{out} term can vary up to 25% without changing the data misfit. The recharge volumes of the WHS and the R^2 values associated with the changes in each parameter are given in Table 4.2.

Table 4.2: Recharge volume and R^2 values associated with changes in C_{out} and H_{out}

Parameter	Percent Parameter Changed	Recharge Volume (m^3)	R^2
C_{out}	-10%	41,000	0.96
	+10%	48,000	0.95
H_{out}	-25%	39,000	0.91
	+25%	50,000	0.87

From the sensitivity analysis, the recharge volume could potentially vary from 39,000m^3 to 50,000m^3.

UNCERTAINTY ANALYSIS

Although a satisfactory result was obtained through the use of the water balance model, the estimation of five unknown parameters suggests a high degree of non-uniqueness. In order to explore the non-uniqueness of this solution, the parameters of H_{in}

and H_{out} were varied and the model was run to fit the new parameters. The infiltration volumes were then compared between each solution.

Solutions can be found if the coefficient of the exponential equation defining H_{in} (α) is changed in by one order of magnitude in either direction (heights of 5m to 500m) with the same level of error, approximately an R^2 of 0.996 and a sum of squared errors of 4.5m^2. The recharge volumes over the study period vary from 39,000m^3 to 53,000m^3. If the height of the downstream aquifer (H_{out}) is altered by one order of magnitude (heights of 0 to -100) the same level of error is obtained as well, approximately an R^2 of 0.995 and a sum of squared errors of 6.6m^2. The infiltration volumes over the study period vary from 34,000m^3 to 38,000m^3. The change in volume is more constrained with changes in the outflow heights than with inflow heights.

FUTURE WORK

In order to calibrate the model, it is suggested that the transmissivity of the upstream aquifer and the downstream aquifer with the sediments in the WHS (C_{in} and C_{out}, respectively) be determined. Since the H_{in} and H_{out} terms are dependent on their respective constant terms, and the constants generally represent the transmissivity the materials of the hypothetical flow tubes, limiting the constants to field parameters should decrease the number of realistic solutions. This constraint would allow for the model to be customized and used in many different field sites.

In addition, the infiltration approximation presented in this study represents only the months of September through December. Ideally, water level data could be collected for the entire year and then modeled to characterize a full year of recharge from the

WHS. Even if data is not available, assumptions could be made about the infiltration over the remainder of the year with prior knowledge of when the WHS is filled and empty.

4.4 Summary

This chapter presented the visualization and water balance modeling of the WHS. The WHS was surveyed and the data were then interpolated to create a surface. A pressure transducer was installed in the WHS which was used to obtain the height of the water in the WHS. The recharge from the WHS was calculated using three models: a simple subtraction of evaporation from the change in volume, a water balance over the WHS, and a second water balance with the incorporation of an addition water loss through spillway overflow. The water balance with the spillway represented the most realistic model of the three.

CHAPTER 5: STRATEGIES FOR WATER MANAGEMENT

5.1 CONCLUSIONS

This study was conducted to assess the effect of water harvesting structures on the hydrology of a water scarce region in rural India. A conceptual model describing the geology and a general hypothesis regarding the flow of water through the geology was formulated. A surface water balance was calculated using the Thornthwaite-Mather approach which was used to estimate the natural recharge to groundwater. A model of the water balance of the WHS was solved numerically and used to estimate the infiltration from the WHS during the months of September through December.

The natural recharge of the total basin study area was estimated to be 256,000 m^3 while the infiltration from the WHS was calculated to be 39,000 m^3. These figures would suggest that the WHS is contributing a volume of water equal to about 15% of the total natural infiltration. This ratio seems realistic and is significant because it suggests that the WHS is contributing a fairly significant volume of water to groundwater.

5.2 FATE OF ARTIFICIALLY RECHARGED WATER

An interesting aspect of this project which has not been discussed is the fate of the recharged water from the WHS. Using the geologic and hydrogeologic interpretations presented in chapter 2 and given the location of the WHS (Figure 5.1), a general hypothesis for the flowpath can be determined.

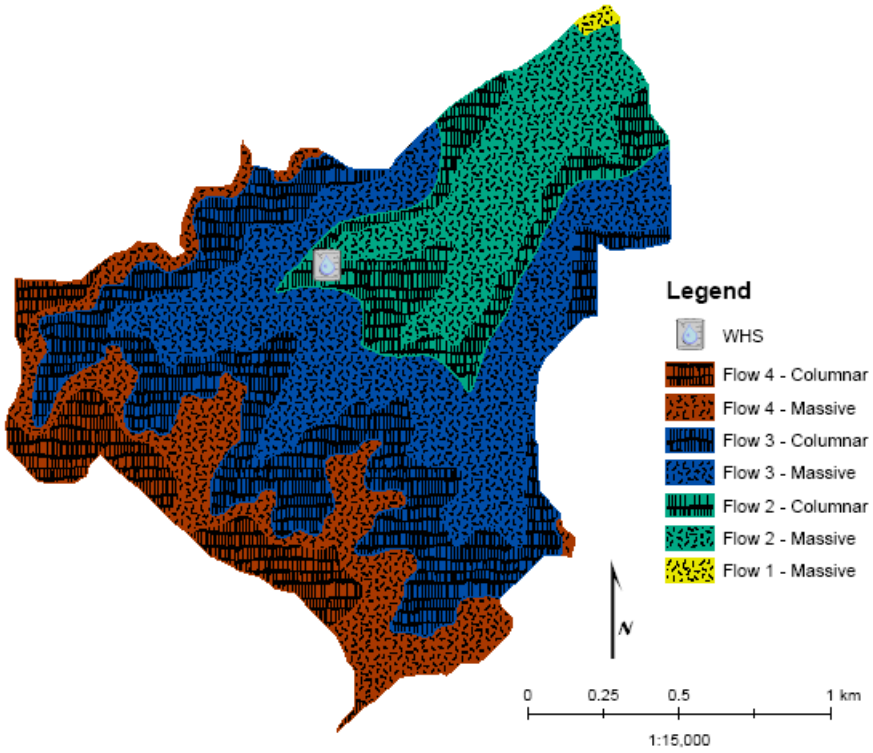

Figure 5.1: WHS location in relation to geology

Assuming the water retained in the WHS actually infiltrates into the ground and given that the WHS was constructed on columnar basalt in which water preferentially flows vertically, it is hypothesized that the water will travel predominantly vertically downward from the WHS. However, a thick sequence of massive basalt, which generally has a lower hydraulic conductivity than the columnar, directly underlies the columnar basalt. This massive basalt would inhibit the downward flow of water and force the recharged water to flow along the surface of the massive basalt in the weathered zone or to be discharged as a spring. Anecdotal evidence supports this hypothesis since the villagers report that the large diameter wells which were constructed within the weathered zone went dry before the construction of the WHS. After the WHS was built, the wells remained productive throughout the year.

However, the integrity of the WHS itself was not examined at all in this study. It is possible that the water retained by the WHS does not infiltrate into the ground but instead continues downstream through leaks in the retention structure itself. At this point in the study, the actual path of water leaving the WHS cannot be determined.

5.3 Effective Data Management

This project was performed with limited primary data, and as such great difficulties were encountered regarding the accuracy of the estimations presented in this study. This work could be partially viewed as a survey of the amount of data that was readily available to the public and what conclusions could be drawn from the meager existing information. Data acquisition rights are not regarded as highly in India as they are in other countries, such as the United States. The United Nations attempted to compile data critical for analyzing groundwater availability and management in 2003 but instead found relatively few sources of usable primary data (Moench, 2003).

Specific water level monitoring data on a consistent time scale in addition to drilling logs and pumping tests are required to conduct meaningful groundwater modeling. Since hydrogeologic data is inherently spatial in nature, a geographic information system (GIS) could be used to effectively maintain and distribute relevant data to researchers who in turn can analyze and model the physical systems and supply these tools to policy makers (Wilson, 2000).

5.3.1 Suggestions for Effective Water Management

First and foremost, all parties involved in water supply in India need to formulate a plan of cooperative management. Water is already a scarce resource, and the current

tactics of separation of information and control is not feasible in the long term (Kulkarni, 2004; Narasimhan, 2006). Data need to be collected on short time scales (i.e. at least weekly) and standard procedures for such collection need to be designed. The data then need to be widely available, ideally on an internet GIS, to enable unhindered development of models and interpretations and to allow for a more efficient policy decision-making process.

A key part to the success of any water management plan is to involve the community in the process. Ultimately, the villagers determine how the water management plan will proceed because they are actively using the resource. The villagers need to have an understanding of where the water comes from and their role in its availability. Wells are currently viewed as individual resources and they are pumped without regard to the effect this behavior will have on other surrounding wells (Kulkarni, 2004). The villagers need to have a basic understanding of hydrogeology in order to effectively self-manage their resources.

5.4 Future Work

The WHS water balance needs to be further tested to obtain a more realistic infiltration estimation. In addition, groundwater models need to be developed and tested which will simulate the flow from the WHS and the role of anisotropy of the basalt layers on groundwater flow. This study has taken the preliminary steps to complete these models. The surface water balance can be used as inputs to the groundwater balance and the conceptual model of the geology of the study area can be used as a setup for the geometry of a numerical model.

APPENDICES

APPENDIX A

PHOTO LOCATIONS

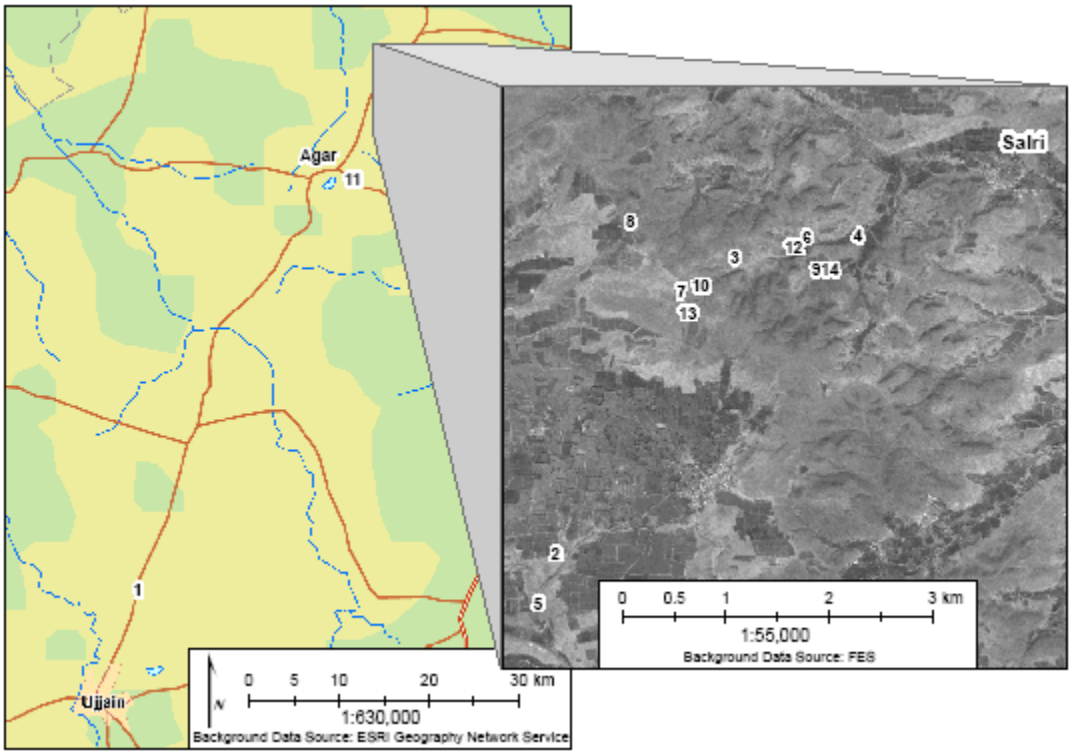

Figure A1: Map of locations of photos presented in document

Table A1: Legend for Figure A1

Map ID	Figure	Description
1	1.2	River between Ujjain and Agar: July 17, 2006
	1.3	River between Ujjain and Agar: May 2, 2007
2	2.2	Thales GPS MobileMapper Setup
3	2.4 A	Alluvial deposits with precipitates as a result of chemical weathering in a dry streambed
4	2.4 B	Alluvial deposits overlying highly chemically weathered material in a dug well
5	2.4 C	Recently disturbed soil transitioning down to weathered basalt cobbles in a WHS construction excavation site
6	2.5 A	Surface view of columns directly downstream of the WHS in basin 1
7	2.5 B	Partially weathered columnar basalt at the ridge
8	2.5 C	Columnar basalt in a dug well on the ridge
9	2.6 A	Surface view of massive basalt in basin 2
10	2.6 B	Partially weathered massive basalt in basin 1
11	2.6 C	Massive basalt at a quarry south of the study area
	2.16	Outcrop illustrating the character of the geologic unit of the boundary aquifer and pocket seep
12	2.8 A	Resistivity setup: wide view of resistivity survey within the reservoir of the WHS
	4.1	WHS reservoir
	4.2	Thales GPS survey setup
13	2.8 B	Resistivity setup: resistivity on the ridge
14	3.2	Examples of two different seeps in massive basalt

APPENDIX B

RESISTIVITY MODELING

The procedure used to model the raw resistivity data and the associated data files associated are listed below.

The raw resistivity data excel file is a collection of resistivity data gathered in or near the Salri watershed, MP, India from May 6-May 8, 2007. The VES resistivity analysis excel file is a collection of resistivity data that has been modeled using forward and inverse methods in order to determine the level of information that can be extracted from the raw data gathered in or near the Salri watershed, MP, India from May 6-May 8, 2007.

RESISTIVITY MODELING PROCEDURE

Figure B1 and Figure B2 display initial hydrogeologic interpretations of the resistivity surveys by Clemson and the Foundation for Ecological Security (FES), respectively based on the assumption that depth of investigation was equal to half the distance between the current electrodes. Generally, low resistivity was interpreted as water bearing zones with high porosity (e.g., sedimentary materials, weathered basalts, or highly fractured basalts) and increasing resistivity indicated decreasing water content and/or more massive formations with fewer fractures present. Water bearing zones were defined by their location within the basalt sequence. A low resistivity region was termed a shallow aquifer if it was located at the base of the weathered zone, a boundary aquifer if it was located between columnar and massive basalts, and a seep pocket (essentially a spring) if it was located within a section of massive basalt.

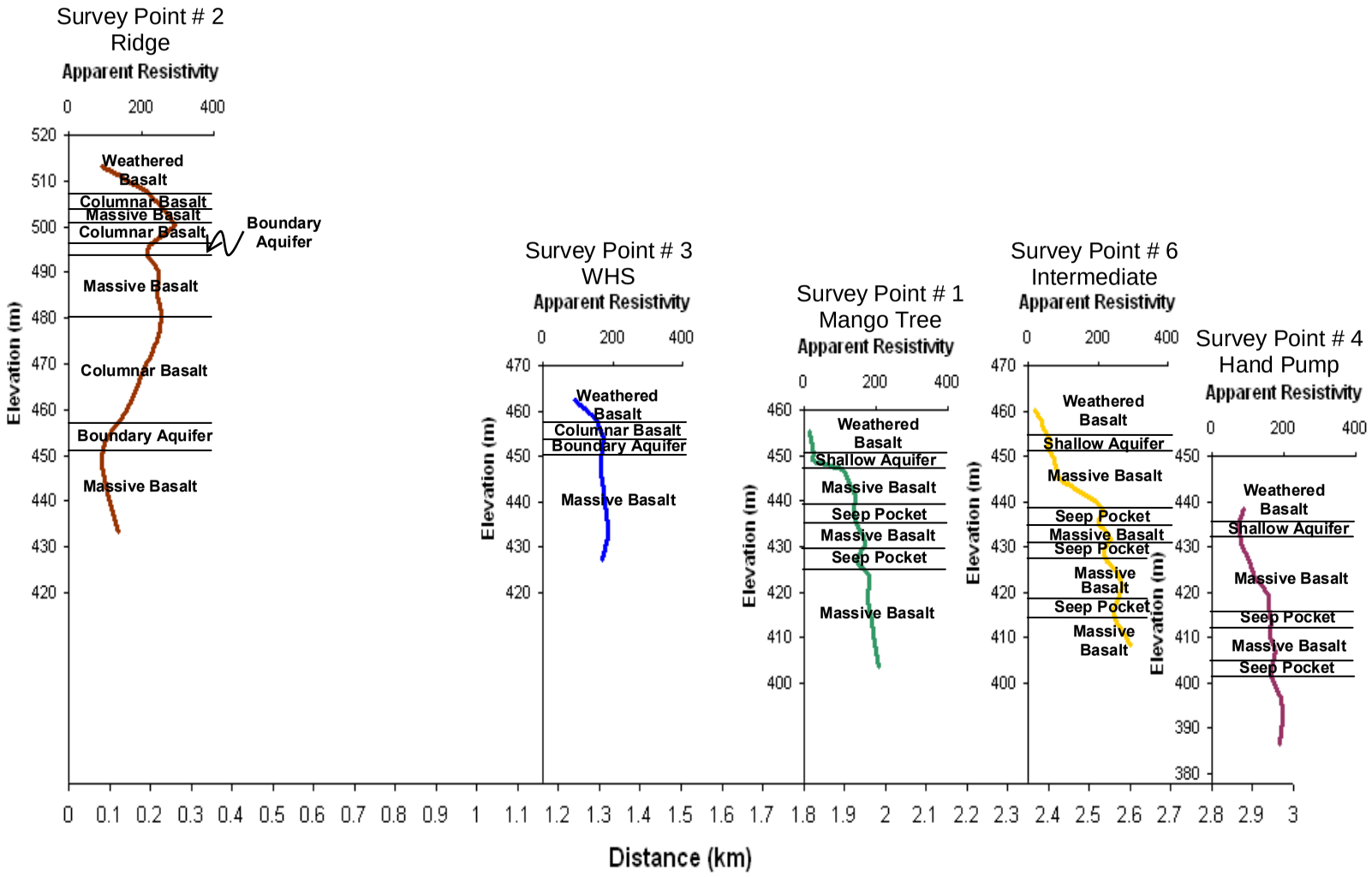

Figure B1: Hydrogeologic interpretation of resistivity surveys by Clemson team

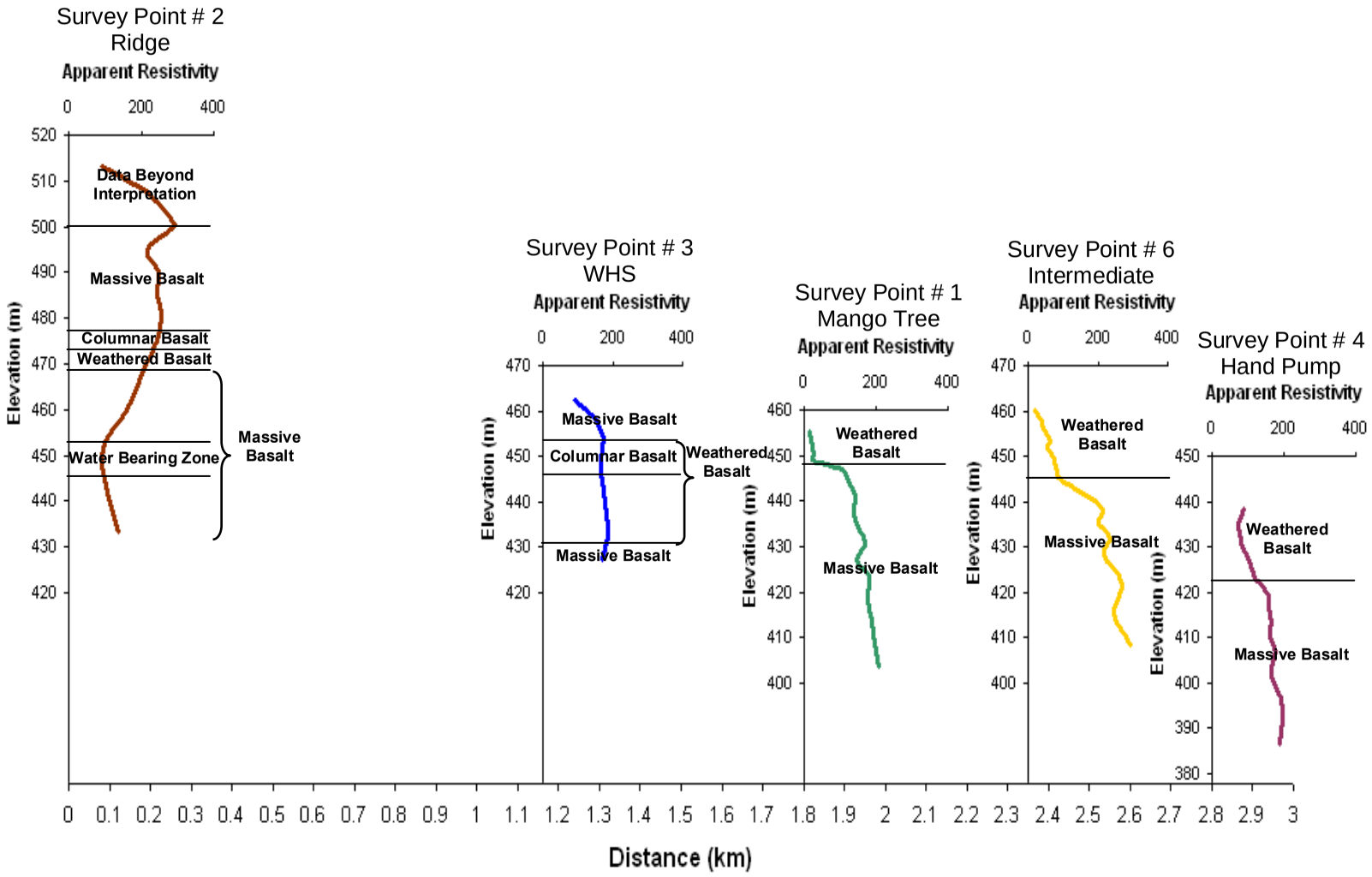

Figure B2: Hydrogeologic interpretation of resistivity surveys by FES team

Forward and inverse modeling was performed to quantify the value of the resistivity data compared to other data collection methods using VES, a freeware program designed by the University of the Witwatersrand (Cooper, 2000). Forward modeling simulates apparent resistivity responses given estimated resistivity and thickness values. Inverse modeling involves altering resistivity or thickness values in order to decrease the least squares misfit between modeled and observed apparent resistivity profiles (i.e., the root mean square of the difference between modeled and observed data points). Initial values of resistivity based upon basalt character were selected from rough averages of the apparent resistivity readings in the near surface and from preliminary forward modeling as in the case of the massive basalt. The initial values used in the modeling process are shown in Table B1; however, to take into account the fact that resistivity generally increases with depth, the resistivity of layers whose character was already expressed at shallower depths was increased by 50Ωm for weathered, columnar, and saturated formations and 500Ωm for massive basalt.

Table B1: Initial resistivity values used for vertical electrical sounding model

Hydrogeologic Character	Resistivity (Ωm)
weathered	150
columnar	200
saturated	100
massive	1500

A comparison of Figure B1 and Figure B2 illustrated using the representation of resistivities presented in Table B1 is given in Figure B3.

Elevation		Ridge		WHS		Mango Tree		Intermediate		Hand Pump	
From	To	Clemson	FES	Clemson	FES	Clemson	FES	Clemson	FES	Clemson	FES
513	510										
510	505										
505	500										
500	495										
495	490										
490	485										
485	480										
480	475										
475	470										
470	465										
465	460										
460	455										
455	450										
450	445										
445	440										
440	435										
435	430										
430	425										
425	420										
420	415										

Figure B3: Comparison of hydrogeologic interpretations of resistivity surveys (note layer thicknesses area approximate)

The goal of the modeling process was to find the best fit of the data with the simplest representation while being consistent with the conceptual model of the hydrogeology. Resistivity inversion was completed using several basic steps:

(1) Initial resistivity values were held constant while thicknesses were inverted,

(2) The model was reset removing any layers that the model was not sensitive to and the parameters of the remaining layers were restored to the initial values,

(3) The thicknesses were held constant while the resistivity values were inverted,

(4) The resistivity of the top layer was set to equal the apparent resistivity data and held constant and the remaining layers' resistivities were inverted.

The modeling process is best explained using an example, in this case, the Clemson interpretation of the ridge location as seen in Table B2 (see VES Resistivity Analysis excel spreadsheet in the electronic appendix for all other locations).

The initial interpretation of number of layers and their respective thickness and resistivity (Figure B and Figure B3) were used as the first guess for forward modeling. At this point, the misfit is large as the root mean square error is 190.3Ωm. The number of layers was then deceased to reduce the number of parameters to be inverted; simple models with as few parameters as possible provide more robust inversion results (Cooper, 2000). Only insensitive layers, those layers which if removed from the model did not alter the error by a significant amount (less than 2 Ωm increase), were removed. The simplest way to identify insensitive layers is to invert the thicknesses while holding the resistivities of each layer constant. If the thickness of a layer increased dramatically, this

indicated that the layers below were inconsequential to the model, or if thickness of a layer was reduced to 0 meters then that layer could be removed.

In this example, the thickness of the saturated layer (fifth layer from the top) increased from 0.3 meters to 983.8 meters. Removing layers increased in error of less than 2Ωm or a decrease in error. Changing the saturated layer mentioned earlier to the half-space (the lowest layer in the model) and removing all subsequent layers did not alter the error at all, thus this simplification is acceptable. As seen in Figure B4, removal of individual layers below layer 5 has no affect on the model since the resistivity curves are exactly the same after the removal of each layer.

Table B2: Example results of modeling technique, Clemson interpretation of ridge resistivity modeling

	Initial Parameters		Modeled Parameters											
			Testing sensitivity of thickness - 100 iterations, resistivity constant, thickness inverted		Testing sensitivity of lower layers - layers 6-9 removed		Confidence in thicknesses		Testing for better resistivity values - 100 iterations, thickness constant, resistivity inverted		Fitting first point		Testing for better resistivity values - 100 iterations, layer 1 resistivity and all thicknesses constant, layers 2-5 resistivity inverted	
	Resistivity (Ωm)	Thickness (m)	Resistivity (Ωm)	Thickness (m)	Resistivity (Ωm)	Thickness (m)	Resistivity (Ωm)	Thickness (m)	Resistivity (Ωm)	Thickness (m)	Resistivity (Ωm)	Thickness (m)	Resistivity (Ωm)	Thickness (m)
	232 Ωm error		40.6 Ωm error		40.6 Ωm error		42.2 Ωm error		49.6 Ωm error		67.3 Ωm error		59.4 Ωm error	
weathered	150	5	150	5.1	150	5.1	150	5	207.1	5	90	5	90	5
columnar	200	2	200	1.3	200	1.3	200	2	509.5	2	509.5	2	1392.5	2
massive	1500	2	1500	2.1	1500	2.1	1500	2	1507.4	2	1507.4	2	1833.2	2
columnar	250	2	250	0.9	250	0.9	250	2	234.8	2	234.8	2	271.2	2
saturated	100	0.3	100	983.8	100	infinite	100	infinite	74.8	infinite	74.8	infinite	15.6	infinite
massive	2000	10	2000	0	0	0	0	0	0	0	0	0	0	0
columnar	300	20	300	706.5	0	0	0	0	0	0	0	0	0	0
saturated	150	0.3	150	25.2	0	0	0	0	0	0	0	0	0	0
massive	2500	infinite	2500	infinite	0	0	0	0	0	0	0	0	0	0

Step 1
Step 2
Step 3
Step 4

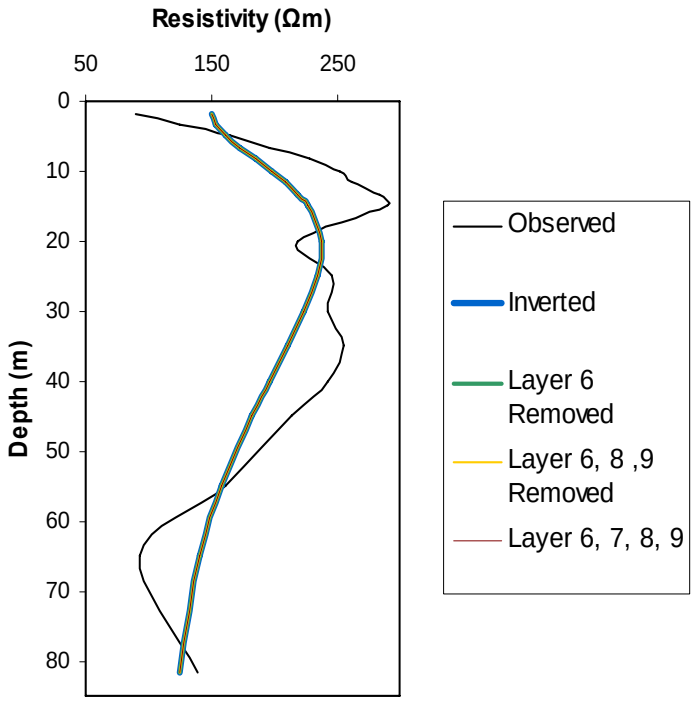

Figure B4: Removal of insensitive layers

With insensitive layers removed in step one, the interpretation was forward modeled with the remaining layer thicknesses reset to the initial values because of the higher confidence in the thickness than resistivity parameter. Although this forward modeling process tends to increase the error of the model (from 40.6Ωm to 42.2Ωm), the change in error is insignificant compared to the geologic logic necessary to maintain the initial thickness.

Step three is the starting point for the analysis of the resistivity values and involves the use of the inversion process to try to find values which decreases the error between the modeled and observed curves. In this example, the error actually increased after inversion of the resistivity values (from 42.2Ωm to 49.6Ωm) indicating that the model is very close to the solution. This result occurred because the VES inversion

program runs the model until the user inputted number of iterations (in this case 100) and not until the model converges (has the lowest error).

The final step attempts to force the model to fit the observed data based upon the assumption that the shallowest apparent resistivity point should have a fairly accurate resistivity since the reading is averaged over a smaller volume of material compared to the subsequent points (Singhal, 1999). Using forward modeling, the resistivity of the shallowest point is set to the field measurement, in this example, approximately 90Ωm. Again, the error typically increases (in this example from 49.6Ωm to 67.3Ωm) because the remaining layers' resistivities are fitted to the previous situation. To overcome this factor and attempt to reduce the error, the resistivity of the layers below the first are inverted. In nearly all cases the error increased when the resistivity of the shallowest layer was forced to equal the field measurement apparent resistivity. This misfit could be due to the fact that the observed resistivity is an average of the material's resistivity and the limited number of modeled parameters cannot eliminate the discrepancy between averaged and absolute values. The only instance where the error decreased with the set value for resistivity of the shallowest layer occurred in FES's interpretation of the WHS. Because the inverted value of the resistivity of the shallowest layer was so close (within 4Ωm) to the observed apparent resistivity value, the inversion process was able to integrate the observed value and reduce the overall error of the model. However, in most situations, the models were reduced to 2 or 3 layers only allowing for 1 or 2 values to be inverted, thus the program was only able to reduce the error by increasing the resistivity of the lower layers to its maximum value, 100,000Ωm, which is logically not feasible

given the geology of the area. Because of these difficulties, the results from fitting the first point were not used in the following analyses or in the final overall interpretation.

Interpretations for all areas were modeled using the same four basic steps. Clemson and FES model results were compared at each point. If the modeling results of each interpretation had more than 2 layers, the models were combined together to attempt to eliminate the differences between them. This combination of interpretations was only simulated at the ridge resistivity point because out of all five locations, the ridge was the sole location where the combination of models would yield an interpretation different from the original elements. The combination of Clemson and FES's model results was conducted by integrating the thinner layers into the thicker layers as seen in Figure B5.

Clemson	
Resistivity (Ωm)	Thickness (m)
49.6Ωm error	
207.1	5
509.5	2
1507.4	2
234.8	2
74.8	infinite

FES	
Resistivity (Ωm)	Thickness (m)
56.2Ωm error	
239.9	10
281.8	20
29.1	10
927	10
3.9	infinite

→

Combined Results	
Resistivity (Ωm)	Thickness (m)
76.9Ωm error	
207.1	5
509.5	2
1507.4	2
281.8	20
29.1	10
927	10
3.9	infinite

Figure B5: Example of combining Clemson and FES results, ridge resistivity modeling

The combined model was then inverted to identify resistivity values that would reduce the error. In the ridge example, after 100 iterations, the error between the observed and modeled resistivity values was 49.2Ωm, which is very similar to the error of the uncombined results for Clemson and FES (49.6Ωm and 56.2Ωm respectively).

Table B3: Forward and inversion model of combined ridge interpretation

	Combining models			
	Initial Parameters		Modeled Parameters	
	Resistivity (Ωm)	Thickness (m)	Resistivity (Ωm)	Thickness (m)
	76.9Ωm error		49.2Ωm error	
weathered	207.1	5	138.1	5
columnar	509.5	2	554	2
massive	1507.4	2	1143.1	2
weathered	281.8	20	227.1	20
saturated	29.1	10	13.3	10
massive	927	10	1003.1	10
saturated	3.9	infinite	12.9	infinite

In addition, Figure B6 indicates that the Clemson interpretation fits the total range of resistivity, with emphasis on the highs and lows, while the FES interpretation fits the middle values of resistivity. The combination model basically appears to expand the range of resistivity values of the FES interpretation. Although the Clemson interpretation has the lowest error, there does not appear to be enough data to confidently distinguish between the Clemson or FES models.

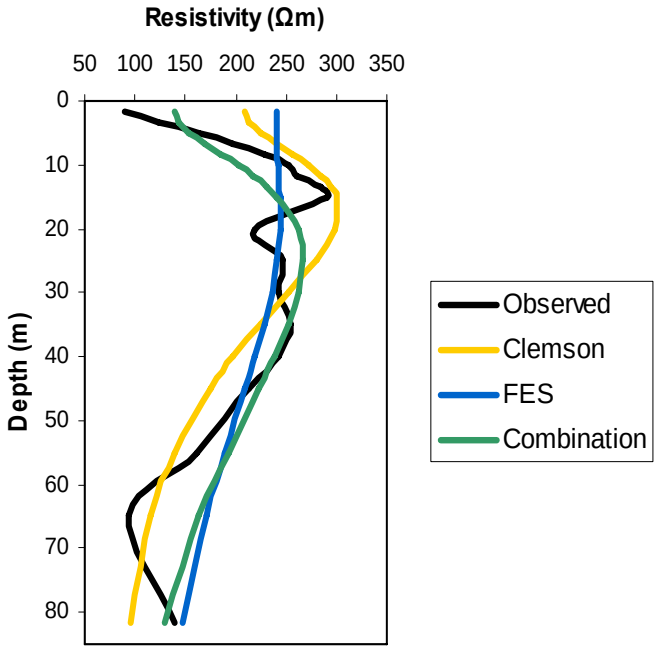

Figure B6: Plot comparing Clemson, FES, and combination resistivity models

The final simulation for each resistivity point was the automatic interpretation. The VES software has two options for modeling resistivity data: the user can enter initial values for resistivity and thickness, or the program can automatically choose the best initial values for either a two or three layered model. The automatic interpretation was used to determine if reasonable interpretations could be found using as few layers as possible.

Table B4: Automatic interpretation results, ridge resistivity modeling

Automatic Interpretation			
2 layer		3 layer	
Resistivity (Ωm)	Thickness (m)	Resistivity (Ωm)	Thickness (m)
53.4Ωm error		24.9Ωm error	
107.1	1.1	107.1	2
216.1	infinite	354.4	13.9
		96.8	infinite

The automatic interpretation commonly had the lowest error because there were no constraints on thickness or resistivity, only number of layers. This process is useful because it gives a sense of the general trend of resistivity and layer thickness that fits the data the best.

Table B5: Classification of hydrogeologic character by modeled resistivity values

Resistivity (Ωm)	Hydrogeologic Character
no data	no data
0-149	saturated
150-249	weathered
250-749	columnar
750+	massive

Overall, after modeling the resistivity interpretations, the differences between the interpretations became less obvious: the number of layers was almost always the same and the patterns of relative resistivity were also consistent, both between Clemson and FES's individual interpretations in addition to site to site. The main difference between each of the models is the thickness of the layers, but this discrepancy is due to holding the thicknesses constant during inversion so as to simplify the problem. However, the modeling process revealed that single site focused interpretations based solely on resistivity data yield very little information; in most cases the resistivity could only confirm two layers with increasing resistivity with depth. Taking all the resistivity site models into account, there appears to be a pattern of at least 2 flows (each composed of columnar and massive basalt) over the 100m investigated. There are a few discrepancies including a third upper flow in Clemson's interpretation and the location of water bearing zones that cannot be resolved only using resistivity observations.

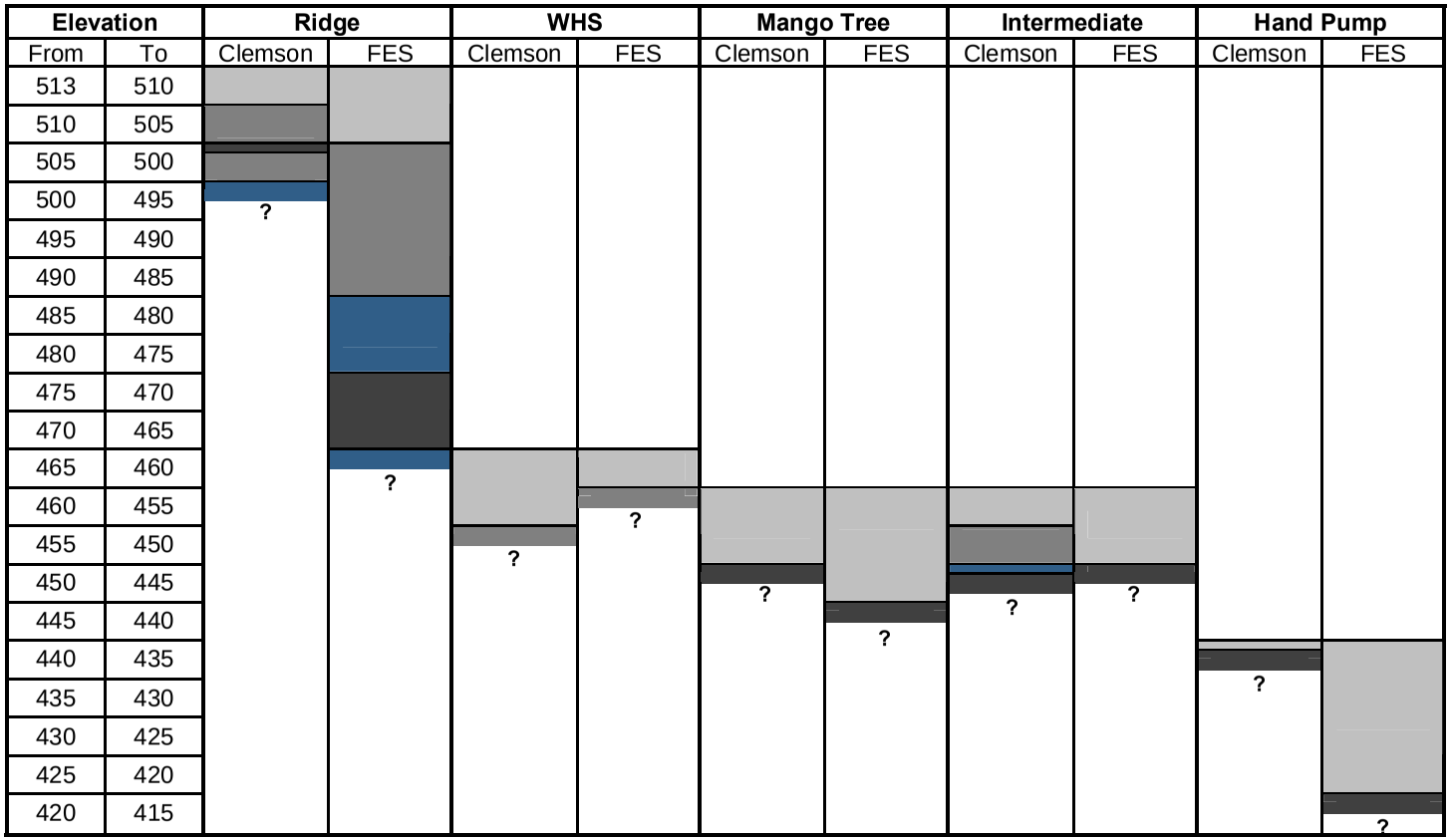

Figure B7: Comparison of modeled hydrogeologic interpretations of resistivity surveys (note layer thicknesses and half-space extent are approximate)

POSSIBLE ERRORS/FUTURE WORK SUGGESTIONS

Because the thicknesses were held constant, the lower of the two layers tended to stabilize at the highest resistivity possible for the program (100,000Ωm) especially when the first point was forced to equal the apparent resistivity value. The actual depth of investigation is at most 20 meters which represents a considerable depth. However, the depths are based upon assumptions which cannot be confirmed without additional data (i.e. logged wells near the resistivity survey points).

APPENDIX C

THORNTHWAITE-MATHER SOIL MOISTURE BALANCE CALCULATION

The Thornthwaite-Mather technique requires an input of monthly precipitation (in millimeters or inches), monthly temperatures (in °C or °F), the latitude of the location of interest, and an estimate of the maximum water holding capacity of the soil. For this study, temperature is in degrees Celsius and all other units are in millimeters unless stated otherwise. Monthly precipitation and temperature data were obtained for a weather station at Agar from the Foundation for Ecological Security.

Table C1: Thornthwaite-Mather soil moisture balance for the year 2007

	Jan	Feb	Mar	Apr	May	Jun	Jul	Aug	Sep	Oct	Nov	Dec
Temperature (°C)	17.6	20.9	22.1	29.6	30.5	30.6	25.2	24.7	26.4	23.2	21.7	17.1
Heat Index, i	6.7	8.7	9.5	14.8	15.5	15.5	11.6	11.2	12.4	10.2	9.2	6.4
Unadjusted Daily PET (mm)	1.3	2.3	2.6	5.3	5.5	5.5	3.9	3.6	4.5	3.1	2.5	1.2
Monthly Duration of Sunlight (units of 12 hours)	27.9	26.7	30.9	31.8	34.5	34.2	34.8	33.6	30.6	29.7	27.3	27.6
Adjusted PET (mm)	36.3	61.4	80.3	168.5	189.8	188.1	135.7	121.0	137.7	92.1	68.3	33.1
Precipitation (P) (mm)	0.0	2.6	0.0	8.6	18.0	68.5	438.8	314.8	141.9	0.0	0.0	0.0
P-PET (mm)	-36.3	-58.8	-80.3	-159.9	-171.8	-119.6	303.1	193.8	4.2	-92.1	-68.3	-33.1
Accumulated Potential Water Loss (mm)	-229.7	-288.5	-368.9	-528.8	-700.6	-820.2			0.0	-92.1	-160.3	-193.4
Storage (mm)	99.0	78.0	56.0	30.0	15.0	9.0	250.0	250.0	250.0	172.0	131.0	114.0
Change in Storage (mm)	-15.0	-21.0	-22.0	-26.0	-15.0	-6.0	241.0	0.0	0.0	-78.0	-41.0	-17.0
Actual ET (mm)	15.0	23.6	22.0	34.6	33.0	74.5	135.7	121.0	137.7	78.0	41.0	17.0
Moisture Deficit (mm)	21.3	37.8	58.3	133.9	156.8	113.6	0.0	0.0	0.0	14.1	27.3	16.1
Moisture Surplus (mm)	0.0	0.0	0.0	0.0	0.0	0.0	197.8	314.8	141.9	0.0	0.0	0.0
Runoff* (mm)	10.9	5.4	2.7	1.4	0.7	0.3	98.9	206.9	174.4	87.2	43.6	21.8
Surface Runoff (mm)	9.3	4.6	2.3	1.2	0.6	0.3	84.1	175.8	148.2	74.1	37.1	18.5
Recharge (mm)	1.6	0.8	0.4	0.2	0.1	0.1	14.8	31.0	26.2	13.1	6.5	3.3

Look up tables referred to in this work can be found in Instructions and Tables for Computing Potential Evapotranspiration and the Water Balance (Thornthwaite, 1957) and will be identified in bold.

Step 1: Heat Index

Using the temperature data in degrees Celsius look up the heat index in **Table 2** for each month.

Table C2: Calculation of heat index

	Jan	Feb	Mar	Apr	May	Jun	Jul	Aug	Sep	Oct	Nov	Dec
Temperature (°C)	17.6	20.9	22.1	29.6	30.5	30.6	25.2	24.7	26.4	23.2	21.7	17.1
Heat Index, i	6.7	8.7	9.5	14.8	15.5	15.5	11.6	11.2	12.4	10.2	9.2	6.4

The monthly heat indices are summed together to obtain the yearly heat index, I, which for this case is 131.8.

Step 2: Unadjusted Daily Potential Evapotranspiration (PET)

Using the monthly temperature data and the yearly heat index (I) look up the unadjusted daily PET in **Table 4** for each month.

Table C3: Calculation of unadjusted daily PET

	Jan	Feb	Mar	Apr	May	Jun	Jul	Aug	Sep	Oct	Nov	Dec
Temperature (°C)	17.6	20.9	22.1	29.6	30.5	30.6	25.2	24.7	26.4	23.2	21.7	17.1
Unadjusted Daily PET (mm)	1.3	2.3	2.6	5.3	5.5	5.5	3.9	3.6	4.5	3.1	2.5	1.2

Step 3: Adjusted Monthly Potential Evapotranspiration (PET)

Using the latitude of the location of interest look up a correction factor for day and month length in **Table 6** for each month. The latitude of this study area is 23.7°N.

Table C4: Monthly duration of sunlight at 23.7°N latitude

	Jan	Feb	Mar	Apr	May	Jun	Jul	Aug	Sep	Oct	Nov	Dec
Monthly Duration of Sunlight (units of 12 hours)	27.9	26.7	30.9	31.8	34.5	34.2	34.8	33.6	30.6	29.7	27.3	27.6

Multiply the correction factor of each month by the unadjusted PET to obtain the adjusted PET.

Table C5: Calculation of adjusted monthly PET

	Jan	Feb	Mar	Apr	May	Jun	Jul	Aug	Sep	Oct	Nov	Dec
Unadjusted Daily PET (mm)	1.3	2.3	2.6	5.3	5.5	5.5	3.9	3.6	4.5	3.1	2.5	1.2
Monthly Duration of Sunlight (units of 12 hours)	27.9	26.7	30.9	31.8	34.5	34.2	34.8	33.6	30.6	29.7	27.3	27.6
Adjusted PET (mm)	36.3	61.4	80.3	168.5	189.8	188.1	135.7	121.0	137.7	92.1	68.3	33.1

Step 4: Precipitation minus Potential Evapotranspiration (P-PET)

Input monthly precipitation in the same units as PET and subtract to obtain P-PET values to be used in subsequent calculations.

Table C6: Calculation of P-PET

	Jan	Feb	Mar	Apr	May	Jun	Jul	Aug	Sep	Oct	Nov	Dec
Adjusted PET (mm)	36.3	61.4	80.3	168.5	189.8	188.1	135.7	121.0	137.7	92.1	68.3	33.1
Precipitation (P) (mm)	0.0	2.6	0.0	8.6	18.0	68.5	438.8	314.8	141.9	0.0	0.0	0.0
P-PET (mm)	-36.3	-58.8	-80.3	-159.9	-171.8	-119.6	303.1	193.8	4.2	-92.1	-68.3	-33.1

Negative P-PET values indicate that the input from rain fails to meet the water needs while positive P-PET values indicate the excess water is input into the system to be used for soil moisture recharge and thus runoff and recharge to groundwater.

Step 5: Accumulated Potential Water Loss (APWL)

Consecutive monthly negative P-PET values are summed together to obtain an estimate on the potential loss of soil water resulting from the deficiency in rain. Before this calculation can be completed, a general sense of the moisture of the location needs to be determined. The moisture status of the location is determined by summing the monthly P-PET values. Positive yearly P-PET values indicate a moist

weather station and thus there is a surplus of water from year to year. Negative yearly P-PET values indicate a dry weather station and thus a deficit of water is carried over from each year. The yearly P-PET value is -319mm in this study signifying that this location is dry. Under normal circumstances, the calculation of the APWL of a dry station would begin with an estimate of the yearly deficit that is carried over from the previous year. However, the Thornthwaite-Mather method was developed for use in the United States and thus it does not take into consideration the special circumstances of the Indian monsoon. It is assumed in this situation that the soil must be saturated at the end of monsoon because there is such a large volume of water input into the system over a short period of time (three months). Therefore, there will not be a deficit carried over from the previous year.

Table C7: Calculation of APWL

	Jan	Feb	Mar	Apr	May	Jun	Jul	Aug	Sep	Oct	Nov	Dec
P-PET (mm)	-36.3	-58.8	-80.3	-159.9	-171.8	-119.6	303.1	193.8	4.2	-92.1	-68.3	-33.1
Accumulated Potential Water Loss (mm)	-229.7	-288.5	-368.9	-528.8	-700.6	-820.2			0.0	-92.1	-160.3	-193.4

Step 6: Storage

An estimate of the maximum soil moisture holding capacity is needed at this point and can be obtained using **Table 10** given the plant and soil type of the location of interest. The maximum water holding capacity of the soil in this study is estimated to be 250mm assuming the area is covered by deep rooted crops, such as pastures, and the dominant soil type is a clay loam.

Using the APWL, look up the storage for the negative P-PET months in **Table 30**. Once all the negative P-PET values are accounted for, each positive P-PET value is

added to the storage of the previous month. If the addition of the positive P-PET value takes the APWL above the water holding capacity, the value of the water holding capacity is entered as the storage and the excess will be accounted for in later calculations of soil moisture surplus.

Table C8: Calculation of soil storage

	Jan	Feb	Mar	Apr	May	Jun	Jul	Aug	Sep	Oct	Nov	Dec
P-PET (mm)	-36.3	-58.8	-80.3	-159.9	-171.8	-119.6	303.1	193.8	4.2	-92.1	-68.3	-33.1
Accumulated Potential Water Loss (mm)	-229.7	-288.5	-368.9	-528.8	-700.6	-820.2			0.0	-92.1	-160.3	-193.4
Storage (mm)	99.0	78.0	56.0	30.0	15.0	9.0	250.0	250.0	250.0	172.0	131.0	114.0

Step 7: Change in Storage

The change in soil moisture storage is calculated by subtracting the previous month storage from the current month storage.

Table C9: Calculation of change in soil storage

	Jan	Feb	Mar	Apr	May	Jun	Jul	Aug	Sep	Oct	Nov	Dec
Storage (mm)	99.0	78.0	56.0	30.0	15.0	9.0	250.0	250.0	250.0	172.0	131.0	114.0
Change in Storage (mm)	-15.0	-21.0	-22.0	-26.0	-15.0	-6.0	241.0	0.0	0.0	-78.0	-41.0	-17.0

Step 8: Actual Evapotranspiration (AET)

The actual evapotranspiration depends on whether the P-PET value of a month is positive or negative. For positive P-PET months, AET equals PET, for negative P-PET months, AET equals the precipitation plus the change in storage of each particular month.

Table C10: Calculation of AET

	Jan	Feb	Mar	Apr	May	Jun	Jul	Aug	Sep	Oct	Nov	Dec
Precipitation (P) (mm)	0.0	2.6	0.0	8.6	18.0	68.5	438.8	314.8	141.9	0.0	0.0	0.0
P-PET (mm)	-36.3	-58.8	-80.3	-159.9	-171.8	-119.6	303.1	193.8	4.2	-92.1	-68.3	-33.1
Change in Storage (mm)	-15.0	-21.0	-22.0	-26.0	-15.0	-6.0	241.0	0.0	0.0	-78.0	-41.0	-17.0
Actual ET (mm)	15.0	23.6	22.0	34.6	33.0	74.5	135.7	121.0	137.7	78.0	41.0	17.0

Step 9: Moisture Deficit

Negative P-PET months indicate the total potential evapotranspiration was not able to be realized. For these months there is a moisture deficit which is the amount the PET and AET differ.

Table C11: Calculation of soil moisture deficit

	Jan	Feb	Mar	Apr	May	Jun	Jul	Aug	Sep	Oct	Nov	Dec
Adjusted PET (mm)	36.3	61.4	80.3	168.5	189.8	188.1	135.7	121.0	137.7	92.1	68.3	33.1
Actual ET (mm)	15.0	23.6	22.0	34.6	33.0	74.5	135.7	121.0	137.7	78.0	41.0	17.0
Moisture Deficit (mm)	21.3	37.8	58.3	133.9	156.8	113.6	0.0	0.0	0.0	14.1	27.3	16.1

Step 10: Moisture Surplus

When the soil moisture storage exceeds the maximum water holding capacity, the potential for surplus is available. For these months the surplus is equal to the precipitation minus the maximum water holding capacity of the soil.

Table C12: Calculation of soil moisture surplus

	Jan	Feb	Mar	Apr	May	Jun	Jul	Aug	Sep	Oct	Nov	Dec
Precipitation (P) (mm)	0.0	2.6	0.0	8.6	18.0	68.5	438.8	314.8	141.9	0.0	0.0	0.0
Storage (mm)	99.0	78.0	56.0	30.0	15.0	9.0	250.0	250.0	250.0	172.0	131.0	114.0
Change in Storage (mm)	-15.0	-21.0	-22.0	-26.0	-15.0	-6.0	241.0	0.0	0.0	-78.0	-41.0	-17.0
Moisture Surplus (mm)	0.0	0.0	0.0	0.0	0.0	0.0	197.8	314.8	141.9	0.0	0.0	0.0

Step 11: Runoff*

The surplus water in the soil is available for runoff and recharge to groundwater. These terms are lumped together into one term, runoff*. For large watersheds only 50% of the water available for runoff actually does runoff while the other half is held over for the next month (Thornthwaite, 1957). Since this study area is a small watershed, another percentage should be used, but given the lack of data on trends of how the runoff percentage changes with watershed size the 50% runoff assumption is used in this study. To calculate runoff*, half of the moisture surplus is taken from the

first month where a surplus is observed. For all consecutive months, half of the moisture surplus of the given month is added to half of the runoff from the previous month.

Table C13: Calculation of runoff*

	Jan	Feb	Mar	Apr	May	Jun	Jul	Aug	Sep	Oct	Nov	Dec
Moisture Surplus (mm)	0.0	0.0	0.0	0.0	0.0	0.0	197.8	314.8	141.9	0.0	0.0	0.0
Runoff* (mm)	10.9	5.4	2.7	1.4	0.7	0.3	98.9	206.9	174.4	87.2	43.6	21.8

Step 12: Surface Runoff and Groundwater Recharge

Since the runoff* term is a lumped parameter of surface runoff and recharge to groundwater, the terms need to be separated. It is assumed that 15% of the runoff* term is groundwater recharge and the remaining 85% is surface runoff. This assumption is based on the fact that recharge is a much slower process than runoff. The actual proportion of runoff to infiltration probably changes throughout the year. The proportion of infiltration could realistically vary anywhere from 5-50% of the available surplus resulting in a variation of the overall basin infiltration from 85,000-850,000m^3. However, lacking streamflow or groundwater level data for calibration, a yearly assumption of 85% runoff to 15% infiltration was used.

Table C14: Calculation of surface runoff and recharge

	Jan	Feb	Mar	Apr	May	Jun	Jul	Aug	Sep	Oct	Nov	Dec
Runoff* (mm)	10.9	5.4	2.7	1.4	0.7	0.3	98.9	206.9	174.4	87.2	43.6	21.8
Surface Runoff (mm)	9.3	4.6	2.3	1.2	0.6	0.3	84.1	175.8	148.2	74.1	37.1	18.5
Recharge (mm)	1.6	0.8	0.4	0.2	0.1	0.1	14.8	31.0	26.2	13.1	6.5	3.3

APPENDIX D

WATER HARVESTING STRUCTURE VISUALIZATION

The procedure used to visually model the water harvesting structure and the associated data files are listed below.

WATER HARVESTING STRUCTURE VISUALIZATION

Data for the WHS survey points were downloaded from the GPS receivers using GNSS solutions. Each day had to be downloaded into a separate project to ensure correct correlation between base station (with prefix BBASE) and rover (prefix BROV). The data files downloaded from both GPS receivers are presented in Table D1.

Table D1: Survey files downloaded from GPS receivers

Name	Station Name	Start Time	Sampling (sec)	Antenna Height (m)
BBASEA07.126	WHB	May 6 2007 00:58:06.00	2.00	1.370 Vertical
BBASEA07.127	BAS2	May 7 2007 01:42:30.00	2.00	1.420 Vertical
BBASEA07.130	LAST	May 9 2007 22:38:10.00	2.00	1.460 Vertical
BROVA07.130	BROVA07	May 9 2007 22:55:30.00	2.00	1.300 Vertical
BROVB07.126	BROVB07	May 6 2007 01:09:42.00	2.00	1.230 Vertical
BROVB07.130	BROVB07	May 10 2007 01:12:48.00	2.00	1.300 Vertical

	Day 1
	Day 3
	No Data

Two projects were created for the two separate data collection days. The first project covered the first day using files BBASEA07.126 and BROVB07.126 and the second project covered the third day using files BBASEA07.130, BROVA07.130, and BROVB07.130. The importing procedure involved defining the control points (base station points) then allowing the program to import the files while only processing single sites as seen in Figure D1.

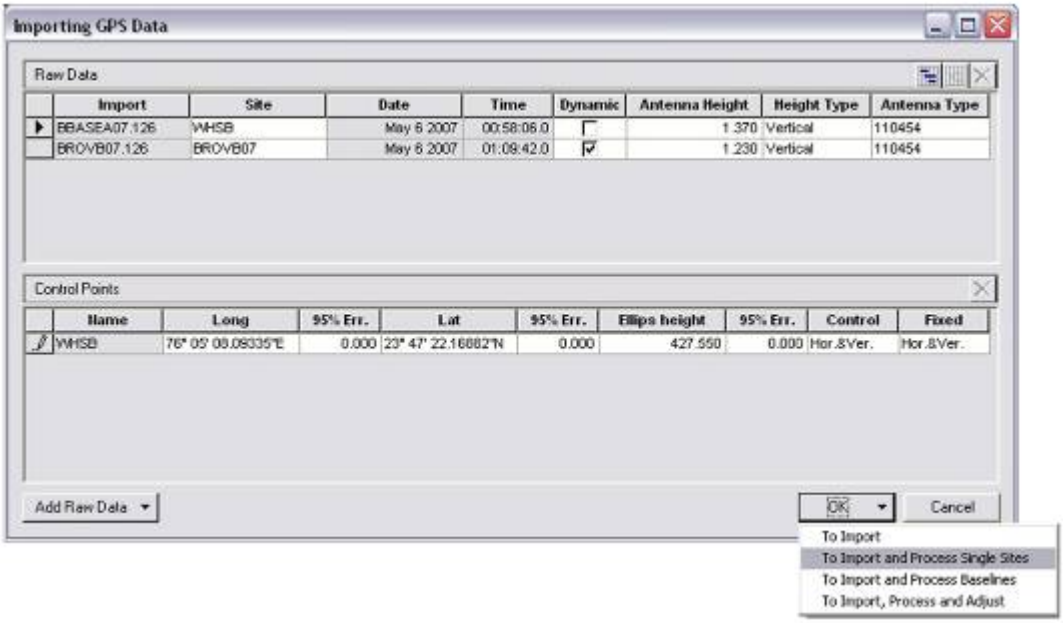

Figure D1: Screenshot of surveying files import

Once the files were imported, the points were exported to a text file and adjusted for import into ESRI's ArcGIS. The text files were combined into one containing all the survey points, and then the file was opened in Microsoft Excel. The latitude and longitude coordinates had to be converted to decimal degrees and the columns had to be correctly formatted as numeric, text, etc. The file was then saved as a dBASE IV format and added to ArcMap. An X-Y event layer was created using the survey database and the spatial reference was set to WGS 84 (the coordinate system the GPS receivers were using). The points (Figure D2) were then projected into UTM coordinates zone 43N and interpolated into a raster using kriging (Figure D3).

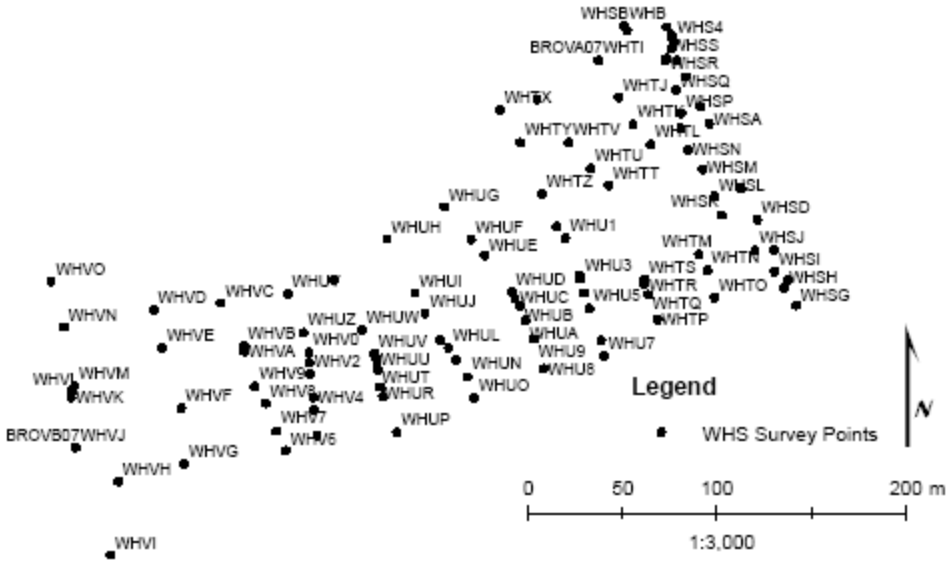

Figure D2: WHS survey points

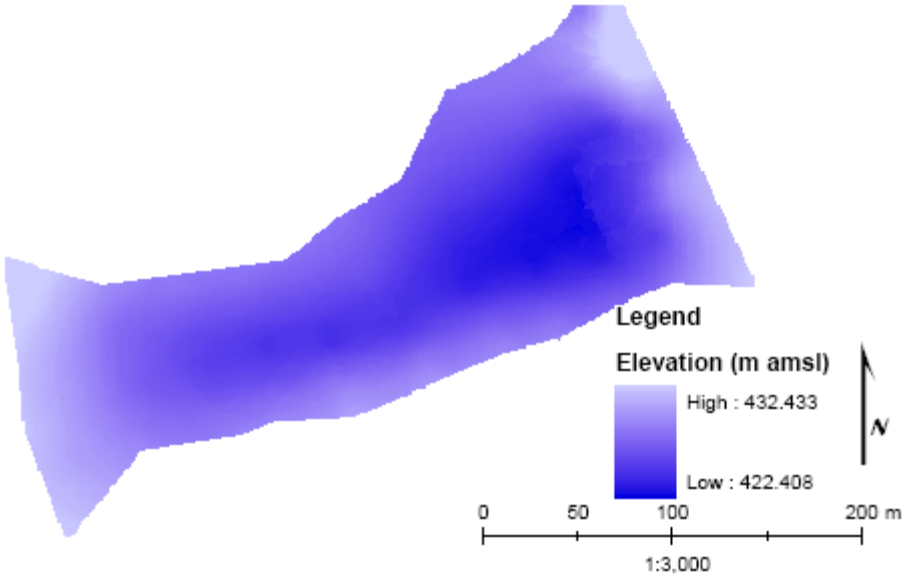

Figure D3: WHS surface obtained through kriging

Contour lines were generated as seen in the ArcMap model in Figure D4.

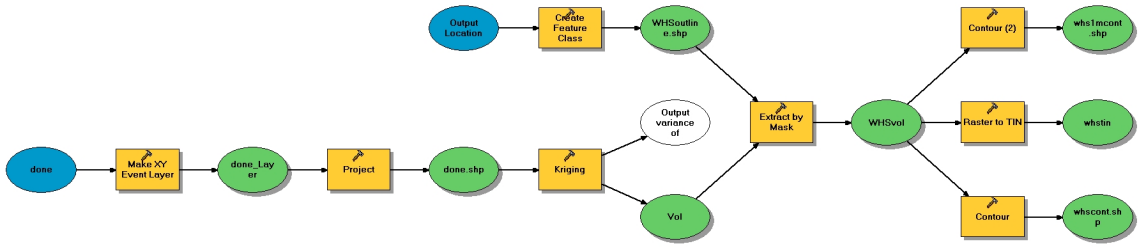

Figure D4: Model used to create 3-D visualization and contours of the WHS

The resulting volume visualization was generated in ArcScene as seen in Figure D5. The area covered is defined by the survey location points and contour lines were created using the surface raster with a contour interval of 1 meter.

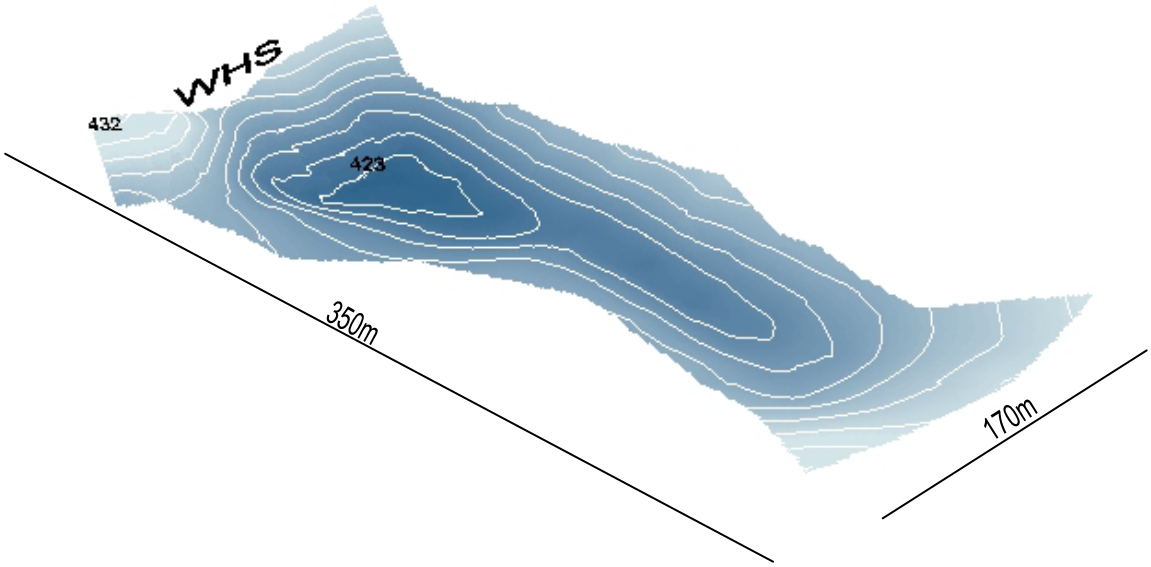

Figure D5: ArcScene visualization of the WHS

Using ArcScene, plots were generated of the WHS volume and surface area verses stage and curves were interpolated to allow for simplified calculations.

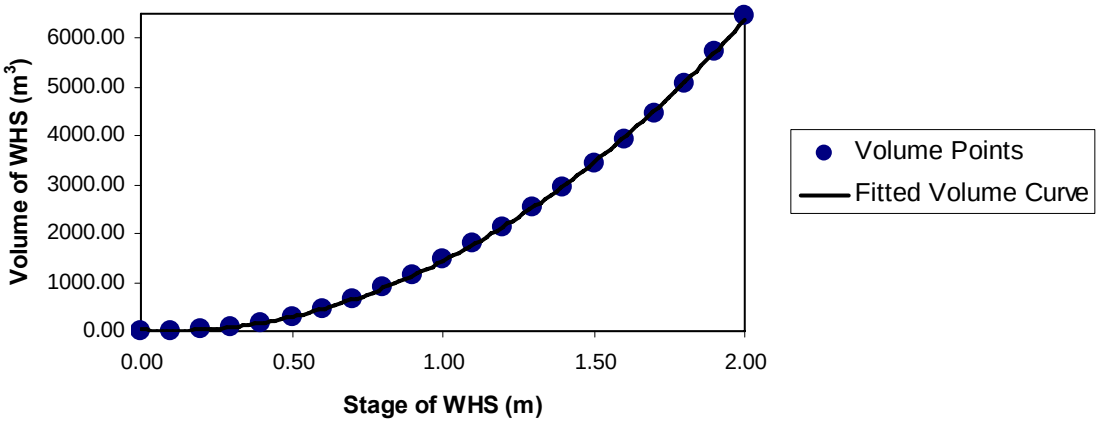

Figure D6: Fitted WHS volume curve for stages 0 – 2 meters

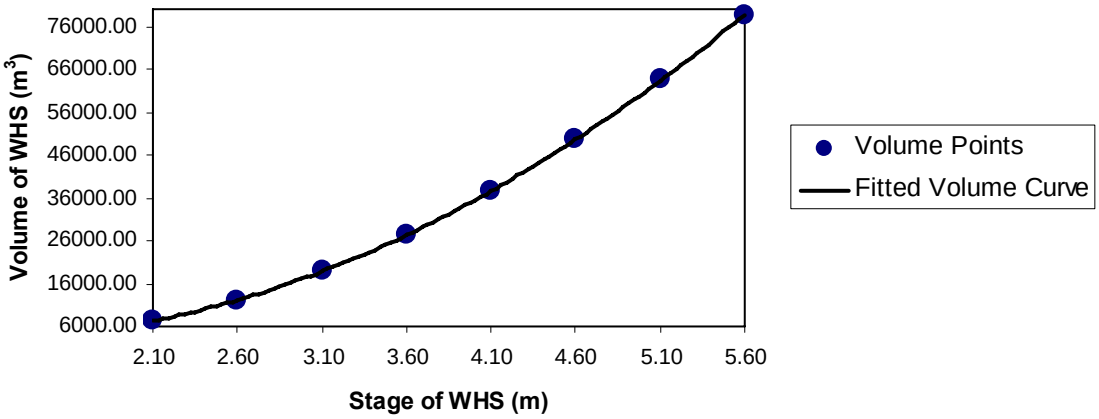

Figure D7: Fitted WHS volume curve for stages 2.1 – 5.6 meters

The volume trend line formula is given in Equation D.1:

$$V_{WHS} = \begin{cases} 1695.5h^2 - 251.99h + 4.5707; & h \le 2 \\ -222.82h^3 + 6090.2h^2 - 16222h + 17106; & h > 2 \end{cases} \quad R^2 = 1 \qquad \text{(D.1)}$$

where V_{WHS} is the volume of water stored in the WHS (m^3) and h is the stage of the water in the WHS (m) with a datum of 422.4m above mean sea level.

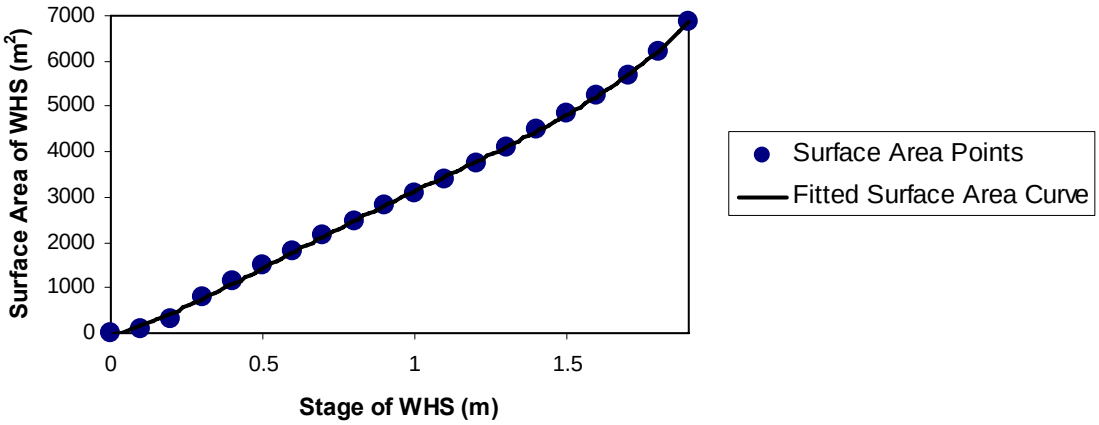

Figure D8: Fitted WHS surface area curve for stages 0 – 1.9 meters

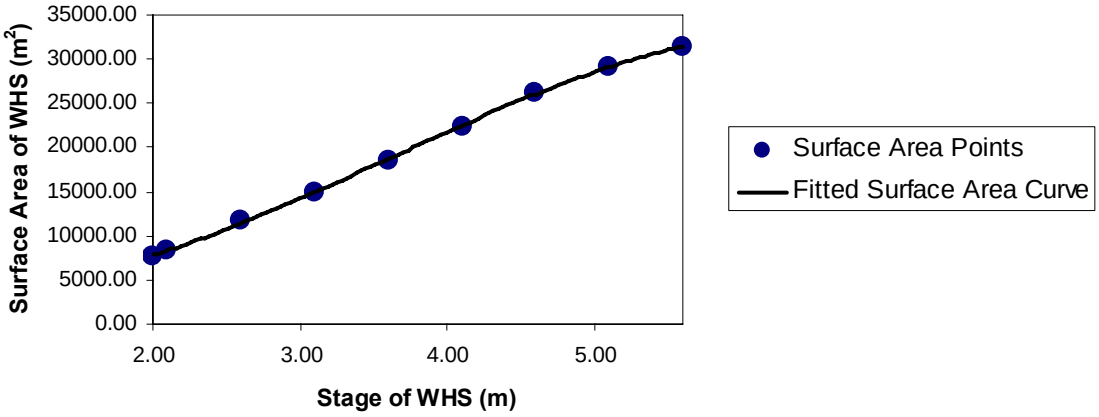

Figure D9: Fitted WHS surface area curve for stages 2 – 5.6 meters

The surface area trend line formula is given in equation D.2:

$$A_{WHS} = \begin{cases} 956.63h^4 - 3164.1h^3 + 3450.4h^2 + 1973.8h - 79.697; & h < 2 \\ -351.15h^3 + 3838.5h^2 - 6307.4h + 8036.2; & h \geq 2 \end{cases} \quad R^2 = 1 \quad \text{(D.2)}$$

where A_{WHS} is the volume of water stored in the WHS (m^3) and h is the stage of the water in the WHS (m) with a datum of 422.2m above mean sea level.

APPENDIX E

WATER HARVESTING STRUCTURE PRESSURE TRANSDUCER CONVERSION

The procedure used to correct the pressure transducer data and convert it to stage of water held within the WHS is listed below.

This document is a collection of data received from a pressure transducer installed in the water harvesting structure (WHS). The transducer was installed in the WHS to record the change in level of surface water stored after the WHS was filled during monsoon. The transducer recorded pressure readings every 30 minutes from September 2, 2007 to December 14, 2007. Data was missing from September 23 to October 12 due to a transducer malfunction.

The transducer recorded the total pressure exerted on the device, meaning the pressure of the water and the barometric pressure of the atmosphere were recorded. In order to obtain the stage of water in the WHS, the effect of the barometric pressure needed to be removed from the data. The barometric pressure was removed in two stages: a moving average to remove the effects of daily fluctuation and regional barometric pressure to remove the effect of weathering systems moving through the area.

APPENDIX F

WATER HARVESTING STRUCTURE NUMERICAL MODEL

The spreadsheet used to estimate the stage of the WHS and the Visual Basic code used to numerically solve the equation is listed below.

WHS Stage Estimation .....Electronic Appendix
WHS Stage Estimation Visual Basic Code.....Electronic Appendix

The WHS stage estimation excel file and associated Visual Basic code is the numerical model used to solve the analytical water balance over the WHS. The file contains three volume estimations. The minimum volume estimate, the numerical solution of the analytical water balance, and the same numerical solution with a spillway added.

WORKS CITED

Arghyam, 2008, India Water Portal.

Athavale, R. N., Ramesh Chand, R. Rangarajan, 1983, Groundwater Recharge Estimates for Two Basins in the Deccan Trap Basalt Formation: Hydrological Sciences Journal, v. 28, p. 525-538.

Cooper, G. R. J., 2000, VES 1.30: Forward Modelling and Inversion of Schlumberger Resistivity Soundings for Microsoft Windows.

FES, 2003, Change Detection Study in Andhra Pradesh, Madhya Pradesh and Rajasthan Project Areas of FES, Foundation for Ecological Security, p. 21-35.

Google, 2008, Agar, Shajapur, Madhya Pradesh India - Google Maps.

Gore, K. P., M. S. Pendke, V. V. S. Gurunadha Rao, C. P. Gupta, 1998, Groundwater Modelling to Quantify the Effect of Water Harvesting Structures in Wagarwadi Watershed, Parbhani District, Maharashtra, India: Hydrological Processes, v. 12, p. 1043-1052.

Healy, R. W., Peter G. Cook, 2002, Using Groundwater Levels to Estimate Recharge: Hydrogeology Journal, v. 10, p. 91-109.

Iyengar, S., ed., 2007, Waternama: Bangalore, Communication for Development and Learning, 124 p.

Jerram, D. A., Mike Widdowson, 2005, The Anatomy of Continental Flood Basalt Provinces: Geological Constraints on the Processes and Products of Flood Volcanism: Lithos, v. 79, p. 385-405.

Kulkarni, H., 2007, Re: Deccan basalt hydraulic conductivity, *in* J. Oblinger, ed.

Kulkarni, H., Anil Lalwani, S. B. Deolankar, 1997, Selection of Appropriate Pumping Systems for Bore Wells in The Deccan Basalt of India: Hydrogeology Journal, v. 5, p. 75-81.

Kulkarni, H., P. S. Vijay Shankar, S. B. Deolankar, Mihir Shah, 2004, Groundwater Demand Management at Local Scale in Rural Areas of India: A Strategy to Ensure Water Well Sustainability Based on Aquifer Diffusivity and Community Participation: Hydrogeology Journal, v. 12, p. 184-196.

Kulkarni, H., S. B. Deolankar, Anil Lalwani, Bijoy Joseph, Suresh Pawar, 2000, Hydrogeological Framework of the Deccan Basalt Groundwater Systems, West-Central India: Hydrogeology Journal, v. 8, p. 368-378.

Kulkarni, H., S. B. Deolankar, Anil Lalwani, V. A. Lele, 1994, Integrated Remote Sensing as an Operational Aid in Hydrogeological Studies of Deccan Basalt Aquifers: Asian-Pacific Remote Sensing Journal, v. 6, p. 9-18.

Kumar, M. D., Santanu Ghosh, O. P. Singh, Rahul Ranade, R. Ravindranath, 2005, Changes in Groundwater Ecology and Its Implication for Surface Flows: Studies from Narmada River Basin, Madhya Pradesh, India, IWMI-TATA Water Policy Program.

Kumar, M. D., Shantanu Ghosh, Ankit Patel, O. P. Singh, R. Ravindranath, 2006, Rainwater Harvesting in India: Some Critical Issues for Basin Planning and Research: Land Use and Water Resources Research, v. 6, p. 1-17.

Lalwani, A., Himanshu Kulkarni, S. B. Deolankar, and P. Paul Thomas, 1995, Program to Calulate Hydraulic Conductivity Using Dugwell Recovery Data: Ground Water, v. 33, p. 144-147.

Macdonald, D. M. J., H. C. Kulkarni, A. R. Lawrence, S. B. Deolankar, J. A. Barker, A. B. Lalwani, 1995, Sustainable Groundwater Development of Hard-Rock Aquifers: The Conflict Between Irrigation and Drinking Water Supplies from the Deccan Basalts of India, Keyworth, Nottingham, British Geological Survey, p. 54.

Madhya Pradesh Irrigation Department, 1981, Report on the Geohydrological Investigation of Agar Block, District Shajapur: Field Season 1974-1975, Bhopal, Government of Madhya Pradesh, Office of the Chief Engineer, Ground Water Surveys, Irrigation Department, M.P., Bhopal.

Moench, M., Jacob Burke, Yarrow Moench, 2003, Rethinking the Approach to Groundwater and Food Security, Rome, Food and Agriculture Organization of the United Nations, p. 17-36.

Naik, P. K., Arun K. Awasthi, A. V. S. S. Anand, Prakash C. Mohan, 2001, Hydrogeologic Framework of the Deccan Terrain of the Koyna River Basin, India: Hydrogeology Journal, v. 9, p. 243-264.

Naik, P. K., Arun K. Awasthi, Prakash C. Mohan, 2002, Springs in a Headwater Basin in the Deccan Trap Country of the Western Ghats, India: Hydrogeology Journal, v. 10, p. 553-565.

Nair, K. K. K., B. Bhusari, 2001, Stratigraphy of Deccan Traps: A Review: Geological Survey of India Special Publications, v. 64, p. 477-491.

Narasimhan, T. N., 2006, Ground Water in Hard-Rock Areas of Peninsular India: Challenges of Utilization: Ground Water, v. 44, p. 130-133.

Narula, K. K., Frank Wendland, D. D. Bhujanga Rao, N. K. Bansal, 2001, Water Resources Development in the Yamuna River Basin in India: Journal of Environmental Studies and Policy, v. 4, p. 21-33.

Patel, A., Dr. M. Dinesh Kumar, 2007, Water Harvesting and Groundwater Recharging in Water Scarce Regions of India: A Case of Ghelo River Basin, Saurashtra, International Water Management Institute, p. 1-21.

ProMark3 Reference Manual, 2005, Magellan Professional.

Ray, S., Mahendra Bijarnia, 2006, Upstream vs Downstream: Groundwater Management and Rainwater Harvesting: Economic and Political Weekly, v. 41, p. 2375-2383.

Reynolds, J. M., 1997, An Introduction to Applied and Environmental Geophysics: Chinchester, John Wiley & Sons Ltd.

Saha, D., A. K. Agrawal, 2006, Determination of Specific Yield Using a Water Balance Approach - Case Study of Torla Odha Watershed in the Deccan Trap province, Maharastra State, India: Hydrogeology Journal, v. 14, p. 625-635.

Saraf, A. K., P. R. Choudhury, 1998, Integrated Remote Sensing and GIS for Groundwater Exploration and Identification of Artificial Recharge Sites: International Journal of Remote Sensing, v. 19, p. 1825-1841.

Scanlon, B. R., Kelley E. Keese, Alan L. Flint, Lorraine E. Flint, Cheikh B. Gaye, W. Michael Edmunds, Ian Simmers, 2006, Global Synthesis of Groundwater Recharge in Semiarid and Arid Regions: Hydrological Processes, v. 20, p. 3335-3370.

Shankar, D., Vidya Kotamraju, S. R. Shetye, 2004, A Quantitative Framework for Estimating Water Resources in India: Current Science, v. 86, p. 543-552.

Singhal, B. B. S., R. P. Gupta, 1999, Applied Hydrogeology of Fractured Rocks: Boston, Kluwer Academic Publishers, 400 p.

Susner Irrigation Department, 1987, Geohydrological Report in Part of Susner Block, Bhopal, Office of the Chief Engineer, Ground Water Surveys, Irrigation Department, M.P., Bhopal.

Sutcliffe, J. V., C. S. Green, 1986, Water Balance Investigation of Recharge in Madhya Pradesh, India: Hydrological Sciences Journal, v. 31, p. 383-394.

Sutcliffe, J. V., R. P. Agrawal, Julia M. Tucker, 1981, The Water Balance of the Betwa Basin, India: Hydrological Sciences Bulletin, v. 26, p. 1981.

The Weather Underground, Inc., 2008, Welcome to Weather Underground : Weather Underground.

Thornthwaite, C. W., J. R. Mather, 1955, The Water Balance: Publications in Climatology, v. 8, p. 1-104.

Thornthwaite, C. W., J. R. Mather, 1957, Instructions and Tables for Computing Potential Evapotranspiration and the Water Balance: Publications in Climatology, v. 10, p. 185-311.

Tiwary, R., 2005, Dalit and Water, *in* S. Moysey, ed., IWMI-TATA.

Wilson, J. P., Helena Mitasova, Dawn J. Wright, 2000, Water Resource Applications of Geographic Information Systems: URISA Journal, v. 12, p. 61-79.